


1-1-2017

Design, Synthesis And Analysis Of Potential Photo-Activatable Cathepsin K Inhibitors

Khalin Evania Nisbett
Wayne State University,

Follow this and additional works at: https://digitalcommons.wayne.edu/oa_theses

 Part of the [Biochemistry Commons](#), [Inorganic Chemistry Commons](#), and the [Organic Chemistry Commons](#)

Recommended Citation

Nisbett, Khalin Evania, "Design, Synthesis And Analysis Of Potential Photo-Activatable Cathepsin K Inhibitors" (2017). *Wayne State University Theses*. 581.
https://digitalcommons.wayne.edu/oa_theses/581

This Open Access Thesis is brought to you for free and open access by DigitalCommons@WayneState. It has been accepted for inclusion in Wayne State University Theses by an authorized administrator of DigitalCommons@WayneState.

**DESIGN, SYNTHESIS AND ANALYSIS OF
POTENTIAL PHOTO-ACTIVATABLE
CATHEPSIN K INHIBITORS**

by

KHALIN EVANIA NISBETT

THESIS

Submitted to the Graduate School

of Wayne State University,

Detroit, Michigan

in partial fulfillment of the requirements

for the degree of

MASTER OF SCIENCE

2017

CHEMISTRY

Approved By:

Jeremy Kodanko, Ph.D.

Date

©COPYRIGHT BY
KHALIN EVANIA NISBETT
2017
All Rights Reserved

Dedication

I know the Lord is always with me. I will not be shaken, for he is right beside me.

-Psalm 16:8

Acknowledgements

“The Lord is my shepherd; I shall not want. He maketh me to lie down in green pastures: he leadeth me beside the still waters. He restoreth my soul: he leadeth me in the paths of righteousness for his name’s sake. Yea, though I walk through the valley of the shadow of death, I will fear no evil: for thou art with me; thy rod and thy staff they comfort me. Thou prepares a table before me in the presence of mine enemies: thou anointest my head with oil; my cup runneth over. Surely goodness and mercy shall follow me all the days of my life: and I will dwell in the house of the Lord forever.”

[A Psalm of David; Psalm 23: 1-6. The Holy Bible]

I am grateful. I am grateful that I am blessed and that my soul has been restored and that above all else I have peace. I must thank God for the people he has placed in my life:

To my father, Evan L. D. Nisbett & my mother, Sherilla I. Nisbett, I have never lacked anything. Your love, support, words of encouragement, prayers, humor, example and understanding have blanketed me through the years. I could not ask for a better King & Queen.

To my sisters, Shevane D. Nisbett and A. Karen Liburd, & my brothers, Clevis H. Nisbett and Kyle A. Weeks, you are my counterweights. What I’m trying to say is, you guys balance me. You hold me together like glue and you catch my screws when they fall. I will forever be indebted to you. I am ever grateful to my closest family, friends and cheerleaders, Colin, Greta, Errol, Esmond, Icilma and Connie Walters, Jeffrey and Judy Nisbett, Lennox and Michelle Zamore, Maureen and Hilton Jeffers, Kitaro Evelyn, Christel Brandy, Nalinie Ramnaraine, Daricia Wilkinson, Keturah Bethel, Y’ Kesha Zamore, Rhonda Roberson and Carol Gardenhire. You are always there when I need you – you have surely facilitated my journey.

The mentors who enabled my education and advised me professionally include Colin Walters, Matthew Allen, Bernard Castillo II, Yakini Brandy, Antonio D. Brathwaite and Justin Shorb, thank you for your input, incite and solicitude.

To my life mentor, Uncle Colin, thank you for your commitment to my success. I am not sure how I would have managed without your advice and guidance. You are truly a great role model. Thank you for every bit of advice, for your honesty and for every feel-good moment. It's been a pleasure learning from you!

Oh, Dr. Allen, you were a mentor when I most needed one. When I walked into your office, scheduled or not, I felt like the world revolved around me for that 5, 15 or 30 minutes. I am easily convinced that you were hoping I would show up. To get that feeling with the chair of this chemistry department, on **any** given day, is extremely remarkable and profound. You were an unexpected blessing.

This thesis and my advancement in this field would not have been possible without my advisor Jeremy Kodanko, who has spent hours teaching and guiding me in the laboratory, and collaborators Izabela Podgorski & Mackenzie Herroon who introduced me to bench biology and answered my bottomless pit of questions. Astute professors, Chuck Winter, Mary Rodgers, Bernard Schlegel, Shane Perrine and Naftali Raz have played noteworthy roles as my professors, and advisers during the final months of my tenure; for this I thank you. I am particularly grateful to the National Institutes of Health who have provided funding for the project discussed in the following pages and to the Wayne State University who has given me this opportunity to learn, teach and mentor.

Associations including the Wayne State University (WSU) African Community, WSU Latin Social & Dance Club, WSU Graduate Employees Organizing Committee, ACS-UVI Student Chapter, as well as friends I met through WSU, UVI and in my home island St Kitts-Nevis, who are absolutely too many to mention will forever be in my heart.

I would change absolutely nothing about this unpredictable & unforgettable journey because of the individuals I have met and the ways in which I have grown. I look forward in anticipation of stronger connections with the persons mentioned above.

Thank you,

Kay

Foreword

“We may make a lot of plans, but the Lord will do what he has decided.”

[Proverbs 19:21; The Holy Bible]

This period is one I will never take back, I will never regret, I will never forget, one that will always *be*. I officially started the research project described within the following pages in January, 2016 and I completed the work by May, 2016. At the end of 5 months and 2 days[†], I learned an incredible amount, but I grew thirstier and more motivated than I was. In this time, I had the pleasure of working and learning from astute professors and colleagues. In the subsequent five months, I began work on a new project, not described here due to its incompleteness. I grew excited and a little bit delusional. I started working weirder hours, 10pm – 8am or 3am – 1pm because the lab became my happy place, I couldn’t wait to succeed and I still can’t. I became so distracted by my obsession that my social life crumbled and my vision became blurred. And then God intervened. A series of events relocated me. It was an odd, ugly time. Truly, a *Fall* of despair and depression, but a *Winter* of hope and ecstasy. Details absent. Suffice it to say, it was necessary, in many ways.

[†] This is an approximate timeline.

“It was the best of times, it was the worst of times, it was the age of wisdom, it was the age of foolishness, it was the epoch of belief, it was the epoch of incredulity, it was the season of Light, it was the season of Darkness, it was the spring of hope, it was the winter of despair, we had everything before us, we had nothing before us.”

[Dickens, C. J. H. (1859). *A tale of two cities* (Vol. 1). Chapman and hall.]

I bought Charles Dickens’ *A Tale of Two Cities* with sincere conviction that he was a graduate student airing his emotions in prose. When I found out this book was based on the French Revolution, I became first, cynical, then disappointed and finally relieved. I felt cheated; the book gave me a false feeling of solidarity. I grew disappointed because this type of falsehood had not been uncommon to me – and I had to acknowledge that it was more rampant than I thought, maybe even dominant.

You must be thinking, I should’ve read further before making the purchase, right? – I should have been more perceptive? Well – But – in my defense, the fact that I didn’t *read* further says less about my baseless assumptions and more about my attention to my career. I had no time to read past what was presented to me. I had papers to write and reactions to set up!

I must be honest, I am glad I bought the book. It’s a classic; it’s one of those experiences you must have – I mean – books you must read to appreciate your surroundings, the culture you are in and how you must maneuver.

“If you are not willing to learn, no one can help you, if you are determined to learn, no one can stop you.”

[Zig Ziglar]

I am truly a small island lady, with big continent dreams. I have this voracious appetite for knowledge that is not well understood by many. I have been asked time and time again, why I work so hard – with true perplexity. And I would respond and say, “I don’t know. Why don’t you?” But the truth is, I have been starved of education and opportunity for so long that every part of me approaches each day hoping to learn something new – anything. I am indisputably hungry for knowledge and undeniably thirsty for a new perspective. I am relentlessly in search of this sustenance.

Until I become satisfied, I will seek to excel in whatever I decide to pursue. I vow to always achieve greatness *in spite of* the obstacles before me – and to chart a new course for small island ladies and gentlemen much like myself. I strive to show those, with obstacles greater and smaller than mine, that it can be done. I seek to encourage & challenge others without uttering a word and to give them permission to find their calling outside of the written expectations. I pray that the light that is within me, will light their path.

Kay

Table of Contents

Dedication	ii
Acknowledgements	iii
Foreword	vi
List of Tables.....	xii
List of Figures	xiii
List of Abbreviations.....	xvii
Chapter 1: About the Investigation.....	1
1.1 Significance of the Investigation.....	1
1.2 Overview of the Investigation.....	4
Chapter 2: Review of the Literature	6
2.1 Enzymes	6
2.1.1 Proteases	6
2.1.2 Papain-like (CA) Cysteine Proteases.....	7
2.1.3 Cathepsin K	8
2.2 Inhibitors	11
2.3 Photo-caging: Metal-Based Alternatives	19
2.3.1 Organic Chromophores	19
2.3.2 Nanoparticles	22
2.3.3 Other Alternatives	23

2.4 Photo-caging: Metal-Based	27
2.4.1 About Metal-Based PACT & PDT	27
2.4.2 Previous work by the Kodanko Group	32
2.4.3 Work by Other Research Teams	36
Chapter 3: Methodology	40
3.1 Materials	40
3.2 Instrumentation	42
3.3 Procedures	43
3.3.1 Syntheses	43
3.3.2 Characterization: Sample Preparation & Data Collection	51
3.3.3 Photolysis of Inhibitor	52
3.3.4 Enzyme Assays	52
Chapter 4: Findings	55
4.1 Characterization Data	55
4.2 Photolysis Data	65
4.3 Enzyme Inhibition Assay Findings	66
Chapter 5: Clarifications & Contributions	68
Chapter 6: Conclusion	76
References	78
Abstract	92

Autobiographical Statement94

List of Tables

(Format: Table [section]. table # in 'section')

Table [2.2.0].1 Major CA cysteine protease inhibitors, categorized by their mechanism of attack12

Table [2.2.0].2 Comparison of the inhibition constants of dipeptide inhibitors by the length and bulk of P₂ binding site.18

Table [5.0.0].1 Evidence for increase in efficacy due to increase in basicity at P₃ residue, contrary to the observation presented here72

Table [5.0.0].2 Comparison of the quantum yields of dissociation for 3 sets of chaperones. The chaperones of each set have different degrees of metal centered bulk.73

List of Figures

(Format: Figure [section]. figure # in 'section')

Figure [1.2.0].1 The inhibitors being investigated.....	4
Figure [1.2.0].2 The Ru ^{II} complex being investigated.....	5
Figure [2.1.1].1 The enzyme subsites and the substrate residues, as named by the Schechter & Berger method. This description considers that the amino acid residues of the substrate (or inhibitor) bind to the corresponding active site	7
Figure [2.1.3].1 Crystal structure of Cathepsin K (A) by amino acid residue (JSmol-Javascript), (B) by secondary structure (PV-WebGL). Image from the RCSB PDB (www.rcsb.org) of PDB ID 5TUN (S. Law, P.M. Andrault, A. Aguda, N. Nguyen, N. Kruglyak, G. Brayer, D. Bromme (2017) Identification of mouse cathepsin K structural elements that regulate the potency of odanacatib <i>Biochem. J.</i> 474: 851-864).....	10
Figure [2.2.0].1 Four of the first inhibitors synthesized	12
Figure [2.2.0].2 Pinner-type inhibitors, the first aminoacetonitrile inhibitors and an example of an azapeptide inhibitor.....	13
Figure [2.2.0].3 Three clinically developed CST-K inhibitors	15
Figure [2.2.0].4 X-ray co-crystal structure of inhibitor 10 lodged into the active site cleft of CST-K and bound by Cys139. (A) show the surface structure; (B) shows a magnified frontal view of the active site; (C) shows the Cys139-S-C=N-R reversible bond via a magnified side view. Image from the RCSB PDB (www.rcsb.org) of PDB ID 1YK8 (D. G. Barretta, D. N. Deaton, A. M. Hassell, R. B. McFadyen, A. B. Miller, L. R. Miller, J. A. Payne, L. M. Shewchuk, D. H. Willard Jr., L. L. Wright (2005) Acyclic cyanamide-based inhibitors of cathepsin K <i>Bioorg. Med. Chem. Lett.</i> 15: 3039-3043).....	16
Figure [2.2.0].5 Proposed mechanism for cysteine inhibition versus serine inhibition.....	17
Figure [2.2.0].6 Depiction of the intermediate oxyanion hole that results from enzyme-carbonyl interactions	17
Figure [2.3.1].1 Organic photo-activatable molecules described in this section	20

Figure [2.3.2].1 The D-luciferin conjugated LD-UCNP described in section 2.3.2.....	23
Figure [2.3.3].1 Jablonski diagram for single- and two-photon absorption.....	24
Figure [2.3.3].2 Illustration of the photo-release of biomolecule such as carbachol form a chromophore-doped lipid vesicle.....	25
Figure [2.3.3].3 An example of sensitized reductive cleaved of an organic carboxylic acid	26
Figure [2.4.1].1 The essential electronic mechanism for the excitation of the $^1\text{O}_2$ species to $^3\text{O}_2$ in PDT	28
Figure [2.4.1].2 The electronic mechanism and energetic arrangements of the excited states that contribute to depopulation/population of the ^3LF , influencing ligand dissociation.....	29
Figure [2.4.1].3 Structural geometry of 32 & 33 via X-ray crystal structures, 32X & 33X . Image 32X from the Cambridge Structural Database. CSD-JIMJUK C. R. Hecker, P. E. Fanwick, D. R. McMillin, Inorganic Chemistry, 1991, 30, 659. DOI: 10.1021/ic00004a013. Image 33X from the Cambridge Structural Database. CSD-ABAHUJ J. D. Knoll, B. A. Albani, C. B. Durr, C. Turro, Journal of Physical Chemistry A, 2014, 118, 10603. DOI: 10.1021/jp5057732	31
Figure [2.4.2].1 The first generation nitrile-bound inhibitors synthesized and investigated by the Kodanko group.....	33
Figure [2.4.2].2 The second generation nitrile bound $[\text{Ru}^{\text{II}}$ -inhibitor] synthesized and investigated by the Kodanko group.....	34
Figure [2.4.2].3 The parent inhibitors as well as their derivatives and caged inhibitors described in section 2.4.2	36
Figure [2.4.3].1 Nitrile-bound inhibitor-chaperone complexes synthesized and investigated by collaborators Turro group (44 & 45) and a non-photo-activatable Ru^{II} complex being clinically developed (46)	38
Figure [2.4.3].2 The PRAMT agent discussed in section 2.4.3	39

Figure [3.3.1].1	Reaction scheme for synthesis of Inhibitor 1.....	43
Figure [3.3.1].2	Reaction scheme for synthesis of Reagent 42.....	44
Figure [3.3.1].3	Reaction scheme for synthesis of Inhibitor 2.....	45
Figure [3.3.1].4	Reaction scheme for synthesis of Inhibitor 3.....	47
Figure [3.3.1].5	Reaction scheme for synthesis of Complex 4.....	49
Figure [4.1.0].1	¹ H NMR of Inhibitor 1.....	55
Figure [4.1.0].2	¹ H NMR of compound 50.....	56
Figure [4.1.0].3	¹ H NMR of compound 52.....	57
Figure [4.1.0].4	¹ H NMR of compound 53.....	58
Figure [4.1.0].5	¹ H NMR of Inhibitor 2.....	59
Figure [4.1.0].6	¹ H NMR of Compound 55.....	60
Figure [4.1.0].7	¹ H NMR of Inhibitor 3.....	61
Figure [4.1.0].8	¹ H NMR of Compound 58.....	62
Figure [4.1.0].9	¹ H NMR of Complex 4.....	63
Figure [4.1.0].10	Superimposed UV-Vis Spectra of Complex 4 & 59.....	64
Figure [4.2.0].1	UV-Vis-Photolysis data.....	65
Figure [4.3.0].1	Enzyme assay data of the uncaged CST-K inhibitors.....	66

Figure [4.3.0].2 Light inhibition enzyme assay data of the caged CST-K inhibitors plot against the respective uncaged inhibitor 267

Figure [5.0.0].1 Schechter and Berger residue assignments for inhibitor 1.....69

List of Abbreviations

(Alphabetically organized)

← – dative bond

[] – complex

¹O₂ – singlet dioxygen

4PA – 4-pyridyl-alanine

5-CNU – 5-cyanocuracil

Ala – Alanine

AMC – 7-amido-4-methylcoumarin

Asn – Asparagine

BMM cells – bone marrow-derived macrophages

Boc – tert-butyloxy carbonyl

BODIPY – Boron- dipyrromethene

bpy – 2,2'-Bipyridine

C4pz – Carboxy-4-pyridylmethyl

CA clan – Calpain & papain family

CALI – Chromophore assisted light inactivation

Cbz – carboxybenzyl

CST – Cathepsin

Cys – Cysteine

DCM – Dichloromethane

DiO – 3,3'-Diocetadecyloxycarbocyanine perchlorate

DiPEA - N,N-Diisopropylethylamine

DLIR – Dark-light IC₅₀ ratio

dmbpy – 6,6'-Dimethyl-2,2'-dipyridine

DMF – Dimethylformamide

DMSO – Dimethyl sulfoxide

DNA – Deoxyribonucleic acid

DTT – 1,4-Dithiothreitol

EDTA – Ethylenediaminetetraacetic acid

FALI – Fluorophore assisted light inactivation

HBTU – N,N,N',N'-Tetramethyl-O-(1H-benzotriazol-1-yl)uronium hexafluorophosphate

HCl – Hydrochloric acid

His – Histidine

HSAB – Hard-Soft Acid-Base Theory

IC₅₀ – Concentration of the inhibitor that produces half maximal response

K_i – thermodynamics of inhibitor binding

k_{inact} – kinetics of inhibitor binding

k_{rel} – relative second order rate inhibition constant; $[(k_{\text{inact}}/K_{\text{i}})_{\text{dark}} \div (k_{\text{inact}}/K_{\text{i}})_{\text{light}}]$

LD-UCNP – Lanthanide-doped up-converting nanoparticles

Leu – Leucine

LF – Ligand field

MeCN – acetonitrile

Met – Methionine

MHC – Major Histocompatibility complex

MLCT – Metal-ligand charge transfer state

MS – Mass Spectrometry

mtpa – tris(6-methyl-2-pyridylmethyl)amine

MTT assay – assay stained with dye: 3-(4,5-Dimethylthiazol-2-yl)-2,5-diphenyltetrazolium bromidefor

N₂ – Dinitrogen

N≡CR – nitrile bounded inhibitor

NIR – Near infrared

NMR – Nuclear Magnetic Resonance Spectroscopy

***o*-** – ortho-

PACT – Photo-activatable Chemotherapy

PC3 – Prostate Carcinoma cell line

PDAMT – Photodynamic Antimicrobial Therapy

PDDS – Photo-responsive drug delivery system

PDT – Photodynamic Therapy

Phe – Phenylalanine

PRAMT – Photo-release Antimicrobial Therapy

pyR – Pyridyl bound inhibitor

RANKL – Receptor Activator of Nuclear factor κ -B Ligand

RNA – Ribonucleic acid

ROS – Reactive oxygen species

Ru^{II} – Ruthenium (II)

terpy – 2,2':6',2''-Terpyridine

TLC – Thin Layer Chromatography

tpa – Tris(2-pyridylmethyl)amine

Tyr – Tyrosine

USFDA – United States Food and Drug Administration

UV – Ultraviolet light

Vis – Visible light

CHAPTER 1. ABOUT THE INVESTIGATION

1.1 SIGNIFICANCE OF THE INVESTIGATION

Cysteine proteases of the 13- membered calpain and papain family (CA clan) play a significant role in the maintenance of normal cellular function and structure.¹⁻⁴ They are essential to the hydrolytic behavior of lysosomes and allow healthy cells to thrive and regenerate. They are known for their unique active site properties and uneven, tissue-specific expression patterns. Of these, cathepsins K, B and S are extremely critical as they are directly involved in osteoclastic bone resorption and macrophage invasion. The downfall of this highly instrumental system is the effects of its malfunction. When CA protease are imbalanced or mislocalized, they contribute instead to the destruction of normal function and structure; they play an active role in the progression of many diseases including osteoporosis, atherosclerosis, lung, breast and prostate cancer and many other systemic diseases. For this reason, they are of high medical importance.

Cathepsin K (CST-K) is important to bone remodeling and function.² The major consequence of upregulated and mislocalized CST-K is the progression of osteoporosis, and bone metastases of lung, breast, and prostate cancers. It is more highly expressed in bone marrow macrophages, and stromal cells in the metastatic environment than that of the primary tumor, this makes metastatic bone cells an optimal target for tumor reduction. Related studies found that the growth and progression of intratibially implanted prostate carcinoma cells (PC3) were significantly reduced in cathepsin K knockout mice versus wild type mice,⁵ thus verifying its importance.

Cancer has been defined as a malignant tumor that results from an uncontrolled division of genetically-mutated cells.⁶ It is a disease, claiming over 17,000 lives daily worldwide,⁷ and as such it is the main focus of numerous research teams and pharmaceutical companies.^{1, 8-13} Currently,

there are numerous clinically developed strategies being employed to combat all the 100+ cancer types. These include surgery, immunotherapy, laser therapy, stem cell transplant, hyperthermia, photodynamic therapy (PDT) and blood transfusion. However, two of the most common treatments are orally administered chemotherapy and radiation therapy. Oral treatments lack the ability to achieve location-specific inhibition.¹¹ The lipophilic character of these therapeutics increases cell permeability, but cell accumulation and anti-target inhibition occur once they are ionized and trapped inside the cell due to the high homology of the CA proteases. This leads to poor therapeutic efficacy, dose escalation, drug resistance and intensified side effects. Radiation therapy uses high doses of radiation to kill cancer cells, but produces side effects such as hair loss, nausea and motion sickness.¹⁴

It is therefore necessary to minimize these risks and costs effects through optimizing drug exposure in future therapies. As scientists probe the current methodologies, new technologies are invented.^{10, 12, 15-21} One such strategy, is photo-activated chemotherapy (PACT).²²⁻²³ In this method, a drug is caged[‡] to a chaperone[§] allowing spatial and temporal control over drug delivery at the infected site. The localization of abnormal proteolysis by CST-K, makes it a prime target for PACT.

The study reported here describes the investigation of a PACT Ru^{II} complex that can be used to permit spatio-temporal control and optimize drug release and exposure for protein inhibition. This strategy has been under development in this research team for approximately 5 years though the pharmacological interest toward cancer treatment has always been central. In the past, inhibitors were bound to the chaperone via a ruthenium-nitrile (Ru^{II}-N≡CR) dative bond.

[‡] Attached by a dative or covalent bond

[§] A Ru^{II} complex, organic protecting group, nanoparticle, or vesicle that can be separated from a drug by photolysis

However, as a result of the instability of these complexes in growth media, a new binding arrangement was sought that will produce similar or better dissociative quantum yields, dark/light IC_{50} ratios (DLIR)** , binding affinities and stabilities in growth media. In this study, derivatives of known cysteine protease inhibitors are synthesized and analyzed for inhibition against recombinant human cathepsin K. The most potent derivative is then complexed to a $[Ru^{II}]^{\dagger\dagger}$ chaperone by a pyridyl substituent and analyzed in the absence and presence of light. Light permits the photo-activation of the $[Ru^{II}$ -inhibitor], allowing the release of the CST-K inhibitor.

**DLIR = IC_{50} (pre-irradiation) \div IC_{50} (post-irradiation)

$\dagger\dagger[]$ = complex; exempli gratia: $[Ru^{II}]$ = Ru^{II} complex

1.2 OVERVIEW OF THE INVESTIGATION

The main goal of this project was to investigate the effect of a new $[\text{Ru}^{\text{II}}]$ -inhibitor binding arrangement on CST-K inhibition, *id est*, $[\text{Ru}^{\text{II}}]\text{-N}\equiv\text{CR}$ binding versus $[\text{Ru}^{\text{II}}]\text{-pyR}$. To do this, we incorporated an N-heteroatom in a known CST-K inhibitor, by exchanging the phenyl substituents of the parent inhibitor **1** (Fig. [1.2.0].1) with a pyridyl substituent. The N-heteroatom would accommodate the dative (L-type) binding necessary for photodissociation. Thus, two derivatives of the parent compound were synthesized, **2** & **3** (Fig [1.2.0].1). It then became necessary to investigate the effect of increasing the basicity of the ligand on CST-K inhibition.

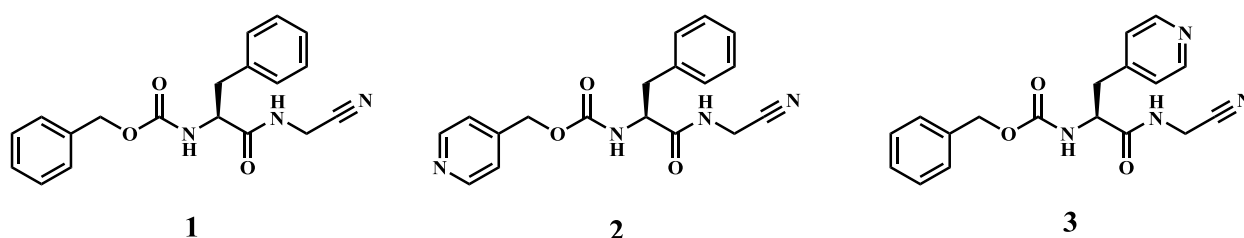


Figure [1.2.0].1 The inhibitors being investigated.

To do this, I synthesized a previously established compound (**1**) and two new derivatives (**2** & **3**). I performed enzyme inhibition assays, and caged the most potent derivative to a Ru^{II} chaperone. This resulted in complex **4** (Fig [1.2.0].2). After characterization and photolysis examination, I performed CST-K inhibition studies in the dark (pre-irradiation) and in the light (post-irradiation). The results were compared to those of previous studies.

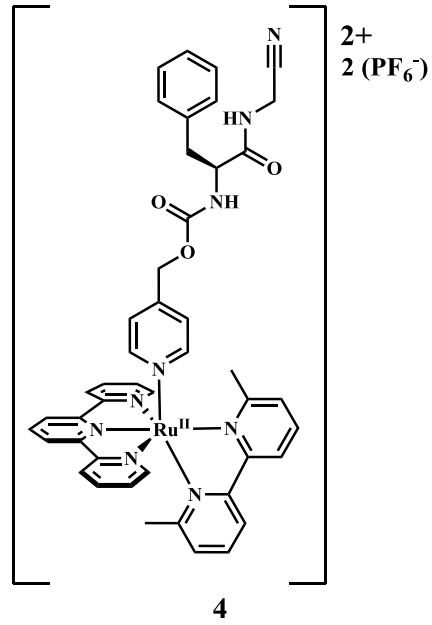


Figure [1.2.0].2 The Ru^{II} complex being investigated.

CHAPTER 2. REVIEW OF THE LITERATURE

2.1 ENZYMES

2.1.1 PROTEASES

Proteases are lysosomal proteolytic enzymes that are essential to the regulation and function of many bio-physiological processes including immune response, growth and cell signaling.²⁴ There are five main types of proteases, named according to their active site residues: aspartic (*exempli gratia*, CST-D), serine (*exempli gratia*, trypsin), threonine (*exempli gratia*, ornithine acetyltransferase), cysteine (*exempli gratia*, CST-K) and metallo-proteases (*exempli gratia*, gluzincin). These proteins are tightly regulated and are responsible for lysing substrates for cellular and structural maintenance. However, when unregulated and mislocalized, proteolysis leads to the development of diseases including inflammation, emphysema and cancer.

There are four main clans of proteases, classed by structure, fold and function. These are the papain- and calpain-like proteases (CA), caspases and related proteases (CD), picornaviral and related proteases (PA) and carboxy- and related proteases as organized by Rawling and Barrett.²⁴ ²⁵ These enzymes typically have an active site nucleophile, such as a thiol or hydroxyl, and a basic residue that can function as an acid during catalysis. Importantly, cysteine proteases are stable to the acidic conditions found in abnormal cells and at the site of bone resorption.¹¹ The enzymes are usually recognized and denoted by their S₂, S₁ and S₁' binding sites according to the Schechter and Berger method, shown in Fig. [2.1.1].1.²⁶

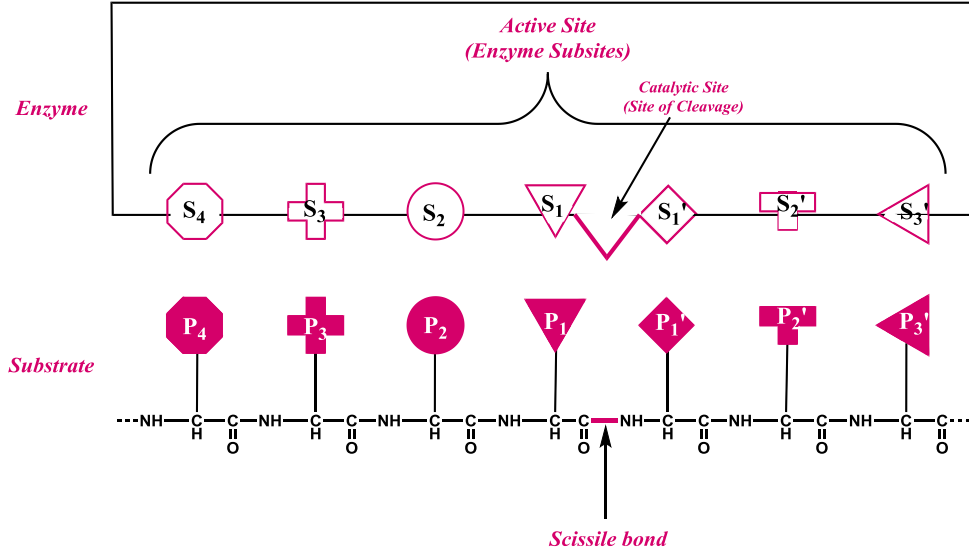


Figure [2.1.1].1 The enzyme subsites and the substrate residues, as named by the Schechter & Berger method. This description considers that the amino acid residues of the substrate (or inhibitor) bind to the corresponding active site.

2.1.2 CA PAPAIN-LIKE (CA) CYSTEINE PROTEASES

Cysteine proteases are enzymes found in various animals, plant and micro-organisms, typically sharing similar sequences and folds.²⁷ This family includes papain and similar plant proteases, cruzipain and similar parasite proteases, and lysosomal (mammalian) cathepsins. There are currently 13 described lysosomal cathepsins; 11 of which are sequentially-known and are expressed in a variety of cells within the lysosome, or extracellularly. These are CST-B, CST-C, CST-F, CST-H, CST-K, CST-L, CST-O, CST-S, CST-V, CST-W and CST-X. The sequentially-unknown two, have been identified as CST-N and CST-T.²⁸

Of the sequentially known cathepsins, CST-B and CST-L have the highest lysosomal concentration.²⁷ CST-V and S are tissue-specific. CST-V is found in the testis/thymus²⁷ and CST-S in lymphatic organs such as the lymph node and the spleen¹¹. In contrast, CST-F, L and X are widely spread.²⁷ Of the CA proteases, CST-L shows the highest proteolytic activity of the lysosomal proteases. Most of the enzymes are endopeptidases with the exception of CST-C which

is an oligomeric aminopeptidase. In addition to their main roles, CST- B and X can behave as carboxypeptidases and CST-H, as an aminopeptidase. Cysteine proteases also process important proteins outside of the lysosome (exempli gratia, thyroglobulin, a thyroid hormone source), and are important for other cellular processes like apoptosis (CST- B and C) and MHC^{‡‡} class II-mediated antigen presentation (CST- S and L).²⁷ Mislocalization of cysteine proteases can contribute to pathologies such as Alzheimer's disease, multiple sclerosis, muscular dystrophy, cancers and bone-related diseases. CST- B, H and L play a major role in cancer progression by directly degrading the extracellular matrix or by activating other important proteases.

In enzyme-inhibitor binding interactions, the S₂ and the S₁' enzyme binding sites contribute most to the selectivity and diversity of these enzymes.²⁷ Interaction of P₂, P₁ and P₁' inhibitor residues with the respective enzyme subsite involves the main- and side-chain atoms, whereas the interaction with P₃ involves only the side chain atoms. Structure characterization has revealed that S₄, S₃' and further binding sites are not present on the cysteine proteases, although P₄ and P₅ residues can interact with the enzyme. As such, the term “substrate binding site” usually refers to the S₂-S₂' region.

2.1.3 CATHEPSIN K

CST-K is an important cysteine protease, mainly found in lysosomes.¹¹ The recombinant CST-K enzyme was characterized in 1996, after CST- B, H and L. The human enzyme is 329 amino acids long with a 215 amino-acid-long catalytic unit, a 99 amino-acid-long propeptide unit and a 15 amino-acid-long N-terminal sequence, see Fig. [2.1.3].1 for the X-ray crystal structure. Inhibitors for this enzyme are rarely selective because the amino acid sequence is 60% identical to CST- L, S and V, and 35% identical to CST- B, F, H, O, and W.^{11, 27, 29} All cathepsins share a

^{‡‡} Major Histocompatibility Complex

common fold and have two domains: an N-terminal (left) and a C-terminal (right) with a V-shaped active site cleft located between S_1 and S_1' as in Fig. [2.1.1].1. The enzymes interact with their substrate at this special pocket called the active site that is decorated with amino acid residues and subsites as seen in Fig. [2.1.1].1.^{9, 25} The active site of CST- K is comprised of residues His159, Cys25 and Asn175. The lysis performed by the enzyme occurs at the catalytic site (V-shaped cleft) within the active site. The surrounding subsites are matt with amino acids as well. As an example, the S_2 subsite of the enzyme is defined by Tyr67, Met68, Ala133, Leu157, Ala160 and Leu205 according to papain residue numbering.

Cathepsin K is predominantly expressed in macrophages and osteoclasts.³⁰ In macrophages, it is 100-fold higher in concentration than CST- L and S. Once it diffuses across the cell membrane it is ionized and sequestered by lysosomes but is transported between endosomes, lysosomes and phagosomes.³ However, it can be secreted as an inactive glycosylated proenzyme precursors from osteoclasts, macrophages, fibroblasts and malignant cells and sequestered into the resorption lacuna in the extracellular environment.

CST-K contributes enormously to skeletal development. It is well-known that a deficiency in the enzyme may induce pycnodysostosis (abnormally dense bones) caused by a reduction in bone reabsorption.³⁰ The inhibition of CST-K causes undigested collagen fibrils to accumulate in lysosomes. CST-K performs regulated functions in physiological processes of normal cells, but is primarily concerned with collagenolytic and bone maintenance. This critical bone reabsorbing protease is responsible for the regulatory functions in bone resorption, and it degrades type I/II collagen, osteopontin and osteonectin (proteins that make up over 90% of bone). Following acid-induced demineralization of the bone, CST-K is secreted from the osteoblasts, causing proteolytic degradation of the organic framework, *id est*, the type 1 collagen fibers. As the activity of CST-K

is not regulated in abnormal cells, the imbalance and secretion is therefore associated with pathological conditions and the onset of various diseases not limited to rheumatoid arthritis, osteoporosis, atherosclerosis, inflammation, and cancer.³ It is the enhanced secretion of CST-K and therefore the enhanced degradation of the collagen matrix that causes osteoporosis.²⁵ CST-K is upregulated by osteoclastogenesis factor, RANKL^{§§}, and down-regulated by estrogen.

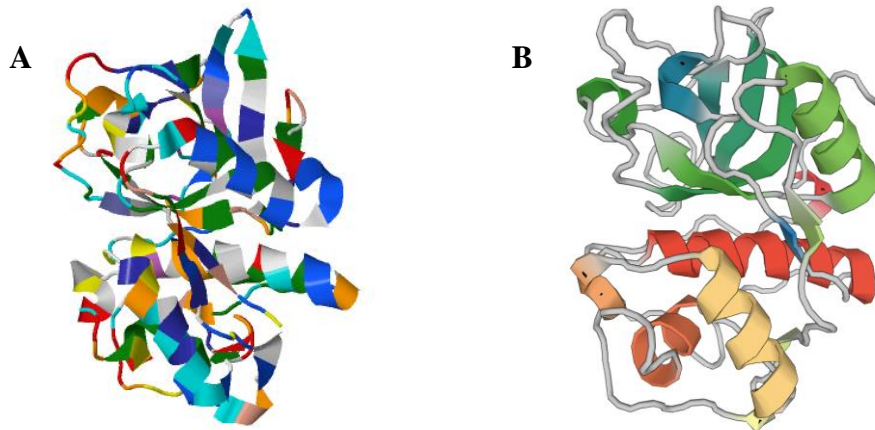


Figure [2.1.3].1 Crystal structure of Cathepsin K (A) by amino acid residue (JSmol-Javascript), (B) by secondary structure (PV-WebGL). Image from the RCSB PDB (www.rcsb.org) of PDB ID 5TUN (S. Law, P.M. Andrault, A. Aguda, N. Nguyen, N. Kruglyak, G. Brayer, D. Bromme (2017) Identification of mouse cathepsin K structural elements that regulate the potency of odanacatib *Biochem. J.* 474: 851-864).

^{§§} Receptor Activator of Nuclear Factor κ -B Ligand

2.2 INHIBITORS

The ideal cysteine protease inhibitor has a low molecular weight, minimal peptide character, high selectivity, high specificity, lipophilic character (to allow cell permeability) and reversible target-binding ability (to avoid antigenic and immunologic complications).¹¹ Additionally, inhibitors are most useful if they have good pharmacokinetic properties such as good oral bioavailability, high membrane permeability, low toxicity, slow elimination rate and align with Lipinski's rule of 5. Most importantly, inhibitors should be unreactive under physiological conditions, but selective and reactive enough to interact with the target. Selectivity of the cysteine protease inhibitors is one of the most important and difficult properties to design due to the high homology of the CA clan. Successful and selective inhibitors of CST-K are used to treat osteoporosis, osteoarthritis, as well as, metastatic bone diseases associated with breast, lung, thyroid and prostate cancers.

The peptide aldehydes, leupeptin and antipain (**5 & 6**; Fig [2.2.0].1), were the first synthetic cysteine protease inhibitors designed.¹¹ They are capable of inhibiting both serine and cysteine proteases. E64 and peptidyl diazomethanes (**7 & 8**; Fig [2.2.0].1) were synthesized shortly after, for the selective inhibition of CST- B, H and L. These were the only known cathepsins of the time. To date, there are several types of inhibitors classed according to their mechanism of interaction with the enzyme. Protease inhibitors can inhibit enzymes by alkylation, acylation, phosphorylation, sulfonylation, metalloid binding, hemiacetal formation, piner-type reaction, *et cetera*. (See Table [2.2.0].1) Due to the extracellular localization of CST-K in cancers and metatheses, non-lysosomotropic inhibitors may increase selectivity and limit the inhibition of intracellular CSTs.

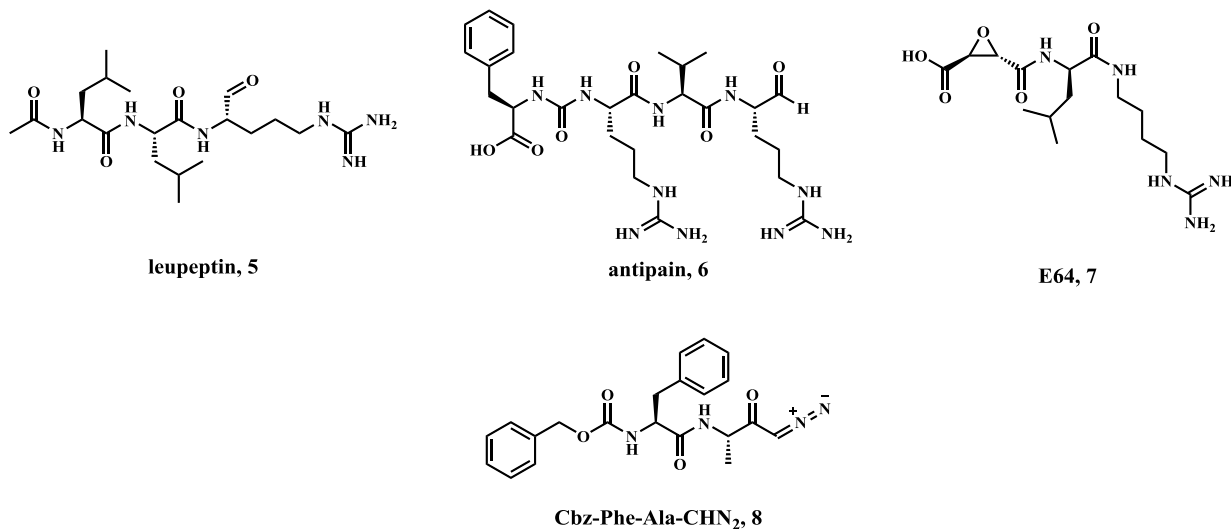


Figure [2.2.0].1 Four of the first inhibitors synthesized.

Alkylation	Acylation/ Imidation	Phosphonylation / Sulfonylation/ Other
Halomethyl Ketones	Aza-peptides	
Diazomethyl Ketones	Carbamates	
Acyloxymethyl Ketones	Peptidyl Acyl Hydroxamates	Peptide Phosphonates
Epoxides	α -Lactams	Phosphonyl Fluorides
☞ Epoxysuccinyl	Heterocyclic Inhibitors	Sulfonyl Fluorides
☞ R, α -Epoxyketone	☞ Isocoumarins	Metalloid binding
☞ R-Aminoalkyl Epoxide	☞ Benzoxazinones	
Aziridine Derivatives	☞ Saccharins	Hemiacetal formation
Vinyl Sulfones	Pinner-type	
Azodicarboxamides	☞ Cyanamides	
	☞ Aromatic nitriles	
	☞ Aminoacetonitriles	

Table [2.2.0].1 Major CA cysteine protease inhibitors, categorized by their mechanism of attack.

Of these inhibitors, irreversible covalent binders including epoxysuccinyl derivatives, ketones and vinyl sulfones are deemed impractical for many pharmacological applications but have been found especially useful in combating drug-resistant cell lines and diseases.³¹ Correspondingly, compounds that contain reactive functional groups may cause an acute or delayed toxic response by binding glutathione and/or DNA and must be well studied.³⁰ The inhibitors listed above are referred to as covalent modifiers because they inhibit the cysteine

proteases by forming an irreversible or reversible covalent bond. Alternative inhibitors do not possess an electrophilic warhead and are referred to as non-covalent modifiers.^{11, 32-34} The most common of these are arylaminoethylamides (**9**, Fig. [2.2.0].2) that were once probed by Novartis Pharma.

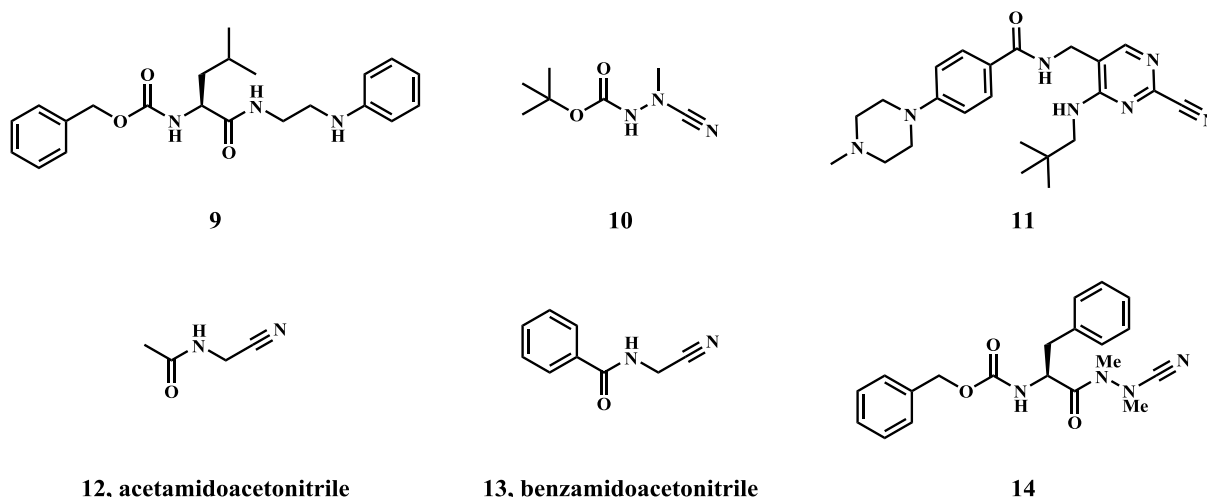


Figure [2.2.0].2 Pinner-type inhibitors, the first aminoacetonitrile inhibitors and an example of an azapeptide inhibitor.

Of significant interest to this thesis are Pinner-type inhibitors. The potency and selectivity of Pinner-type inhibitors are due to the nitrile warhead that covalently bind the substrate.³⁰ The authentic Pinner reaction is an acid-catalyzed reaction between a nitrile and an alcohol that proceeds to form an amidine or an ester. In contrast, the enzyme-inhibitor pinner-type reactions are reversible; they form a thioimidate adduct and dissociate to reform the nitrile and substrate. There are three major classes, each of which are structurally related: cyanamides, aryl-nitriles and aminoacetonitriles.^{30, 35} In cyanamides ($R_2N-C\equiv N$; *exempli gratia* **10**, Fig [2.2.0].2), the nitrile is connected to an N-heteroatom. The presence of the N-heteroatom increases the electrophilicity of the group due to the inductive effect, improving its CST-K activity, however, it is only moderately selective. In aromatic nitriles ($R_5Ph-C\equiv N$; *exempli gratia* **11**, Fig [2.2.0].2), the warhead is attached to an aromatic group. The electrophilicity of the warhead increases with increasingly electron

withdrawing substituents and heterocycles. In aminoacetonitriles ($R_2N-R_2C-C\equiv N$; *exempli gratia* **12** & **13**, Fig [2.2.0].2), the nitrile warhead is terminal to an amino group. These are typically potent and selective, although they have intermediate and lowest electrophilicity. Clinically developed odanacatib (**17**, Fig [2.2.0].2) is an example of this inhibitor type. The first nitrile compounds used for cysteine protease inhibition are acetamidoacetonitrile (**12**) and benzamidoacetonitrile (**13**) (Fig [2.2.0].2).⁹ Currently, dipeptide aminonitriles (as presented in this thesis) and azapeptides (**14**, Fig [2.2.0].2) are being competitively developed for CST-K inhibition. In azapeptides, the $C_{\alpha}H$ group of a peptide is replaced by an N-heteroatom. When this is done at P_1 , a more potent and stable inhibitor was observed in comparison to the carboanalogue.³⁶ Increasing electrophilicity and reactivity of the nitrile, can produce irreversible covalent binding to cysteine proteases.³⁵ Naturally occurring CST-K inhibitors include proteins of the cystatin, stefin, kininogen, thyropan, serpin families and α_2 -macroglobulin.³

To date, three of the most promising CST-K inhibiting drugs were Balicatib (**15**), Relcatib (**16**) and Odanacatib (**17**), see Fig. [2.2.1].3.¹¹ Balicatib (AAE-581) is a highly potent, basic peptidic nitrile having an IC_{50} of 1.4 nM with, however, low selectivity in cell based assays.^{2, 11} In 2006, the testing of the drug was discontinued by its developer, Novartis, during phase II clinical trials when rare dermatological side effects, including lesions, pruritus, skin-thickening and other phenotypes were observed.^{8, 37} Relcatib (SB-462795) is a monobasic, extremely potent, azepanone analogue developed by GlaxoSmithKlein having a K_{iapp} of 41 pM and an oral bioavailability of 89% among other suitable pharmacokinetic characteristic.^{2, 11} Clinical trials toward the approval of this drug were however discontinued in 2007, possibly as a result of its low selectivity, high lysosomal accumulation and off-target selectivity.^{8, 37} Until 2016, Odanacatib (MK-0822) showed promise and quickly approached approval.⁸ It is a non-basic, non-

lysosomotropic, nitrile based inhibitor, with a high potency and selectivity for CST- K with an IC_{50} of 0.2 nM. Its selectivity was owed to the 4-fluoroleucine side chain at P₂.¹¹ It also showed great pharmacokinetic parameters such as long half-life, slow elimination and metabolism. However, after 12 years of clinical development, Merck & Co. were forced to discontinue development due to an increased risk of cardiovascular events to clinical patients.³⁷

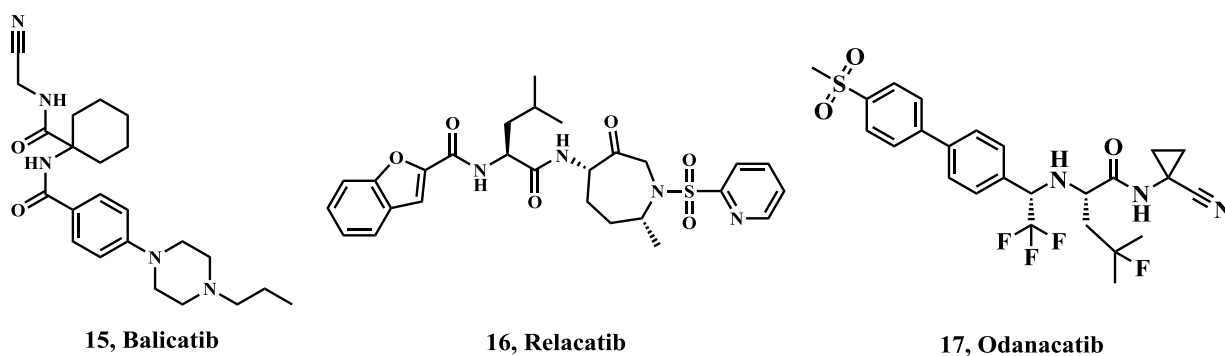


Figure [2.2.0].3 Three clinically developed CST-K inhibitors.

This thesis is based on the use of nitriles inhibitors, because they are both selective for the CA cysteine protease clan, as well as, within the clan depending on the structure of the inhibitor.²⁵ Once the inhibitor locks into the active site cleft where it is stabilized by a number of amino acid residues, it is attacked by the thiol catalytic site, see [Fig. 2.2.0].4. Nitrile inhibitors have a higher inhibitory activity toward cysteine proteases versus serine proteases. This observation is supported by a number of theories. Firstly, the Hard-Soft Acid-Base (HSAB) theory, presumes that the soft cyano ($C\equiv N$) electrophile binds much more tightly to the soft sulphur (S) nucleophile than the hard oxygen (O) nucleophile. Secondly, the peptide nitriles reversibly bind the thiol of the cathepsin via a covalent thioimidate linkage (**18**, Fig [2.2.0].5).^{25, 30} When the nucleophilic thiol attacks the sp carbon of the $C\equiv N$, a trigonal planar thioimidate is formed. As a result, the trigonal planar intermediate is less prone to hydrolysis; it resembles the acyl enzyme rather than the hydrolysis-prone tetrahedral intermediate of the sp^2 carbonyls. Thirdly, the transition state of the nitrile

interaction is less constrained in comparison to the serine-nitrile transition state due to the large atomic radius of the S-heteroatom. As such, it is more likely for the adduct to revert than for hydrolysis to take place. This is in contrast to serine proteases: the small size of the oxygen atom may influence the reaction to proceed irreversibly to the competing hydrolysis of the substrate molecule (see **19**, Fig [2.2.0].5). In addition, the intermediate due to nitrile inhibition does not require hydrogen bond stabilization since there is not an oxyanion hole formed as with carbonyl inhibition.³⁸

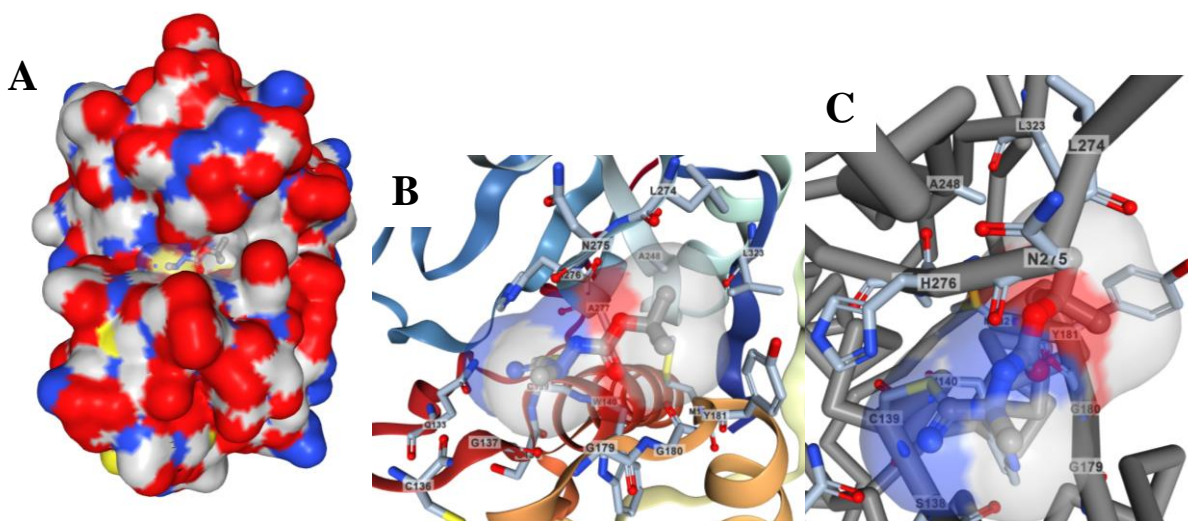


Figure [2.2.0].4 X-ray co-crystal structure of inhibitor **10** lodged into the active site cleft of CST-K and bound by Cys139. (A) show the surface structure; (B) shows a magnified frontal view of the active site; (C) shows the Cys139-S-C=N-R reversible bond via a magnified side view. Image from the RCSB PDB (www.rcsb.org) of PDB ID 1YK8 (D. G. Barretta, D. N. Deaton, A. M. Hassell, R. B. McFadyen, A. B. Miller, L. R. Miller, J. A. Payne, L. M. Shewchuk, D. H. Willard Jr., L. L. Wright (2005) Acyclic cyanamide-based inhibitors of cathepsin K *Bioorg. Med. Chem. Lett.* 15: 3039-3043).

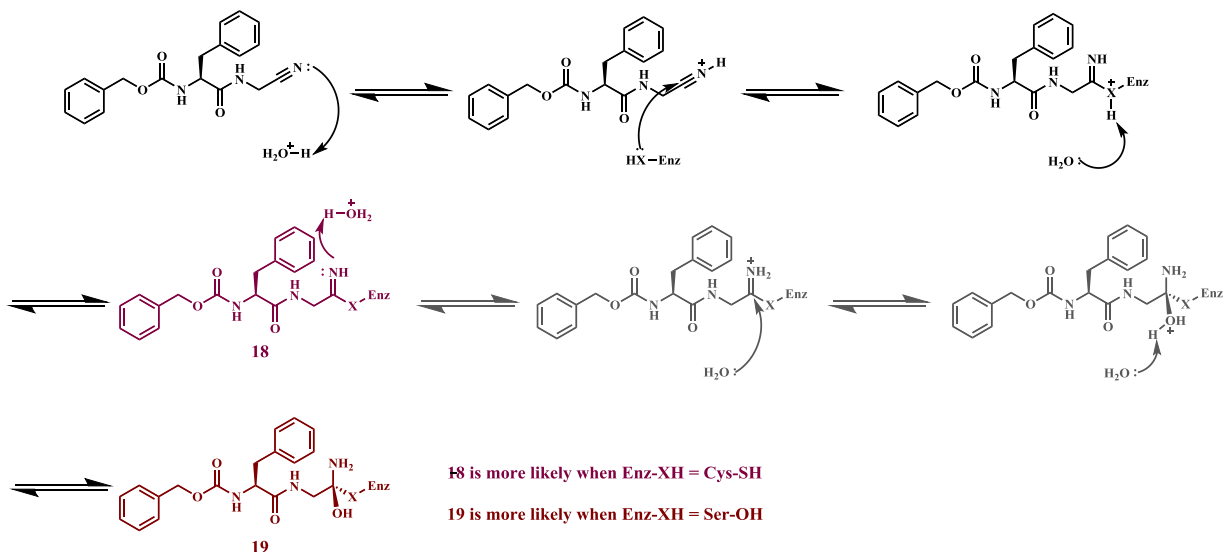


Figure [2.2.0].5 Proposed mechanism for cysteine inhibition versus serine inhibition.

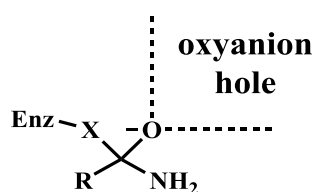


Figure [2.2.0].6 Depiction of the intermediate oxyanion hole that results from enzyme-carbonyl interactions.

Other structural implications of the dipeptide inhibitor play a large role as well. A study by Löser *et alia* show that the P₂ residue produces a different IC₅₀ for cathepsins K, L and S in accordance with the nature of the substituent: aliphatic/aromatic, bulky/compact, short/long, *et cetera*.²⁵ The authors noted the particular importance of the P₂ residue in comparison to other residues (P₁ and P₃). With reference to cathepsin K, the leucinyl substituent at P₂ had the highest binding affinity for subsite S₂. The phenylalanyl substituent also displayed favorable binding and inhibitory activity. Table [2.2.0].1 shows that there is a specific length and bulk requirement for high binding affinity to S₂. The IC₅₀ also increased with aromatic bulk on the N-terminal group (P₃); enhanced inhibitory activity was observed when carboxybenzyl (Cbz) substituent was used at P₃ rather than the *tert*-butyloxycarbonyl (Boc) substituent. The hydrogen bonding (HB) donation from the N-H amide bond was shown to play a significant role in adduct stabilization; upon

methylation of the amide N-heteroatom (N-Me), the affinity of the inhibitor for cells expressing CST-K decreased by 3 orders of magnitude. Studies also show that the high cooperativity between covalent and non-covalent interactions of the inhibitors and protease play a significant role, though time independent inhibition was observed. Substrate specificity of CST-K is such that leucine is favored over phenylalanine at P₂. Cathepsin K inhibition with a basic P₃ substituent was shown to increase the enzyme selectivity as well as the lysosomal concentration. This increase in lysosomal concentration can contribute to an increase in anti-target potency, and can reduce selectivity over time.³⁰

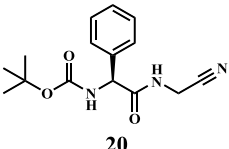
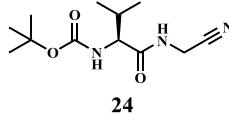
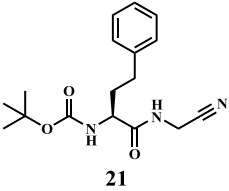
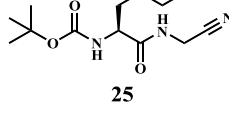
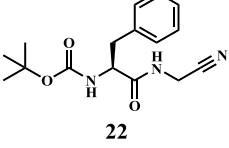
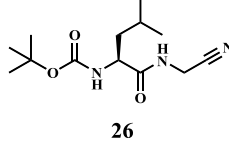
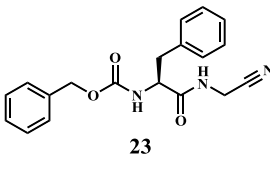
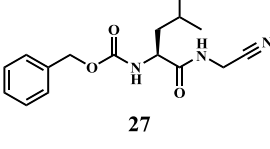
Inhibitor	K _i (mM) human CST-K	Inhibitor	K _i (mM) human CST-K
	90 ± 7		6.5 ± 0.4
	8.5 ± 3		1.1 ± 0.1
	4.1 ± 0.2		0.12 ± 0.01
	0.26 ± 0.01		0.035 ± 0.001

Table [2.2.0].2 Comparison of the inhibition constants of dipeptide inhibitors by the length and bulk of P₂ binding site.

2.3 PHOTO-CAGING: METAL-BASED ALTERNATIVES

2.3.1 ORGANIC CHROMOPHORES

The studies regarding organic-based chromophores and fluorophores far out-number the investigation of the metal-based systems, and are continuously being developed as alternatives to metals in renewable energy and medicine.³⁹⁻⁴¹ Like metal-based chromophores, organic chromophores are used to enable controlled, light-assisted protein inactivation or other cellular functions. Of the most promising and grandfathered approaches are CALI and FALI, *id est*, Chromophore/ Fluorophore-assisted light inactivation.⁴²⁻⁴⁶ This method has primarily been used to elucidate biological structure and function; it is useful in high-throughput applications because of its characteristic efficiency.

For protein inhibition, an antibody labeled with malachite green dye is allowed to bind the target protein followed by irradiation with laser light of suitable energy that excites the chromophore.³⁹ Coupling the dye to a protein-specific antibody leads to generation of singlet oxygen ($^1\text{O}_2$). This causes irreversible damage to the bound protein, disturbing its normal function and the function of proteins in its immediate vicinity. The inactivation is restricted to the protein bound by the antibody. This method has been adapted for many different proteins including membrane receptors, signal transduction molecules as well as transcription factors.

Commonly, the fluorophore fluorescein (**28**, Fig. [2.3.1].1) has been used for protein labeling. It is water soluble, stable at and above pH 7 and is commercially available as an isothiocyanate derivative.³⁹ The absorbance of fluorescein, over the UV-vis range, increases linearly with the dye concentration. Binding fluorescein to an antibody in an air-saturated solution slightly increases the triplet lifetime. This is in contrast to the decrease in the triplet lifetime observed when the solution is anaerobic. Collision with oxygen will potentially quench the

chromophore since its photochemical (ground, singlet, triplet state) properties do not change upon coupling. As such, binding an antibody to the chromophore (spatial shielding) protects the photo-efficiency by preventing collision with oxygen. However, this method is prone to light-induced protein inactivation, depending on the irradiation energy, enzyme, fluorophore concentration, oxygen quenching, *et cetera*. Photo-bleaching is also an undesired side reaction that is independent of protein inactivation.

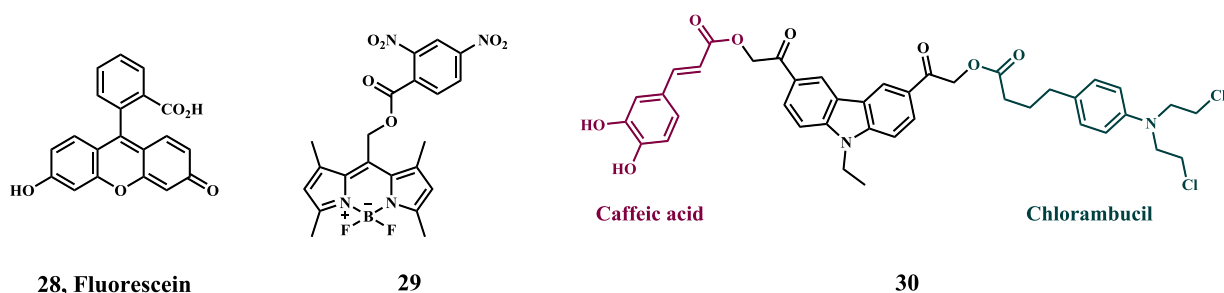


Fig [2.3.1].1 Organic photo-activatable molecules described in this section.

Organic fluorophores have also been used as drug chaperones or photo-responsive drug delivery systems (PDDSs), affording spatio-temporal control over biological activity or inhibition. A wide range of organic groups are useful for application as PDDSs⁴⁷⁻⁴⁸, these include but are not limited to *o*-nitrobenzyl¹⁵, acridin-9-ylmethyl⁴⁹, acetylpyrene⁵⁰, hydroxyquinoline⁵¹, hydroxynaphthyl⁵² and coumarinyl^{19, 53} derivatives.

Boron-dipyrromethene- (BODIPY-) derived photo-caging groups (**29**, Fig. [2.3.1].1), have been proposed as an alternative to popular *o*-nitrobenzyl photo-caging systems resulting from their superior optical properties, ease of synthesis and biocompatibility.⁵⁴ Goswami *et alia* reported successful photo-release of a carboxylic acid from the organic chaperone using visible light. The authors also observed an increase in fluorescence (green light excitation) upon release; this likely results from the carboxylic acid quenching the fluorescence while attached.

Of late, a hybridized strategy is the use of dual PDDSs that allow simultaneous photo-release of different therapeutics. Venkatesh *et alia* have probed the acetyl carbazole group for this application with carboxylic acid and aminoacids.⁵⁵ Carbazoles are deemed useful due to their wide band gaps, luminescence efficiency and flexible functionalization making them potential fluorescent PDDSs. Acetyl carbazole (**30**, Fig. [2.3.1].1) was reported as both a fluorescent imaging agent as well as a potential PDDS. Caffeic acid (anti-tumor, anti-metastatic agent) and chloroambucil (methylating agent in leukemia) are the photo-releasable drugs used (see **30**, Fig [2.3.1].1). Synergistic effects are also reported. With irradiation of the organic compound for 60 minutes with UV light (365 nm), 91 and 94% of the drugs were released with quantum yields of 0.046 and 0.051, respectively. Photo-decomposition of the free carbazole after 60 minutes of irradiation is however, a drawback. The authors also reported biocompatibility and cellular uptake activity using confocal microscopy studies on glial cancer cells U87MG, as well as high to low cell viability before and after irradiation.

While organic-CALI provides the generation of a chimera of molecules that can selectively bind and inhibit target proteins, polypyridyl-[Ru^{II}]-CALI is superior.²³ Both the organic- and [Ru^{II}]-based systems are highly efficient. These chemical reagents allow biological scientists to carry out time-resolved studies on cellular dynamics. Organic chromophores are sensitive to self-bleaching and are often cell impermeable. They also lack high affinity and selectivity for the proteins of interest. [Ru^{II}]-CALI chromophores have surpassed organic chromophores as they are more resistant to photo- and self-bleaching (stable to singlet oxygen), are cell permeable and can quantitatively inactivate selected proteins. They also have a longer triplet state lifetime, a higher turnover of singlet oxygen, high affinity to synthetic binding proteins due to photo-physical and photo-chemical properties.

2.3.2 NANOPARTICLES

Lanthanide-doped up-converting nanoparticles (LD-UCNP) are of growing interest to the field of spatio-temporal controlled therapy.¹⁶ The most prominent feature of these systems is the anti-stokes property. This involves the vibrational excitation of a photon to a higher rather than lower energy level (up-conversion) and results from the photo-physical property of the lanthanide atom used. This is a property that renewable energy and data storage scientist have used for decades and is now being probed for use in biological systems. LD-UCNP are known for their high photostability, deep tissue penetration and activation with low energy near-infrared light (NIR) which makes them even more attractive for use in bio-imaging with a diverse number of functional groups.⁵⁶

Li *et alia* have suggested the use of LD-UCNP in the study of biological processes, regenerative medicine and cell isolation therapy.⁵⁷ The researchers presented a strategy for non-invasive, spatio-temporal controlled therapy through the regulation of cell-material interactions: photo-controlled cell adhesion. Prior to irradiation the cells were immobilized to TmYb-doped, silica-coated, NaYF₄ nanoparticles using a photo-cleavable molecule, a polyethyleneglycol spacer and a bio-adhesive ligand. The up-converting property becomes necessary because ultraviolet (UV) light is needed to activate the controlled photo-release of adhesion cells. As such, NIR of 980 nm irradiates the LD-UCNP that converts it to UV light. The UV light is absorbed by photolabile linkers that activate the photo-cleavage reaction and this changes the cell binding state of the surface, causing adhesive cells to dissociate. In contrast, the use of intense UV light limits tissue penetration and results in cellular and DNA damage. This strategy has the advantage of causing little cell damage and extraordinary tissue penetration. The rate and the amount of cells

released is also variable depending on the time of exposure to light and the power intensity of the light used.

LD-UCNP are also being developed for use with the uncaging of photo-labile compounds and bioluminescence imaging studies.⁵⁶ Yang *et alia* report the use of the same UCNP listed above for the enhancement of bio-imaging protocols. In this study, a D-luciferin-conjugated LD-UCNP (**31**, Fig. [2.3.2].1) is activated by NIR irradiation, it then converts the energy to UV irradiation which triggers the release of the D-luciferin which enhances the fluorescence and bioluminescence signals in vitro and in vivo with light penetration of up to 10 mm of tissue. This procedure allows non-invasive monitoring of dynamic biological systems.

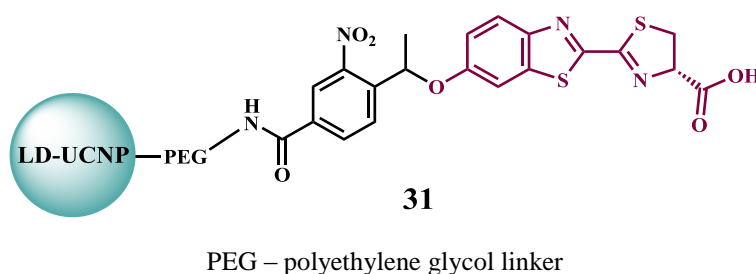


Figure [2.3.2].1 The D-luciferin conjugated LD-UCNP described above.

2.3.3 OTHER ALTERNATIVES

Other methods to improve the bio-imaging and photolysis protocols include multiphoton photolysis^{20, 58-60}, uncaging of biological stimuli from nanocapsules⁶¹ and photo-induced electron transfer⁶².

Multiphoton excitation

The most common type of multiphoton photolysis used is two-photon photolysis; a process through which a photo-activated system simultaneously absorbs two photons of pulsed, low-energy, visible, NIR or (far-infrared) FIR light using sufficiently intense laser illumination.⁶³ The

excitation produces results equivalent to that of single-photon excitation; however, the two are quantum-mechanically different. Single-photon excitation is linear, whereas multiphoton excitation is quadratic, *id est*, the fluorescence emission increases quadratically with excitation intensity.⁶⁴ Contrary to the popular notion, single and two photon excitation produce equivalent results when the sum of the energies of the two photon excitation is greater than the energy gap between the ground and excited state. (Fig [2.3.3].1)⁶³

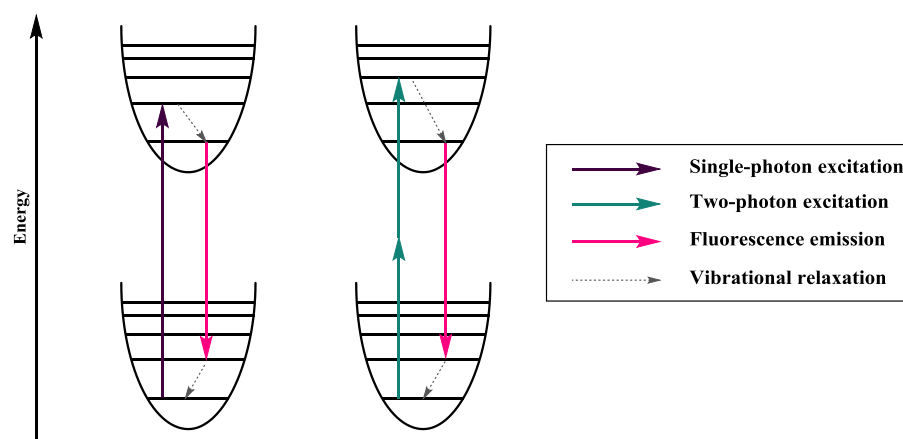


Fig [2.3.3].1 Jablonski diagram for single- and two-photon absorption.

The two-photon excitation process benefits from depth discrimination and enhanced 3D resolution, for tissue penetration and imaging.⁶⁴ With the new method, a wider range of fluorophores are now available with limited cellular damage, but the probes must have long wavelength absorption properties. Although two-photon excitation minimizes photo-bleaching and photo-damage, cells and biological systems still experience these effects.⁶³ Two-photon damage may be caused by the production of reactive oxygen species (ROS), thermal damage from high power infrared irradiation, as well as dielectric breakdown of proteins from the intense electromagnetic field of the femtosecond laser. Two-photon excitation processes also have lower conversion efficiencies due to the narrow absorption cross-section and require a more elaborate

experiment set-up. The chemical probes used are required to have a high two-photon cross-sections in reference to fluorescein.¹⁸ Brown *et alia* have reported the use of two photon excitation to photocleave chelates and calcium dyes thus giving researchers an opportunity to determine the role of Ca^{2+} in cellular regulation and second messenger signaling using pulsed 700 nm light from a 7 mW powered laser.⁵⁸

Chromophore-gated vesicles

Another attractive platform involves the use of lipid, polymer or silica vesicles to cage an array of biologically active compounds, from small neutral and charged molecules to large proteins, peptides and DNA (Fig [2.3.3].2).⁶¹ It avoids dark hydrolysis which usually causes background activity, displays high photolytic efficiency and fast uncaging times. Their photolysis wavelengths can be tuned by doping the nano-capsule shell with highly absorptive chromophores such as 3,3'-dioctadecyloxycarbocyanine perchlorate (DiO C₁₈). The biomolecules are caged in the vesicle by extrusion in phosphate-buffered saline containing 0.5–1 mM of the cageable biomolecule, and occasionally with freeze-thaw cycles to increase capsulation efficiency. When activating the vesicles *in vivo*, they can be visualized with a wavelength of light different to that used for photolysis. Dendramis *et alia* were able to tune vesicles for uncaging in the FIR.⁶¹

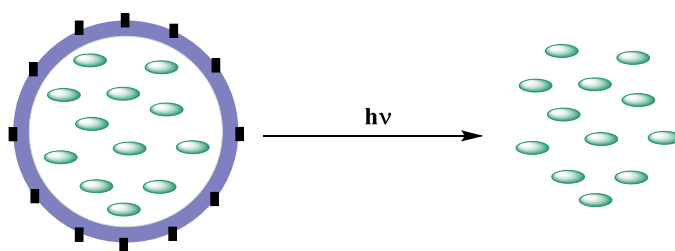


Fig [2.3.3].2 Illustration of the photo-release of biomolecule such as carbachol from a chromophore-doped lipid vesicle.

Electron-controlled ligand release

Another method by which biological scientists can gain spatio-temporal control is via biomolecule-release mediated by photo-induced electron transfer.⁶² It involves the design of systems such that caging groups are removed by electron transfer rather than by direct photolysis, *id est*, the bond-breaking step is independent of the light absorption step. This allows for even greater control over the wavelength of light used in the release process. Mechanistically, a sensitizer molecule and a quencher molecule are used. After the sensitizer is photolyzed, it encounters the quencher while in its excited state. An electron is then transferred from the sensitizer to the quencher creating a radical pair that partitions between ^(a) returning to the ground state and ^(b) proceeding toward the desired products. The reactions are generally of four types: sensitized reductive cleavage, direct reductive cleavage, sensitized oxidative cleavage and direct oxidative mechanism. An example of this was reported using phenacyl esters via the sensitized reductive cleavage by Banerjee and Falvey;^{62, 65} N-dimethylaniline as the sensitizer and phenacyl ester as the quencher to produce a carboxylic acid, see Fig. [2.3.3].3.

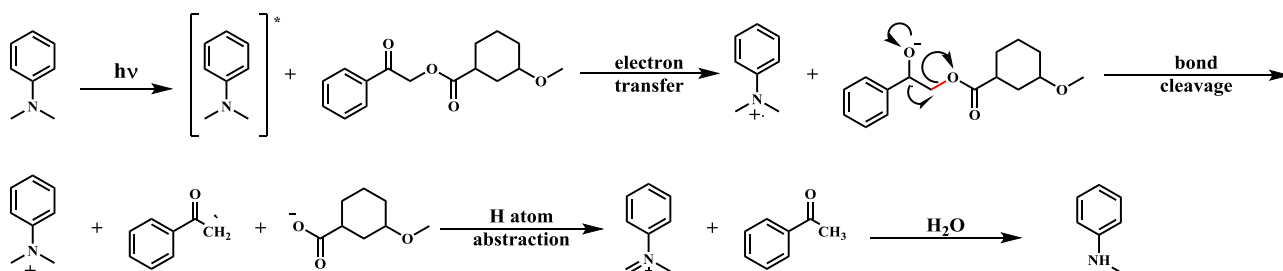


Figure [2.3.3].3 An example of sensitized reductive cleavage of an organic carboxylic acid.

2.4 PHOTO-CAGING: METAL-BASED

2.4.1 ABOUT METAL-BASED PACT & PDT

Ru^{II} complexes are being developed extensively for use in renewable energy production and medicine. The use of Ru^{II} -complexes ($[\text{Ru}^{\text{II}}]$) in renewable energy includes the design of photo-sensitizers and catalysts for high power output⁶⁶ and for carbon dioxide reduction⁶⁷. In medicine, they are used as chemotherapeutics,⁶⁸ and are being developed as photodynamic therapy (PDT) agents⁶⁹ and photo-activated chemotherapeutics (PACT)⁷⁰⁻⁷². The interest in metal-based therapeutics increased shortly after 1978,⁷³⁻⁷⁴ when cisplatin became the first metal-based anticancer therapy approved by the USFDA.⁷⁵ Interest in $[\text{Ru}^{\text{II}}]$ in particular, began with investigations into transition metal.

Though it is not my focus, it is important to mention the alternative to photo-activatable chemotherapy, PDT. PDT is continually being developed for use in cancer therapy, dermatology and infections.⁷⁶⁻⁷⁷ Like PACT, it involves the excitation of a metal complex or an organic molecule to the singlet excited state, after a photon of the appropriate energy is supplied. The molecule can then return to ground state by radiative (fluorescent) or non-radiative (thermal) decay. However, in an efficient photosensitizer the electron spin will rearrange to create a long-lived triplet excited state. This is referred to as intersystem crossing. Upon decay from the triplet excited state, the released energy can excite $^1\text{O}_2$ to $^3\text{O}_2$ (Fig [2.4.1].1). $^3\text{O}_2$ will then be able to react with other important molecules and proteins to trigger cell death. This is the main PDT mechanism for biological damage, but the reliance on oxygen prevents its use in hypoxic microenvironments. PDT agents are also prone to photo-bleaching, poor solubility and poor tissue retention. Other methods of PDT include photo-initiated DNA binding.²¹ By this method, metal complexes bind DNA after the photo-initiated release of a ligand. This strategy can be used in hypoxic environments.

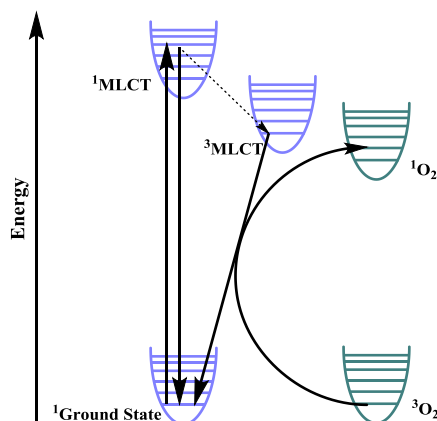


Figure [2.4.1].1 The essential electronic mechanism for the excitation of the $^1\text{O}_2$ species to $^3\text{O}_2$ in PDT.

Development concerning $[\text{Ru}^{\text{II}}]$ in PACT requires a solid understanding of its electronic dynamics. $[\text{Ru}^{\text{II}}]$ are characterized by strong absorption throughout the UV-vis region, long excited state lifetimes and chemical stability in solution. Added to these, $[\text{Ru}^{\text{II}}]$ are highly reactive once photo-excited but are generally inert at the ground state. When a photon is absorbed by a $[\text{Ru}^{\text{II}}]$, an electron is excited from the ground state to a region of higher energy, $^1\text{MLCT}$. Intersystem crossing then occurs as the electron is transferred to the $^3\text{MLCT}$. The MLCT can decay, *id est*, return to ground state, via a radiative and non-radiative process or may populate thermally accessible ^3LF states (Fig [2.4.1].2). Ligand dissociation is completely dependent on the population of this ^3LF state.

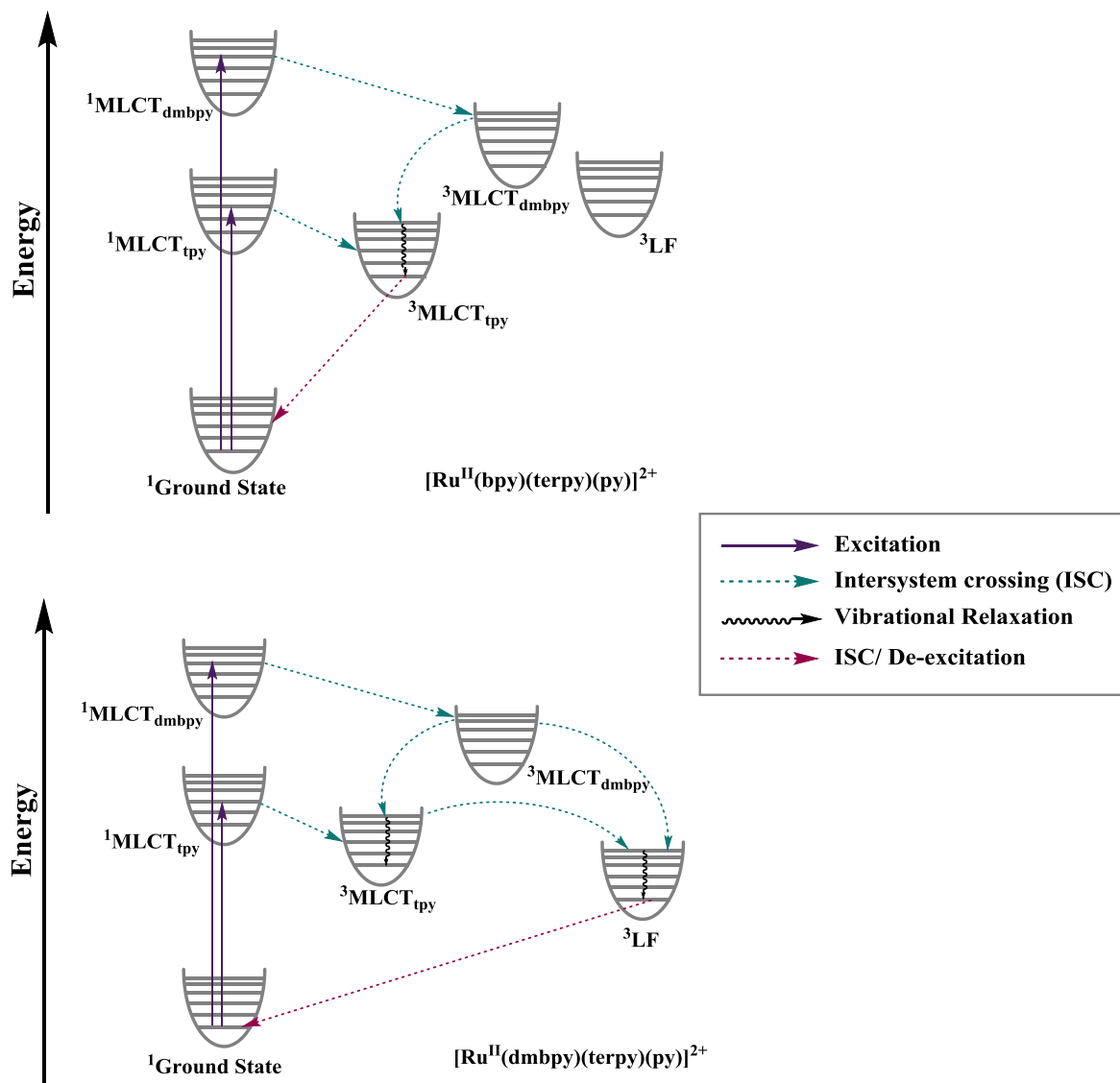


Figure [2.4.1].2 The electronic mechanism and energetic arrangements of the excited states that contribute to depopulation/population of the ^3LF , influencing ligand dissociation.

The investigation presented in this thesis is a product of this *tried, true and refined* property. Our work is in collaboration with the Turro group at Ohio State University.^{5, 78-79} The Turro group has tuned the ^3LF state of the $[\text{Ru}^{\text{II}}]$ such that bound cyano and pyridyl ligands would easily dissociate from the $[\text{Ru}^{\text{II}}]$ once irradiated. In the most recently tuned $[\text{Ru}^{\text{II}}]$, an ancillary tridentate ligand, 2,2':6',2''-terpyridine (terpy), has been used, accompanied by a bidentate ligand, 2,2'-bipyridine (bpy). The presence of the terpy ligand helps to distort the octahedral bond angles

from the expected 90 and 180 degrees slightly, though most of the octahedral distortion is due to the steric bulk of the bidentate ligand used, see Fig [2.4.1].3. Increasing the steric bulk on the bpy ligand was found to increase the propensity of 3LF to be populated and therefore the lability of the axial, monodentate ligand in low energy light. These researchers observed an increase of the quantum yield for pyridine dissociation when 6,6'-dimethyl-2,2'-bipyridine (dmbpy) was used in place of bpy on the $[Ru^{II}]$. These complexes were stable in the dark.

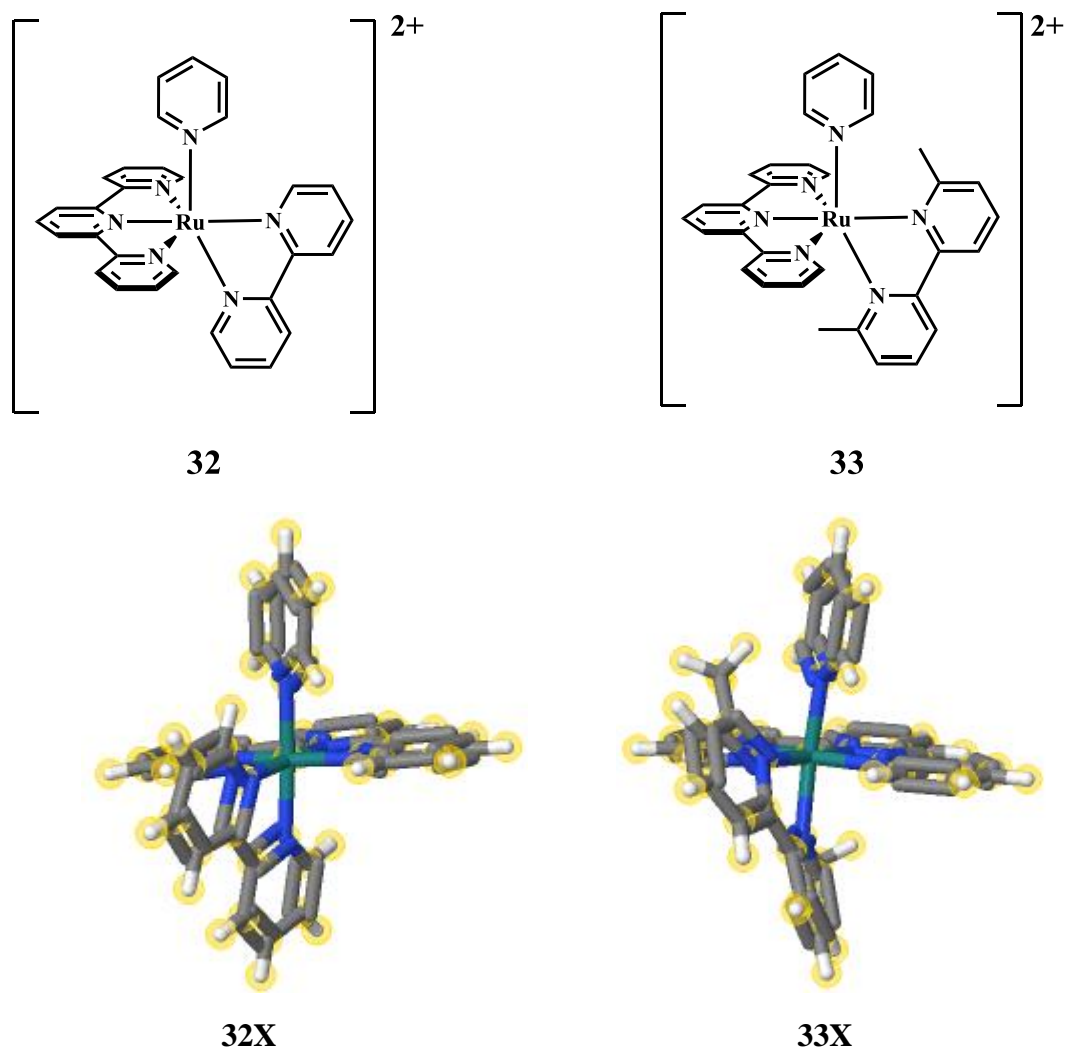


Figure [2.4.1].3 Structural geometry of **32** & **33** via X-ray crystal structures, **32X** & **33X**. Image **32X** from the Cambridge Structural Database. CSD-JIMJUK C. R. Hecker, P. E. Fanwick, D. R. McMillin, *Inorganic Chemistry*, 1991, 30, 659. DOI: 10.1021/ic00004a013. Image **33X** from the Cambridge Structural Database. CSD-ABAHUJ J. D. Knoll, B. A. Albani, C. B. Durr, C. Turro, *Journal of Physical Chemistry A*, 2014, 118, 10603. DOI: 10.1021/jp5057732.

Increasing the steric bulk of the bidentate ligand, distorts the pseudo octahedral geometry of the complex even further and significantly tilts the active ligand. A 15 degree decrease in the dihedral angle of the dmbpy is observed in comparison to the analogous bpy complex. Consequently, the [Ru^{II}]-pyridine overlap decreases, the Ru^{II}-py bond is weakened and the pyridine dissociation occurs more rapidly. Essentially, the energy of the ³LF state is lowered and

is more easily populated; the σ and π donation from pyridine is worsened and bond dissociation is activated by photons. The energy of the lowest MLCT is not significantly changed because it is unreactive toward substitution.

2.4.2 PREVIOUS WORK DONE BY THE KODANKO GROUP

An ideal chaperone is cleanly removable but has a high binding affinity to its substrate.⁶² It is stable prior to irradiation but removable with wavelengths of light that are not absorbed by other components in its vicinity. It also has a high quantum yield for dissociation.

In organic chaperones it is difficult to satisfy all of the above features. Theoretically speaking, once an inhibitor and a chaperone⁸⁰ have been fine-tuned for inhibitory activity and favorable dissociation, spatio-temporal control over protein inhibition can be gained by coupling the two.⁷⁹ Photo-activated compounds are constantly being developed due to their potential to act as localized, specific, selective, time-gated therapeutics. This strategy has become essential in *in vitro* and *in vivo* research applications and is being developed for clinical use.

$[\text{Ru}^{\text{II}}(\text{bpy})_2]^{2+}$ is one of the most commonly used chaperones today. Prior to the developments to be discussed in this thesis, senior authors of the Kodanko lab presented $[\text{Ru}^{\text{II}}(\text{bpy})_2]^{2+}$ as a chaperone for cysteine protease inhibitors.^{5, 79, 81} When $[\text{Ru}^{\text{II}}(\text{bpy})_2]^{2+}$ is used, two molecules of the monodentate inhibitors are bound to the metal center. The chaperone therefore has dual-release capacity.⁵

In 2014, CST-K activity in osteoclast cells was targeted in an effort to spatially control apoptosis, inflammation and cell signaling.⁷⁹ The developed complex (**34** & **35**) were bound to the Ru^{II} metal center via a dative bond to the nitrile ($\text{Ru}^{\text{II}} \leftarrow \text{N} \equiv \text{CR}$) and had lower quantum yields than the parent acetonitrile complex, **36**, much like the CST-B complex described below. **34** & **35**

showed rapid and efficient dissociation of the first molecule, but inefficient dissociation of the second identical ligand. The decreased efficiency for the release of the second inhibitor is a result of ^(a)steric bulk around the complex preventing aquation, ^(b)the polarity and ^(c)larger size of the monodentate inhibitor compound. In spite of this, the authors observed spatial and temporal control over inhibition; the uncaged inhibitor and the irradiated complex inhibited the enzyme to the same degree and the compound showed neither toxicity or growth inhibitory effects of BMM or PC-3 cells by MTT assays.

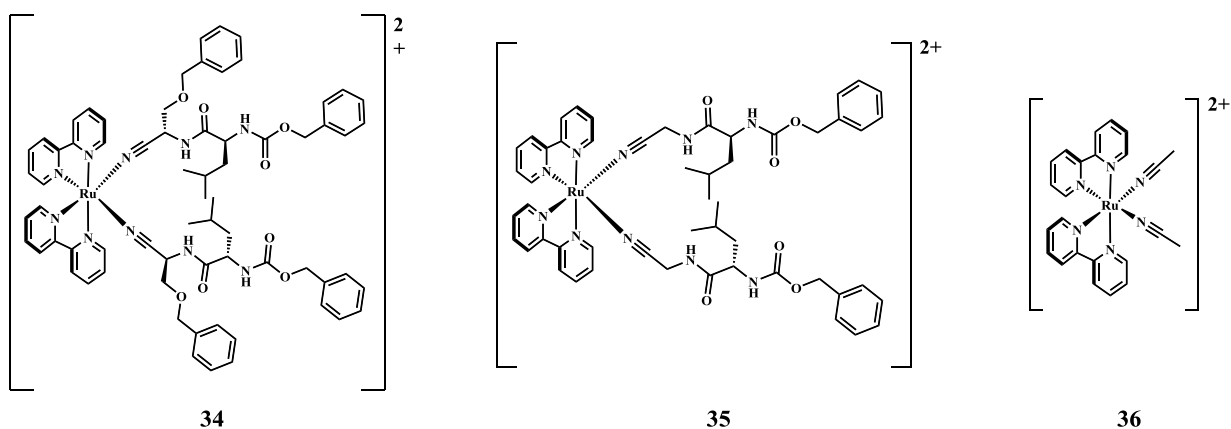
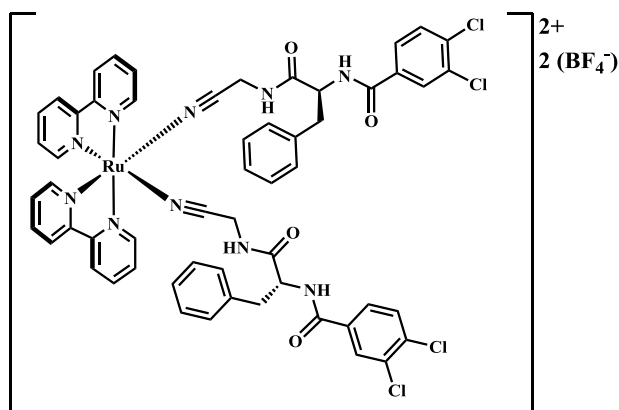


Figure [2.4.2].1 The first generation nitrile-bound inhibitors synthesized and investigated by the Kodanko group.

In a related study, a similar complex (**37**) was synthesized for the inhibition of CST-B. CST-B is one of the most abundant proteases, overexpressed in human breast cancer. Upon irradiation with 395 nm visible light, the protease inhibitors were released *in vitro*.



37

Figure [2.4.2].2 The second generation nitrile bound $[\text{Ru}^{\text{II}}\text{-inhibitor}]$ synthesized and investigated by the Kodanko group.

The reported IC_{50} values were determined using the CST-B enzyme assay protocol.⁵ The potency of the free inhibitor was similar to that of the caged inhibitor showing that inhibition was prohibited once the inhibitor was caged to the chaperone fragment. The DLIR of the $[\text{Ru}^{\text{II}}\text{-inhibitor}]$ complex was found to be 12 via a CST-B enzyme assay. The inhibitory activity of the complex increased once irradiated providing further evidence that the dissociation of the inhibitor molecules is light controlled. Given that two inhibitor molecules were attached to the chaperone, the IC_{50} value was expected to be at least half that of the free inhibitor. However, dual release was restricted as a result of the low dissociation efficiency of the second caged inhibitor. The inhibitor was also shown to be selective for cathepsin B using *in vitro* assays. In the triple negative breast cancer cell line MDA-MB-231, the DLIR increased to 79.6; but did not change for Hs578T breast cancer cell line. This is likely due to differences in protein complexation within each cell line. The live cell proteolysis assay demonstrated that the irradiated complex was more potent than the free inhibitor and could be used at lower concentrations. When $1 \mu\text{M}$ of the compound (**37**) was photo-activated in a 3D MAME culture, the degradation of DQ-collagen IV (green fluorescence) was significantly reduced. However, at higher concentrations significant inhibition was observed in the

dark. This may be due to the release of inhibitor over the 4-day timescale of the experiment. The complexes were not found to be toxic.

As we continued to develop photo-activatable inhibitors for CST-K⁸², we observed that the stability of complexes in growth media was compromised when a Ru^{II}-N≡CR bond was present in comparison to a Ru^{II}-pyridyl bond (Li, A.; Kodanko, J. Unpublished results). As such we investigated pyridyl containing CST inhibitors and derivatives.

Our first publication displaying a pyridyl-bound [Ru^{II}-inhibitor] was targeted at CST-L and papain inhibition via spatio-temporal controlled irreversible binding.⁸³ Cathepsin L is a target because of its influence in inflammation, cancer and other pathologies. Although the warhead was not directly bound to the [Ru^{II}] as in the previously described complexes, the bulk of the metal complex was expected to inhibit binding until photo-release. Previously established epoxysuccinyl CLIK inhibitors were synthesized (**38** & **41**) and modified for caging (**39** & **42**). The second order rate constant for inhibition (K_i) of CST-L by **38**, **39**, **40** (pre-irradiation) were experimentally equivalent within error. Complexes **41** and **42** had similar inhibitory effects but **43** (pre-irradiation) had a much lower inhibitory effect than **42**. **43** ($\lambda_{\max} = 471$ nm) was only effective post-irradiation. As such, **40** was presented as a homing agent whereas as **43** was presented as a spatio-temporally controlled chaperone. The contribution of these investigations continue to pave the way for targeting other enzymes and live cell systems and future *in vivo* work. The complexes continue to be tuned and technology developed such that inhibition can be achieved spatio-temporally in the PDT window^{***}.

*** Range of light wavelengths (650–800 nm) suitable for photochemical excitation that avoids significant absorption of other plasma components, including hemoglobin and water

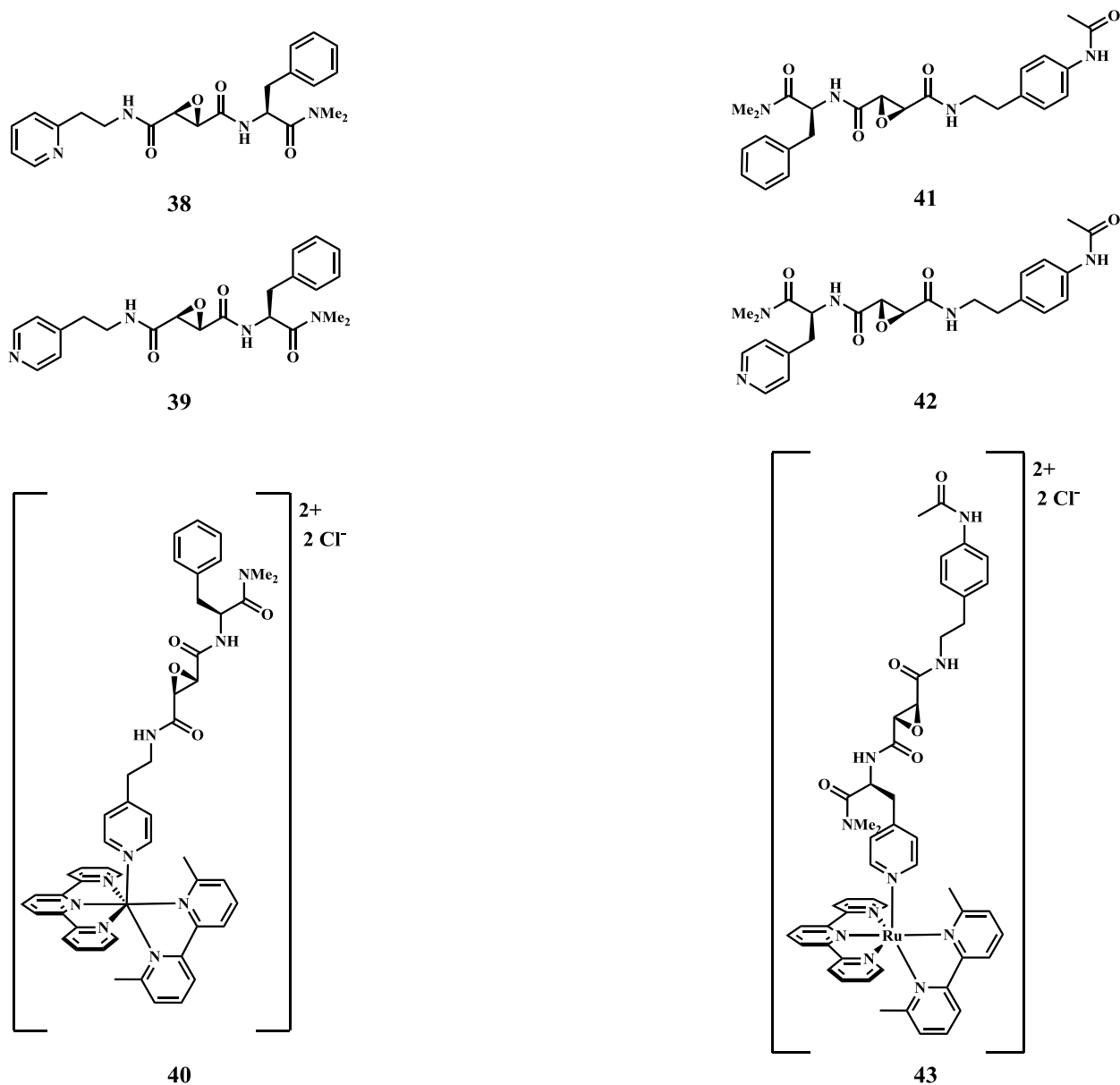


Figure [2.4.2].3 The parent inhibitors as well as their derivatives and caged inhibitors described above.

2.4.3 WORK BY OTHER RESEARCH TEAMS

Fighting cancer

Garner *et alia* reports a dual-action therapeutic agent, monitored by UV-vis spectroscopy, ^1H NMR and agarose mobility shift gels.⁸⁴ Here, a derivative of uracil and an analogue of 5-fluorocil, 5-cyanouracil (5-CNU), was complexed to $[\text{Ru}^{\text{II}}(\text{bpy})_2]^{2+}$ via the nitrile substituent, see

44, Fig [2.4.3].1. Once complexed, 5-cyanouracil was biologically inactive but activate upon irradiation in water. The authors discern that the complex displays dual-therapeutic capabilities since both the chaperone and the nucleobase (5-CNU) are functional after irradiation. As 5-cyanouracil is released from the complex, simultaneous aquation of the metal complex enables binding to DNA, initiating apoptosis in a mechanism similar to cisplatin. The authors propose that 5-cyanouracil disrupts the pyrimidine catabolism cycle pharmacologically. Importantly, the dual-therapeutic ability of the unit can also be controlled spatio-temporally and can therefore selectively target malignancies, tumors and other effects with lower risks.

In 2013, the Turro group enhanced their photo-activatable system by using a new Ru^{II} chaperone: [Ru^{II}(terpy)]²⁺.⁸⁵ The chaperone was now bound to three 5-cyanouracil ligands; having triple-release capacity, see **45**, Fig. [2.4.3].1. Once irradiated with 395 nm light, the 5-CNU ligands are photolyzed from the [Ru^{II}], which simultaneously undergoes aquation, then covalently binds DNA. The individual biological activity of the 5-CNU and the [Ru^{II}] makes this complex an attractive, potential dual-therapeutic agent. The authors observed that nitrile bound [Ru^{II}] display a greater ligand-exchange quantum yield in comparison to other complexes. Importantly the drug absorbs in the PDT window. This, and the increased cytotoxicity of the compound make [Ru^{II}(terpy)]²⁺ a more favorable chaperone than [Ru^{II}(bpy)₂]²⁺. The trans-effect also plays a large role here such that the 5-CNU ligand trans to the pyridine of terpy is least likely to dissociate; the axial ligands are more reactive. The complex is being further developed to increase the quantum yield of aquation and cell penetration ability. Importantly, this new system can be irradiated selectively and specifically, unlike other [Ru^{II}] that have undergone clinical trials, such as **46** – KP1019, that have a lower selectivity.

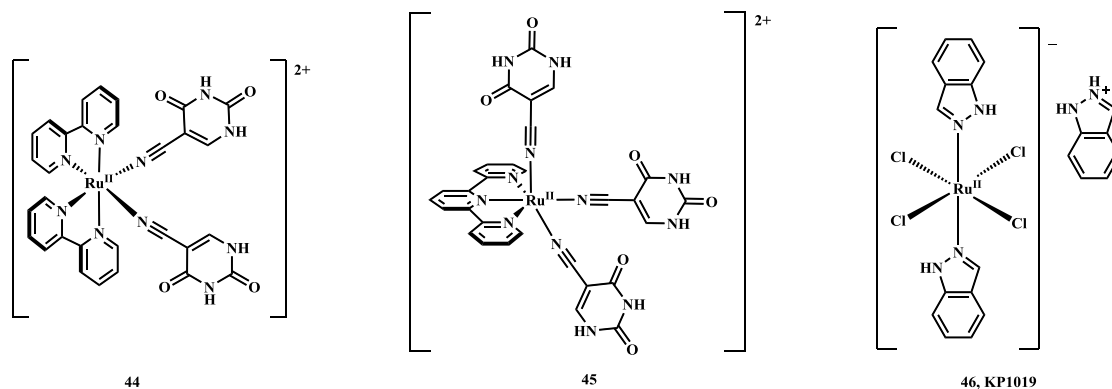


Figure [2.4.3].1 Nitrile-bound inhibitor-chaperone complexes synthesized and investigated by collaborators Turro group (**44** & **45**) and a non-photo-activatable Ru^{II} complex being clinically developed (**46**).

Fighting Antimicrobial Resistance

Like photo-active oncotherapy, photo-active antimicrobial therapy types include: photodynamic antimicrobial therapy (PDAMT) and photo-release antimicrobial therapy (PRAMT).⁸⁶ Much like PDT, PDAMT works via generation of ROS and causes non-specific damage to the bacteria, whereas PRAMT, like, PACT, allows spatial and temporal control achieving targeted therapy and reduced systemic toxicity to the host as well as reduced antimicrobial resistance.

This technology is currently being advanced to combat antimicrobial resistance.⁸⁶⁻⁸⁹ Antibiotic resistance results from the bacterial mutations and reduces the impact of drugs on its reproduction and life. Bacterial infection and resistance, lead to increased mortality and increase health expenditure. Smith *et alia* tackles this growing problem by using $[Ru^{II}(bpy)_2]^{2+}$ as a chaperone for an antimicrobial drug, isoniazid (INH).⁸⁶ The photo-activated complex, $[Ru^{II}(bpy)_2(INH)_2]^{2+}$ (**47**) was shown to be 5.5 times more potent toward *Mycobacterium smegmatis* than the unbound clinical drug, with a minimum inhibitory concentration of 4 μM after irradiation. Both INH ligands were released in less than two hours when irradiated with 465 nm light, forming the diaqua complex: $[Ru^{II}(bpy)_2(H_2O)_2]^{2+}$. The first ligand dissociated within one

minute of irradiation, or in less than 500 ps according to DFT calculations. It is likely that the chaperone plays a role in either transporting the drug across the membrane or has an additional antimicrobial mechanism in synergy with the released drug. The successful development of this system as a therapy would mean the treatment of the third most important, multi-drug resistant, mycobacterial disease worldwide, tuberculosis would be possible.

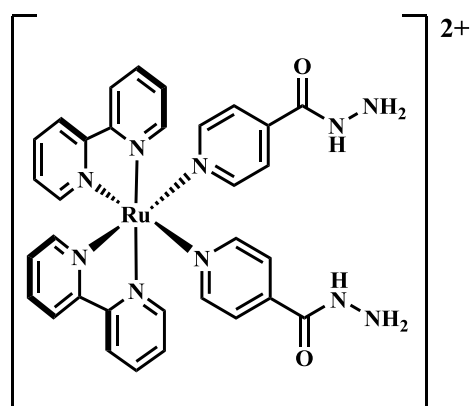


Figure [2.4.3].2 The PRAMT agent discussed above.

Chapter 3. Methodology

3.1 MATERIALS

All declared materials were used as received without further purification from commercial suppliers. Cbz-Phe-OH, Boc-4PA-OH, Boc-Phe-OH, HBTU and 4-nitrophenylcarbonate were obtained from Chem-Impex International, Inc. Trifluoroacetic acid, 12 N hydrochloric acid, sodium bicarbonate, sodium sulfate, sodium hydroxide, N-methylmorpholine, terpyridine, acetone, ethanol, methanol and dry diethyl ether were obtained from Sigma-Aldrich Co. LLC. Triethylamine, sodium chloride, dichloromethane, ethyl acetate and hexanes were obtained from Fisher Chemical-Thermo Fisher Scientific, Inc. Celite and dry dimethylformamide were obtained from Merck & Co., Inc. Formic acid, lithium chloride and toluene were obtained from EMD Millipore Corporation. Diisopropylethylamine, benzyl chloroformate and sodium carbonate were obtained from Acros Organics-Thermo Fisher Scientific, Inc. Aminoacetonitrile hydrochloride was obtained from Alfa Aesar-Thermo Fisher Scientific, Inc. Pyridine-4-methanol was obtained from Matrix Scientific. Ruthenium (III) chloride trihydrate was obtained from Strem Chemicals, Inc. Dmbpy was obtained from Ark Pharma, Inc. Deuterated NMR solvents were obtained from Cambridge Isotope Laboratories, Inc. Recombinant human procathepsin K (0.023 mg/mL; purity > 95%) and Cbz-Phe-Arg-AMC (10 mg; purity > 99%) was commercially obtained from Enzo Life Sciences, Inc. and the appropriate aliquots were prepared and frozen. Air sensitive reactions were conducted in an atmosphere of nitrogen gas or argon gas obtained from Airgas, Inc. Column chromatography was performed using silica gel obtained from Sigma-Aldrich Co. LLC and alumina gel (activated, neutral, Brockmann Grade I) obtained from EMD Millipore Corporation.

Synthesis of compounds **1**, **2**, **3** and **4** were accomplished using advanced intermediates. All compounds were prepared using methods as stated in the literature, or using slightly modified versions.

3.2 INSTRUMENTATION

Thin layer chromatographs were collected using silica gel glass plates with UV-254 fluorescent indicator and alumina gel glass plates with UV-254 fluorescent indicator obtained from Merck & Co., Inc. The ^1H NMR spectra were collected on a Varian Fourier Transform (FT) Nuclear Magnetic Resonance (NMR) Mercury 400, processed using Varian Vnmrj 2.2D software or Varian FT-NMR Agilent 400, processed using Varian Vnmrj 3.2A software. The mass spectra were obtained using Waters High Performance Liquid Chromatography (HPLC) ZQ2000 Single Quadrupole Mass Spectrometer coupled with electrospray ionization. The UV-vis spectra were obtained using a Varian Cary 50 spectrophotometer. Enzymatic assay plates were read using a Tecan Infinite M200 microplate reader with Tecan i-control 1.10.4.0 software. Enzyme assays were irradiated with an Osram Xenophot HLX 24 V/250 W Tungsten Halogen Lamp. A 10 cm water cell was used to absorb unwanted infrared light. Inhibition data was fit using Igor Pro 7.00 32-bit software.

3.3 PROCEDURES

3.3.1 SYNTHESSES

Synthesis of Inhibitor 1

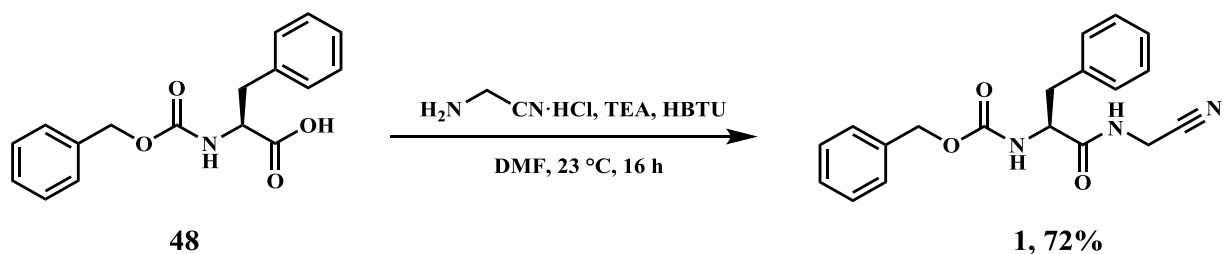


Figure [3.3.1].1 Reaction scheme for synthesis of Inhibitor **1**.

Inhibitor **1** was prepared following a previously established method.⁸¹ A 10 mL round bottom flask containing **48**, Cbz-Phe-OH (250 mg; 0.84 mmol), was purged with N₂ gas for 5 minutes; the flask was maintained under N₂ gas for the remainder of the experiment. Dry DMF (6 mL) was then added to the flask and the mixture was stirred until dissolution of **48**. HBTU (380 mg; 1.0 mmol), aminoacetonitrile hydrochloride (92.7 mg; 1.00 mmol) and triethylamine (0.28 mL; 2.0 mmol) were then added. The reaction mixture was stirred at room temperature (23 °C) for 16 h. Complete conversion of reactant to product was verified by TLC analysis. The organic layer was extracted using DCM (8 mL) and washed with 0.1 M HCL (10 mL; 2 times), followed by saturated sodium bicarbonate (10 mL; 2 times) then brine (10 mL) and dried using sodium sulfate. The organic layer was then filtered, concentrated *in vacuo* and the product was recrystallized from ethyl acetate/hexanes. Yield 204 mg; 72%. The product was characterized by ¹H NMR and MS, see chapter 4. The characterization data agreed with previously reported data.

Synthesis of Reagent 50

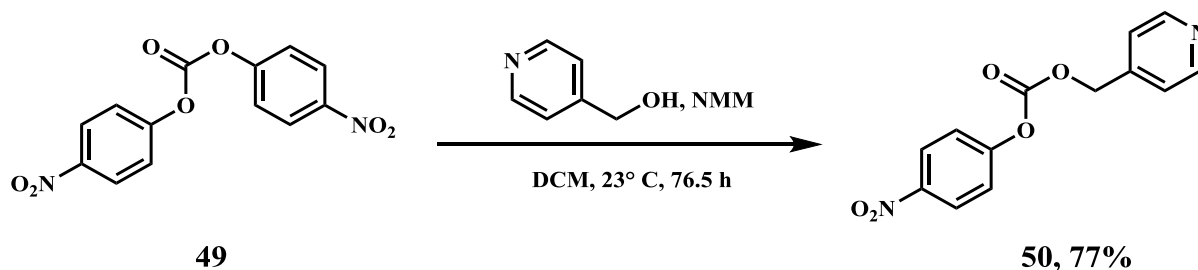


Figure [3.3.1].2 Reaction scheme for synthesis of Reagent 42.

Reagent **50** was prepared following a previously established method.⁹⁰ A 50 mL round bottom flask containing pyridine-4-methanol (1.00 g; 0.00916 mmol) and **49**, 4-nitrophenylcarbonate (3.07 g; 0.0100 mmol), was purged with N₂ gas for 5 minutes and maintained under an N₂ atmosphere. DCM (17 mL) was added, followed by N-methylmorpholine (1.00 mL; 0.00916 mmol). The mixture was stirred at room temperature (23 °C) for 76.5 h. The reaction mixture changed from a cloudy off-white colloid to a dark red-orange solution. Upon completion, as determined by TLC analysis, the solvent was evaporated *in vacuo*. The residue was then dissolved in ethyl acetate (40 mL) and filtered through sterile cotton. The compound was extracted using 1 M HCl (50 mL; 4 times). The aqueous layers were combined, the pH increased to 9 using saturated sodium carbonate. The pH was monitored with universal indicator paper. The product was then extracted with DCM (30 mL; 4 times) then washed with brine (50 mL), dried over anhydrous sodium sulfate and concentrated *in vacuo*. The product was recrystallized from ethyl acetate/hexanes. Yield: 1.92g; 77%. The product was characterized by ¹H NMR and MS, see chapter 4. The characterization data agrees with previously reported data.

Synthesis of Inhibitor 2

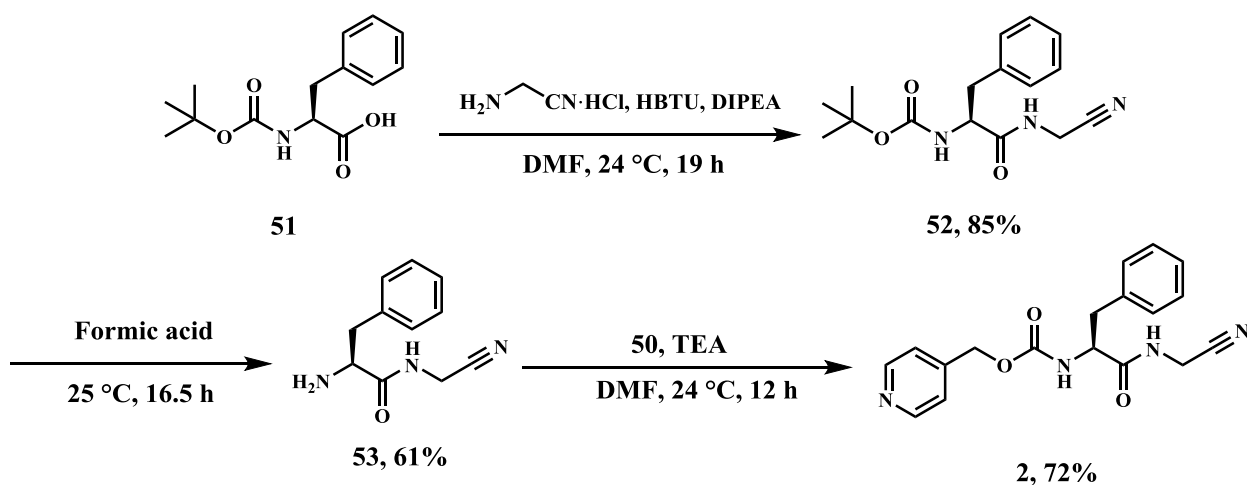


Figure [3.3.1].3 Reaction scheme for synthesis of Inhibitor 2.

Compound **52** was prepared following a method modified from the literature.⁸¹ A 100 mL round bottom flask containing **51**, Boc-Phe-OH (3.00 g; 0.0113 mol) was purged with N_2 gas for 5 minutes; the flask was maintained under N_2 gas for the remainder of the experiment. Dry DMF (60 mL) was added and the mixture was stirred until dissolution of **51**. HBTU (5.15 g; 0.0136 mol), aminoacetonitrile hydrochloride (1.15 g; 0.0124 mol) and DIPEA (7.10 mL; 0.0396 mol) were then added. The reaction mixture was stirred at room temperature ($24\text{ }^\circ\text{C}$) for 19 h. Complete conversion was verified by TLC analysis. The organic layer was extracted using ethyl acetate (75 mL) and washed with saturated sodium bicarbonate (100 mL; 2 times), then brine (100 mL) and dried over anhydrous sodium sulfate. The organic layer was then filtered, concentrated under reduced pressure and recrystallized from ethyl acetate to yield white crystals. Yield: 2.93 g; 85%. The product was characterized by ^1H NMR, see chapter 4. The characterization data agrees with previously reported data.

Compound **53** was prepared following previously established methods.^{25, 91} Compound **52** (550 mg; 1.8 mmol) was added to a 20 mL round bottom flask. Formic acid (8 mL) was added and

the mixture and allowed to stir at room temperature (25 °C) for 16.5 h. DCM (5 mL) was added to the round bottom flask and the mixture was evaporated *in vacuo*. Water (10 mL) was added and the solution was basified to pH 9 using saturated sodium bicarbonate. The pH was monitored with universal indicator paper. Compound **53** was extracted using DCM (10 mL). The organic layer was dried over anhydrous sodium sulfate and concentrated *in vacuo*. Yield: 224 mg; 61%. The product was characterized by ¹H NMR, see chapter 4. The characterization data agrees with previously reported data.

Inhibitor **2** was prepared following a method modified from the literature.⁹⁰ A 10 mL round bottom flask containing **50** (148.5 mg; 0.5416 mmol) and **53** (135 mg; 0.492 mmol) was purged with N₂ gas for 5 minutes; the flask was maintained under N₂ gas for the remainder of the experiment. Dry DMF (5 mL) was added and the mixture stirred until dissolution of **50** and **53**. Triethylamine (0.08 mL; 0.5 mmol) was then added. The reaction mixture was stirred at room temperature (24 °C) for 12 h. Complete conversion was verified by TLC analysis. The organic layer was extracted using ethyl acetate (10 mL) and washed with sodium bicarbonate (10 mL; 2 times), then brine (10 mL) and dried over anhydrous sodium sulfate. The organic layer was then filtered, concentrated *in vacuo* and recrystallized from ethyl acetate/hexanes to yield white crystals. Yield: 120 mg; 72%. The product was characterized by ¹H NMR and MS, see chapter 4. The characterization data agrees with previously reported data.

Synthesis of Inhibitor 3

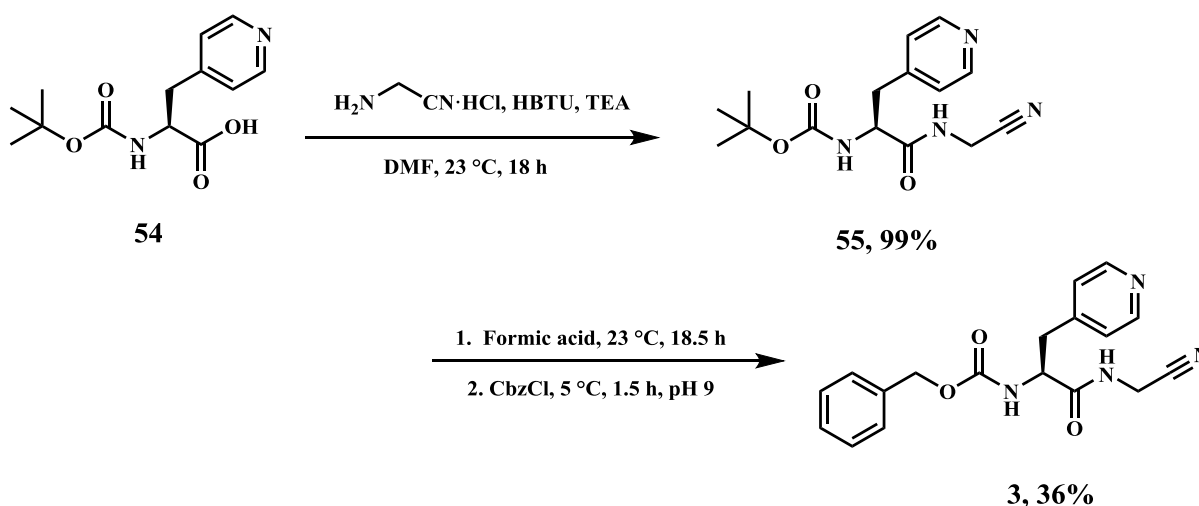


Figure [3.3.1].4 Reaction scheme for synthesis of Inhibitor 3.

Compound **55** was prepared following a previously established method.⁸¹ A 25 mL round bottom flask containing **54**, Boc-4PA-OH (500. mL; 1.88 mmol), was purged with N₂ gas for 5 minutes; the flask was maintained under N₂ gas for the remainder of the experiment. Dry DMF (10 mL) was added and the mixture stirred until dissolution of **54**. HBTU (854 mg; 2.25 mmol), aminoacetonitrile hydrochloride (191 mg; 2.07 mmol) and DIPEA (1.10 mL; 2.25 mmol) were then added. The reaction mixture was stirred at room temperature (23 °C) for 18 h. Complete conversion was verified by TLC analysis. The organic layer was extracted using ethyl acetate (15 mL) and washed with saturated sodium bicarbonate (20 mL; 2 times), brine (20 mL) and dried over anhydrous sodium sulfate. The organic layer was then filtered, concentrated *in vacuo* and recrystallized from ethyl acetate/hexanes to yield white crystals. Yield: 563 mg; 99%. The product was characterized by ¹H NMR, see chapter 4. The characterization data agrees with previously reported data.

Inhibitor **3** was prepared following previously established methods.^{25, 91} Compound **55** (20.0 mg; 0.657 mmol) was added to a 5 mL round bottom flask. Excess formic acid (1 mL) was

added and the mixture was allowed to stir at room temperature (23 °C) for 18.5 h. DCM (5 mL) was added to the round bottom flask and the mixture was evaporated *in vacuo*.

The concentrated product was then basified to pH 9 with saturated sodium bicarbonate and cooled to 5 °C. The pH was monitored with universal indicator paper. The flask was maintained under ice cooling. Benzyl chloroformate was then added dropwise to the mixture. Upon completion, as monitored by TLC analysis, the product was extracted with DCM (5 mL), dried over anhydrous sodium sulfate, evaporated *in vacuo* and recrystallized from ethyl acetate/hexanes to yield white crystals. Yield: 8 mg; 36%. The product was characterized by ¹H NMR and MS, see chapter 4. The characterization data agrees with previously reported data.

Synthesis of Complex **4** $[Ru^{II}(terpy)(bpy)(2)](PF_6)_2$

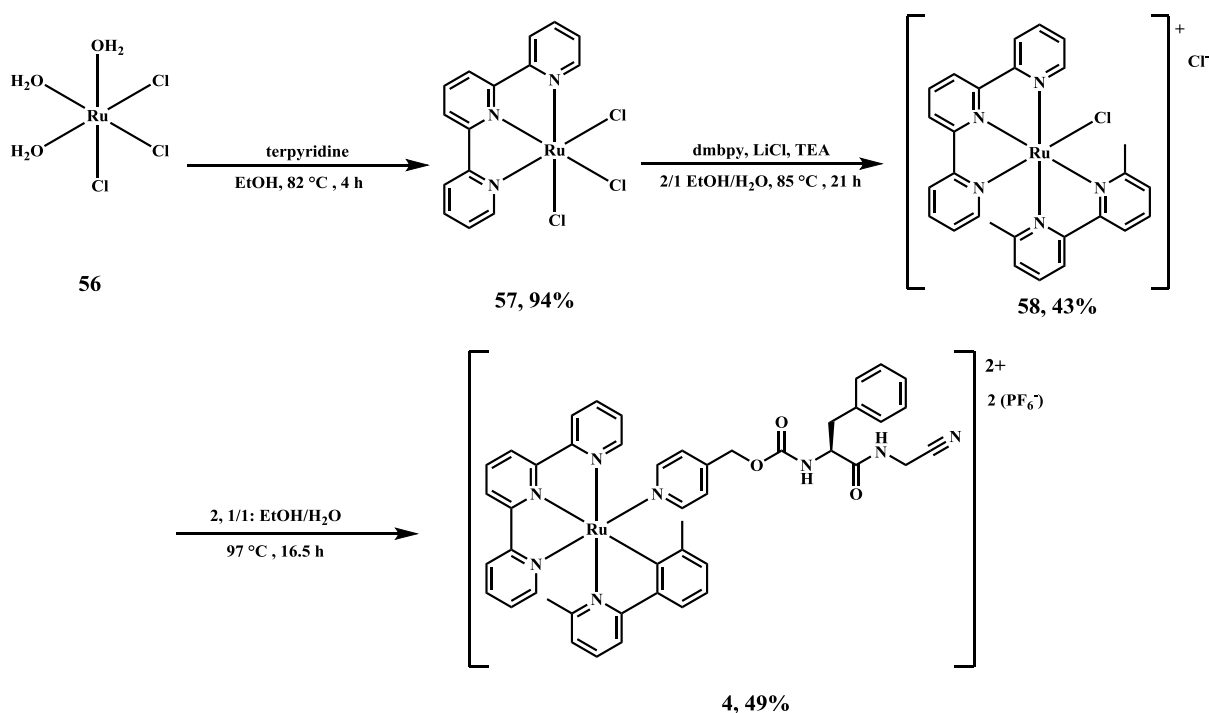


Figure [3.3.1].5 Reaction scheme for synthesis of Complex **4**.

Complex **57** was prepared following a method modified from the literature.⁹² A 150 mL sealed flask containing **56**, $Ru^{III}Cl_3 \cdot 3H_2O$ (500. mg; 1.91 mmol) and terpy (446 mg; 1.91 mmol) was purged with argon gas for 10 minutes in the dark. Ethanol (134 mL) was then added and the flask was sealed. The reaction was allowed to proceed under reflux (82 °C) for 4 h. The mixture was then allowed to cool to room temperature and the deep purple crystals were collected after centrifuging and washing with ethanol. The crystals were allowed to dry *in vacuo* for 16 h. Yield: 796 mg; 94%. The product was characterized by ¹H NMR. The characterization data agrees with previously reported data.

Complex **58** was prepared following a method modified from the literature.⁹³ A 75 mL sealed flask containing compound **57** (262 mg; 0.589 mmol), dmbpy (163 mg; 184.24 mmol), lithium chloride (250 mg; 5.89 mmol) was purged with argon gas for 15 minutes. Ethanol (32 mL)

and water (16 mL) were then added under continued purging. TEA was subsequently added. The reaction was allowed to proceed under reflux (85 °C) for 21 h. The mixture was filtered through celite while hot and the filtrate was evaporated *in vacuo*. The compound was purified over alumina in the dark. (Solid phase: alumina; Mobile phase: 0–5% Methanol/DCM) and recrystallized from 1% methanol/DCM/hexanes. Yield: 148.8 mg; 43%. The product was characterized by ¹H NMR, see chapter 4. The characterization data agrees with previously reported data.

Complex **4** was prepared following a method modified from the literature.⁷⁸ A 15 mL sealed flask containing compound **58** (10. mg; 0.017 mmol) and **2** (17 mg; 0.050 mmol) were purged with argon gas for 15 minutes. Ethanol (2.5 mL) and distilled water (2.5 mL) were then added. The reaction was allowed to proceed under reflux (97 °C) for 16.5 h. The solvent was evaporated *in vacuo* and the product was washed with toluene. Product was purified via column chromatography (solid phase: alumina; mobile phase: 0–10% methanol/DCM), and solvent layering (ethanol/diethyl ether, 3 times) and vapor diffusion (ethanol/diethyl ether; 2 times). Yield: 7 mg; 49%. The product was characterized by ¹H NMR and MS, see chapter 4. The characterization data agrees with previously reported data.

3.3.2 CHARACTERIZATION: SAMPLE PREPARATION AND DATA COLLECTION

NMR

Approximately 20 mg or twenty drops of the compound was dissolved in 0.6–0.8 mL of the deuterated NMR grade solvent in an appropriately sized vial. The solution was then filtered through cotton into another vial then transferred to a 7 inch, borosilicate glass NMR tube (with an inner diameter of 0.5 mm and an outer diameter of 10 mm). ^1H NMR solvents were either methanol- D_4 or chloroform- D_1 and the resonances were referenced to the residual methanol and chloroform signals on the Varian FT-NMR Mercury 400 or the Varian FT-NMR Agilent 400 for all applicable samples. Mass spectroscopy was performed in methanol for all applicable samples. See chapter 4 for details specific to each compound and section 3.2 for details specific to the instrument.

Mass Spectrometry

Approximately 0.1 mg or one droplet of sample was dissolved in 1–5 mL of HPLC-grade methanol. A gradient of concentrations were prepared. The methanol was first injected into the NMR three times, followed by 1 to 3 injections of the dissolved sample of varying concentrations. The solvent peak was subtracted from the sample peak. The spectrum was compared to the isotope mass model. See chapter 4 for details specific to each compound and section 3.2 for details specific to the instrument.

Electronic Absorption Spectroscopy

Approximately one drop or 0.5 mg of the sample was dissolved in 1 mL of ACS reagent grade solvent in a vial. The solution was then transferred to a 1 X 1 cm quartz cuvette, sealed with a plastic septum and placed in the Varian Cary 50 UV-Vis Spectrophotometer at ambient temperature. Absorbance versus wavelength data was plot using Igor Pro 7.0.

3.3.3 PHOTOLYSIS OF INHIBITOR

The sample was prepared as stated above and transferred to a 1 x 1 cm quartz cuvette. The electronic absorption spectrum was taken after 0, 1, 3, 5, 10, 15 and 30 minutes of irradiation with white light from Osram Xenophot HLX 24 V/250 W Tungsten Halogen Lamp. Photolysis data is shown in section 4.2.

3.3.4 ENZYME ASSAYS

Free CST-K Inhibition assay for 1, 2 & 3

Cathepsin K activity was determined using a method previously reported in the literature.⁵
⁷⁹ All solutions and substrates were kept on ice prior to and between uses during experiment set-up. The primary buffer contained 400 mM sodium acetate, 4 mM EDTA, 0.01% Triton-X at pH 5.5. The activator buffer contained 400 mM sodium acetate, 4 mM EDTA, 8 mM DTT, 0.01% Triton-X at pH 5.5. The experiment was carried out in triplicate on Corning® 96 Well Flat Bottom Black Polystyrene TC-Treated Microplates.

The enzyme was activated with activator buffer (100 μ L; 8 nM CST-K) and 30 minutes of incubation at 25 °C. Substrate (5 mL; 20 μ L) was prepared from 100 mM aliquot of Cbz-Phe-Arg-AMC. 100 μ L solutions of the free inhibitor of various concentrations were prepared via serial dilution from a DMSO stock solution of the inhibitors. Concentrations ranged from 4 nM to 0.4 mM. After incubation of the enzyme, 96-well flat black plates were filled with 25 μ L of activated enzyme, and 25 μ L of inhibitor solution. A blank cell was also prepared. The plate was covered with foil and the reaction was allowed to take place for 15 minutes, with gently agitation every 3 minutes. 50 μ L substrate solution was added to each well and the plate was immediately placed in the plate reader and processed. Final concentrations are: 2 nM CST-K, 10 μ M Cbz-Phe-Arg-AMC, 1 nM–0.1 mM inhibitor, <1% DMSO.

CST-K activity was determined by kinetic measurements via fluorometric detection of the AMC hydrolysis product at 37 °C, every 1 minute for 30 minutes. The enzyme activities are expressed as ratios; 100% activity is the activity observed in the absence of inhibitor. The IC₅₀ values are shown in section 4.3 and were determined by plotting percent activity versus log₁₀ of the inhibitor concentration. The data was fit using a sigmoidal curve (Igor Pro 7.0).

Caged CST-K dark-light Inhibition assay for 4

CST-K activity was determined using a method previously reported in the literature.^{5,79} As above, all solutions and substrates were stored on ice when not in use in the experiment. The primary buffer contained 400 mM sodium acetate, 4 mM EDTA, 0.01% Triton-X at pH 5.5; this buffer was used for all dilutions with the exception of that of the enzyme. The activator buffer contained 400 mM sodium acetate, 4 mM EDTA, 8 mM DTT, 0.01% Triton-X at pH 5.5. The experiment was carried out in triplicate on Corning® 96 Well Flat Bottom Black Polystyrene TC-Treated Microplates. Light and dark experiments were done separately.

The enzyme was diluted 110 times with activator buffer (100 µL; 8 nM CST-K) and incubated for 15 minutes at 37 °C. Substrate (5 mL; 200 µM) was prepared from 100 mM aliquot of Cbz-Phe-Arg-AMC. 100 µL solutions of the free inhibitor were prepared in vary concentrations via serial dilution (concentrations varying from 4 nM to 0.4 mM). After incubation of enzyme, 96-well flat black plates were filled with 25 µL of activated enzyme, and 25 µL of inhibitor solution. A blank cell was also prepared.

For the “light” experiment, photolysis was allowed to take place by placing the plate under the Osram Xenophot HLX 24 V/250 W tungsten halogen lamp for 15 minutes. Infrared light was absorbed using a 10 cm water cell between the lamp and the sample. The plate was gently shaken every 3 minutes.

For the “dark” experiment, all room lights were switched, the plate was covered with foil and the reaction was allowed to take place for 15 minutes. The plate was gently shaken every 3 minutes.

50 μ L of the substrate solution was added to each well and the plate was immediately placed in the plate reader and processed. Final concentrations are: 2 nM CST-K, 100 μ M Z-Phe-Arg-AMC, 1 nM–0.1 mM inhibitor.

CST-K activity was determined by kinetic measurements via fluorometric detection of the AMC hydrolysis product at 37 °C, every 2 minutes for 14 minutes. The enzyme activities are expressed as ratios; 100% activity is the activity observed in the absence of inhibitor. The IC_{50} values are shown in section 4.3 and were determined by plotting percent activity versus \log_{10} of the inhibitor concentration. The data was fit using a sigmoidal curve (Igor Pro 7.0).

Chapter 4. Findings

4.1 CHARACTERIZATION DATA

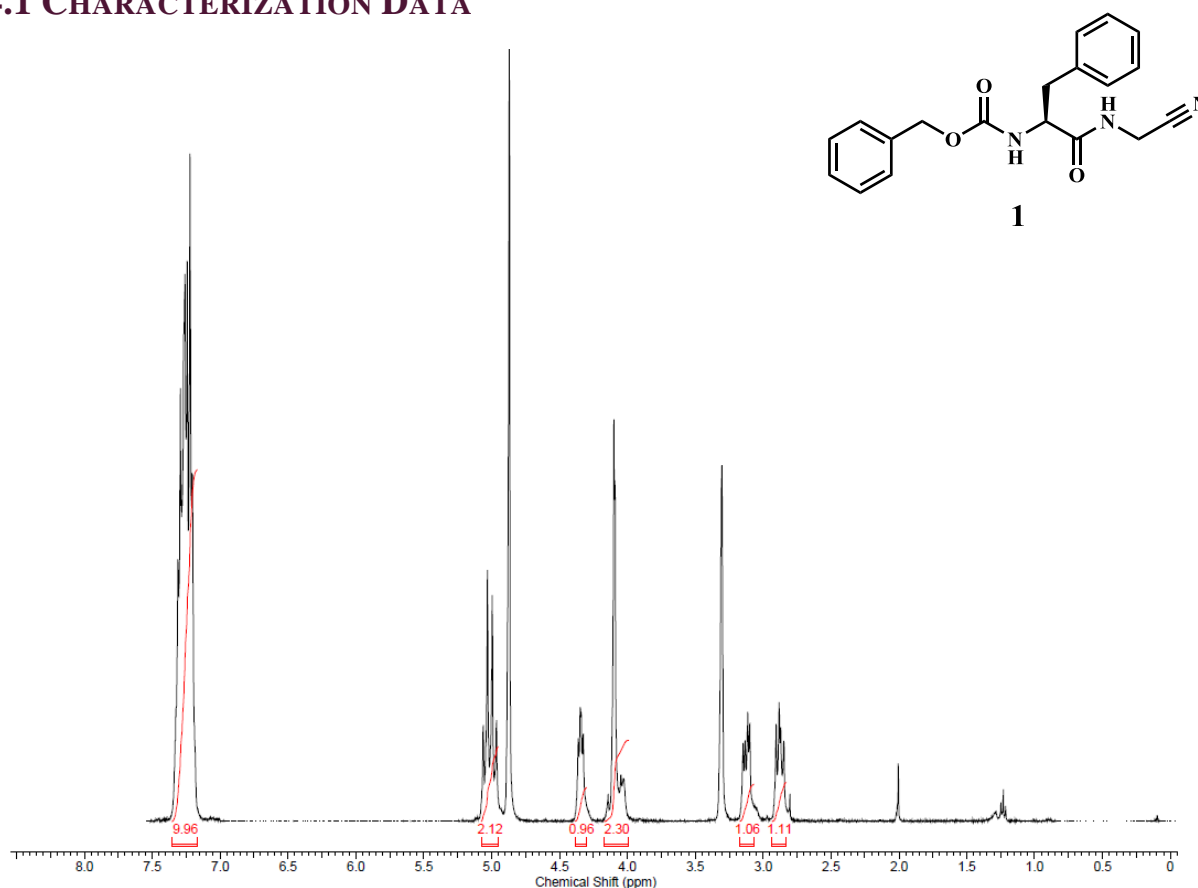


Figure [4.1.0].1 ¹H NMR of Inhibitor 1.

¹H NMR spectroscopy of **1** was performed in methanol-d₄, and the resonances were referenced to the residual methanol signal on the Varian FT-NMR Mercury 400: δ 7.26 (m, 10H), δ 5.01 (q, 2H, 12.56, 14.19), δ 4.34 (dt, 1H, 2.43, 6.08), δ 4.10 (d, 2H, 2.84), δ 3.12 (dd, 1H, 6.08, 13.78), δ 2.88 (dd, 1H, 13.78)

MS (ESI) performed in methanol. m/z: [M + H]⁺ Calcd for C₁₉H₁₉N₃O₃: 337.14; Found : 337.96

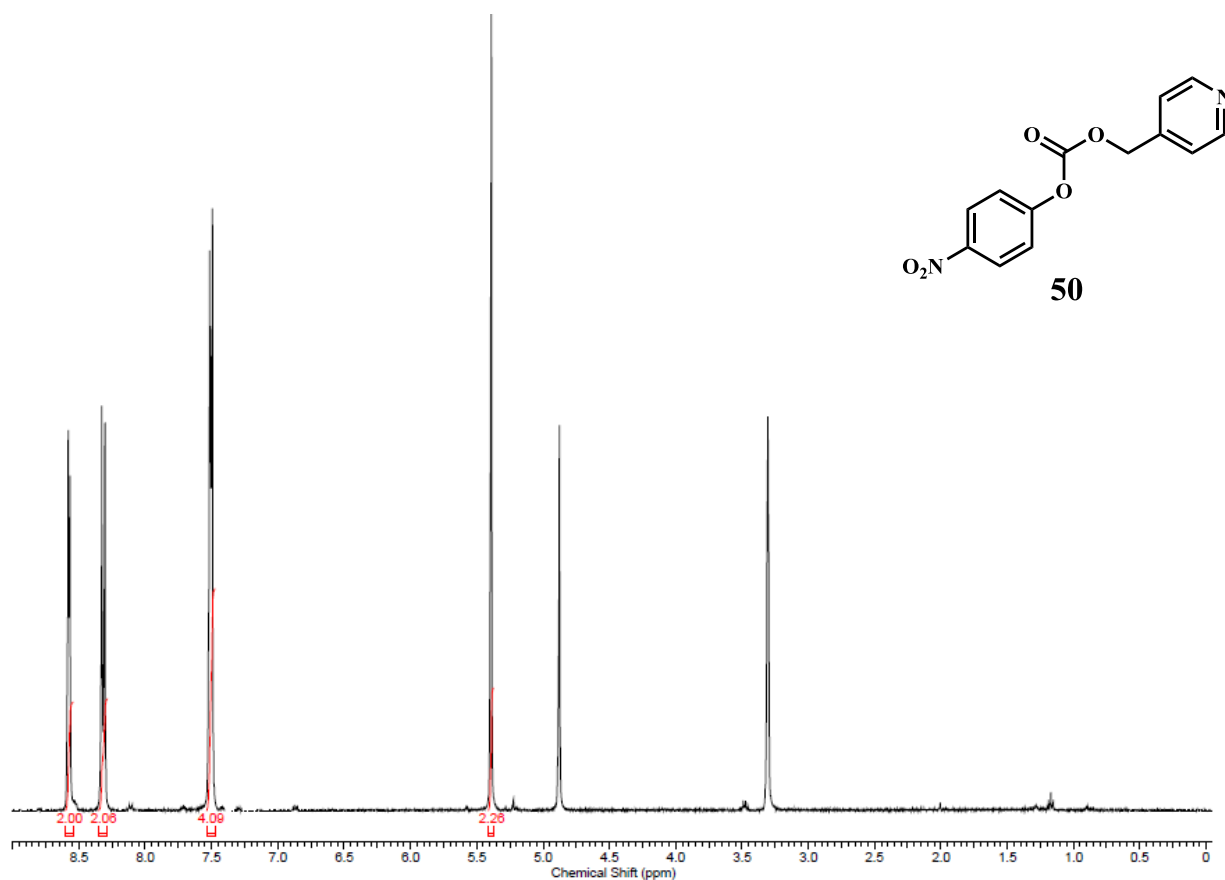


Figure [4.1.0].2 ^1H NMR of compound **50**.

^1H NMR spectroscopy of **50** was performed in methanol- d_4 , and the resonances were referenced to the residual methanol signal on the Varian FT-NMR Mercury 400: δ 8.57 (m, 2H), δ 8.32 (m, 2H), δ 7.52 (m, 4H), δ 5.39 (s, 2H)

MS (ESI) performed in methanol. m/z : $[\text{M} + \text{H}]^+$ Calcd for $\text{C}_{13}\text{H}_{10}\text{N}_2\text{O}_5$: 274.06; Found: 274.87

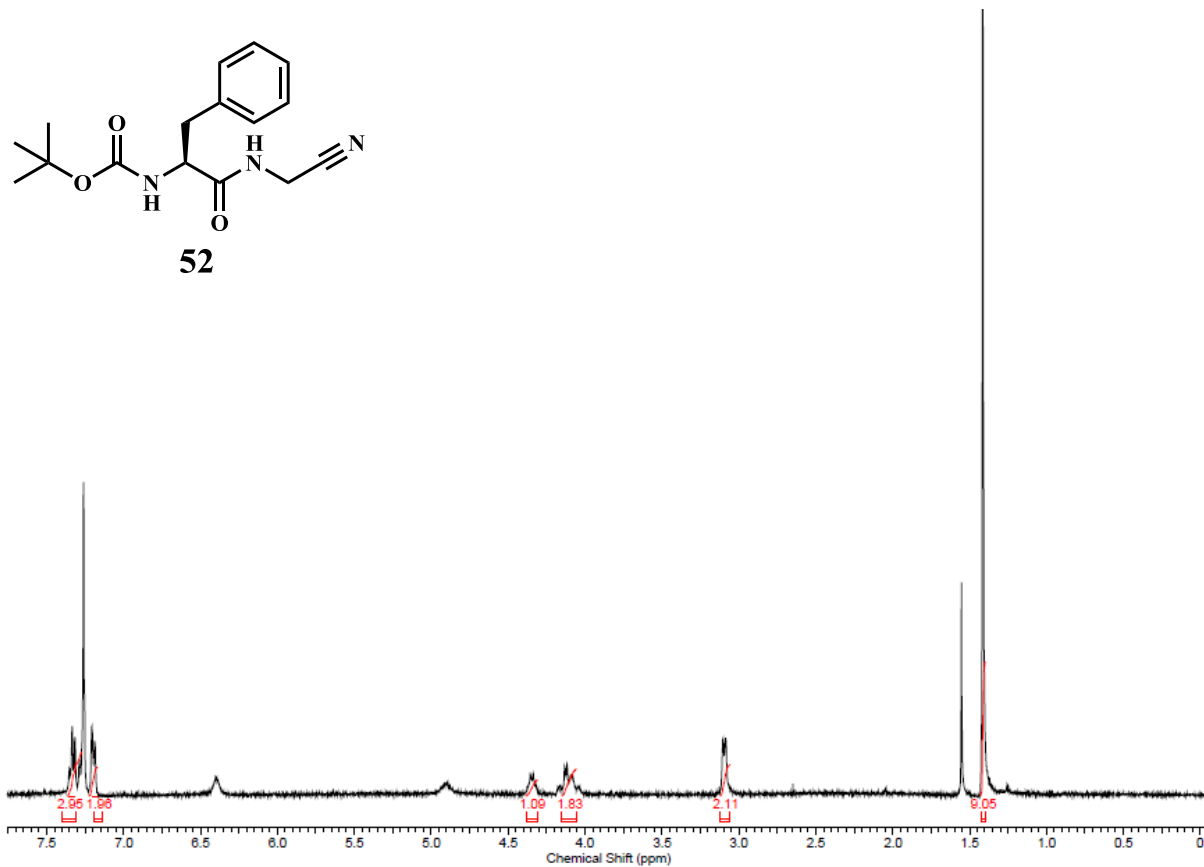


Figure [4.1.0].3 ^1H NMR of compound **52**.

^1H NMR spectroscopy of **52** was performed in chloroform- d_1 , and the resonances were referenced to the residual chloroform signal on the Varian FT-NMR Mercury 400: δ 7.33 (m, 3H), δ 7.20 (d, 2H, 7.30), δ 4.34 (m, 1H), δ 4.10 (m, 2H), δ 3.09 (d, 2H, 6.89), δ 1.41 (s, 9H)

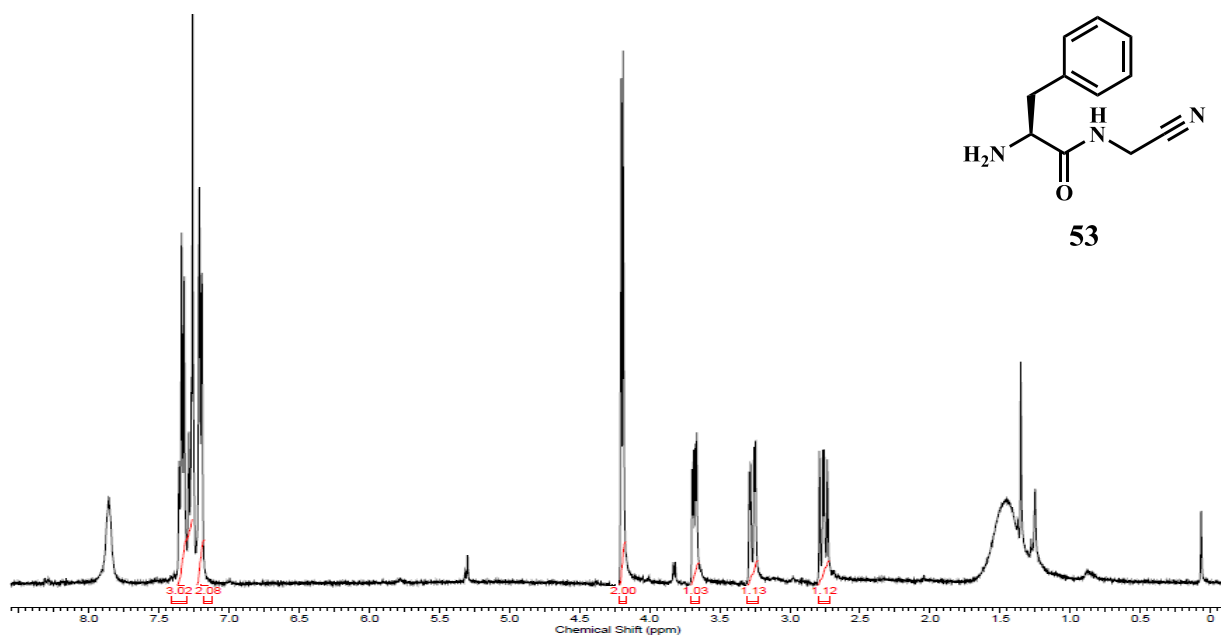


Figure [4.1.0].4 ^1H NMR of compound **53**.

^1H NMR spectroscopy of **53** was performed in chloroform- d_1 , and the resonances were referenced to the residual chloroform signal on the Varian FT-NMR Mercury 400: δ 7.33 (m, 3H), δ 7.20 (d, 2H, 7.30), δ 4.19 (d, 2H, 5.67), δ 3.68 (dd, 1H, 4.05, 8.92), δ 3.26 (dd, 1H, 4.05, 13.78), δ 2.76 (dd, 1H, 8.05, 13.78)

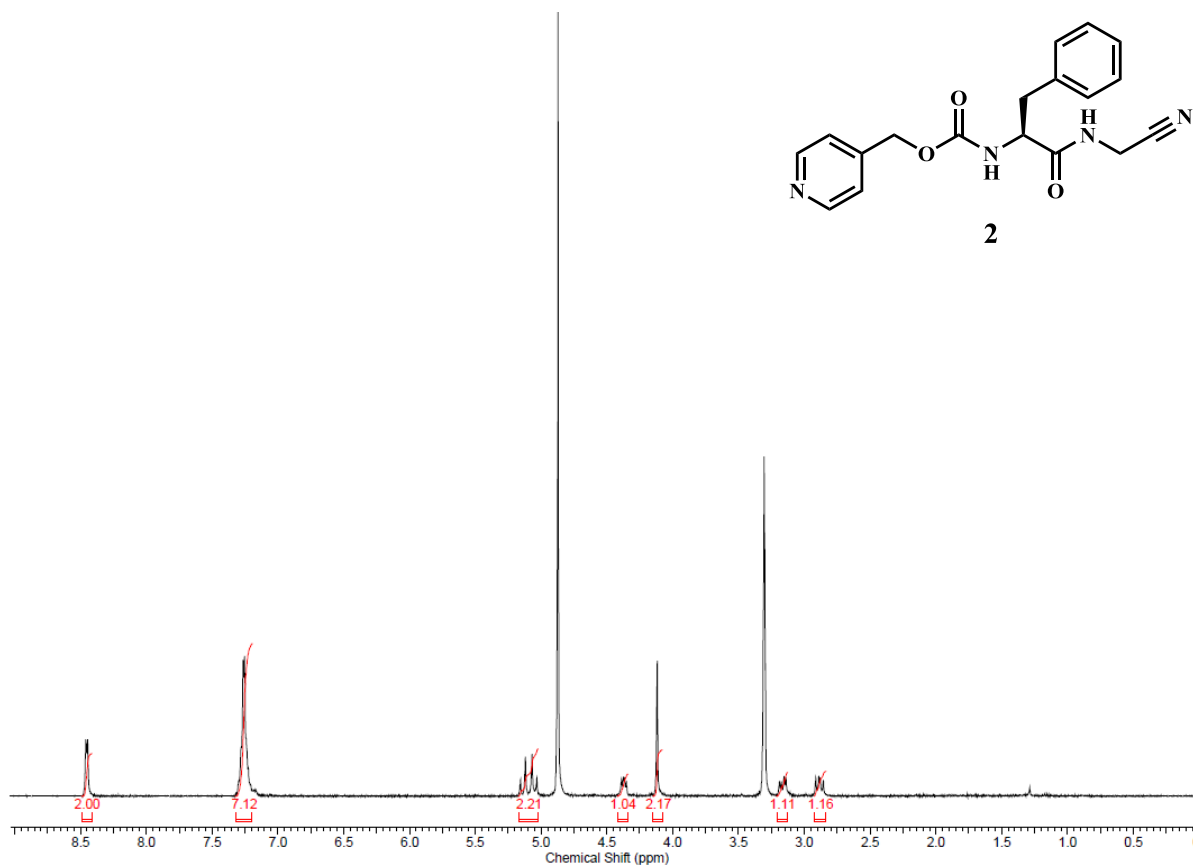


Figure [4.1.0].5 ^1H NMR of Inhibitor **2**.

^1H NMR spectroscopy of **2** was performed in methanol- d_4 , and the resonances were referenced to the residual methanol signal on the Varian FT-NMR Mercury 400: δ 8.45 (d, 2H, 4.05), δ 7.26 (m, 7H), δ 5.10 (dd, 2H, 14.59, 20.27), δ 4.37 (dt, 1H, 5.67, 9.68), δ 4.12 (d, 2H, 0.81), δ 3.16 (dd, 1H, 5.67, 14.59), δ 2.88 (dd, 1H, 9.68, 14.59)

MS (ESI) performed in methanol. m/z : $[\text{M} + \text{H}]^+$ Calcd for $\text{C}_{18}\text{H}_{18}\text{N}_4\text{O}_3$: 338.14; Found: 338.87

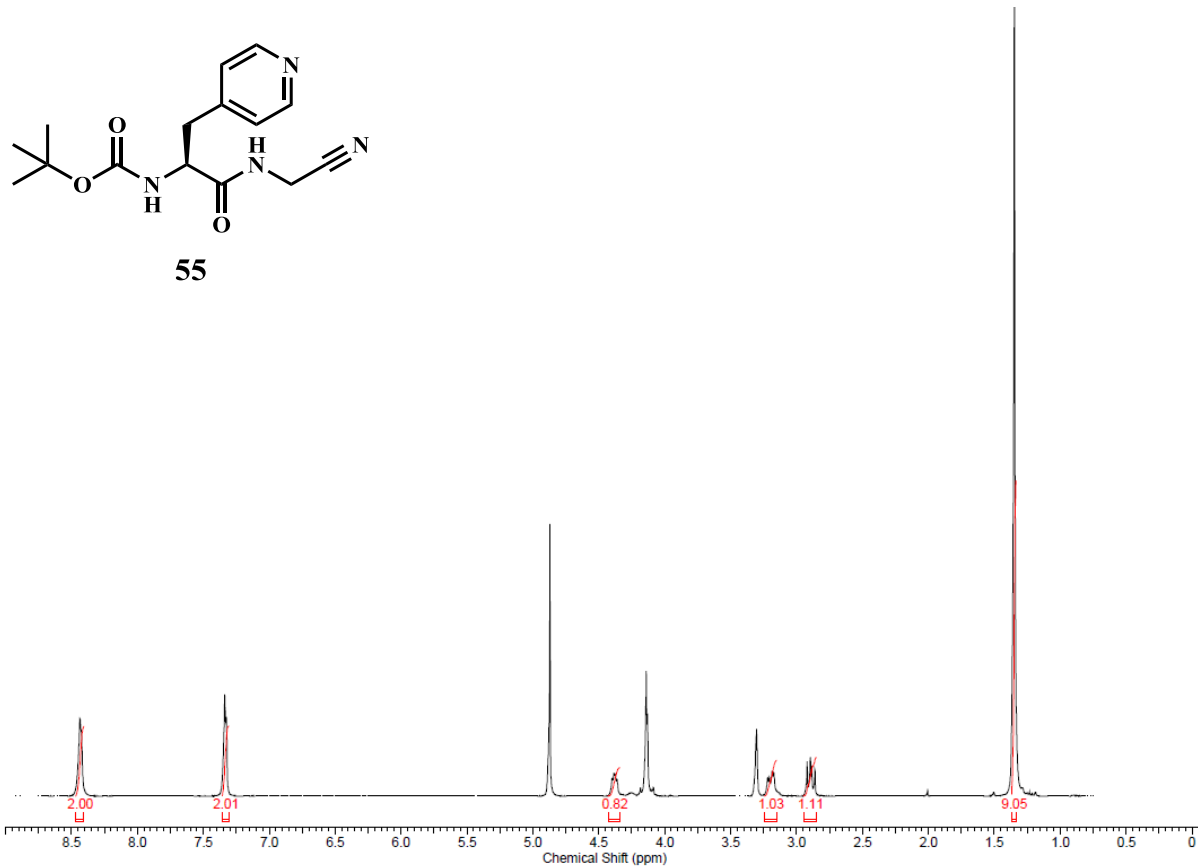


Figure [4.1.0].6 ^1H NMR of Compound **55**.

^1H NMR spectroscopy of **55** was performed in methanol- d_4 , and the resonances were referenced to the residual methanol signal on the Varian FT-NMR Mercury 400: δ 8.45 (d, 2H, 4.46), δ 7.33 (d, 2H, 4.46), δ 4.38 (dt, 1H, 3.24, 5.67), δ 3.20 (dd, 1H, 5.67, 13.78), δ 2.89 (dd, 1H, 13.78), δ 1.35 (s, 9H).

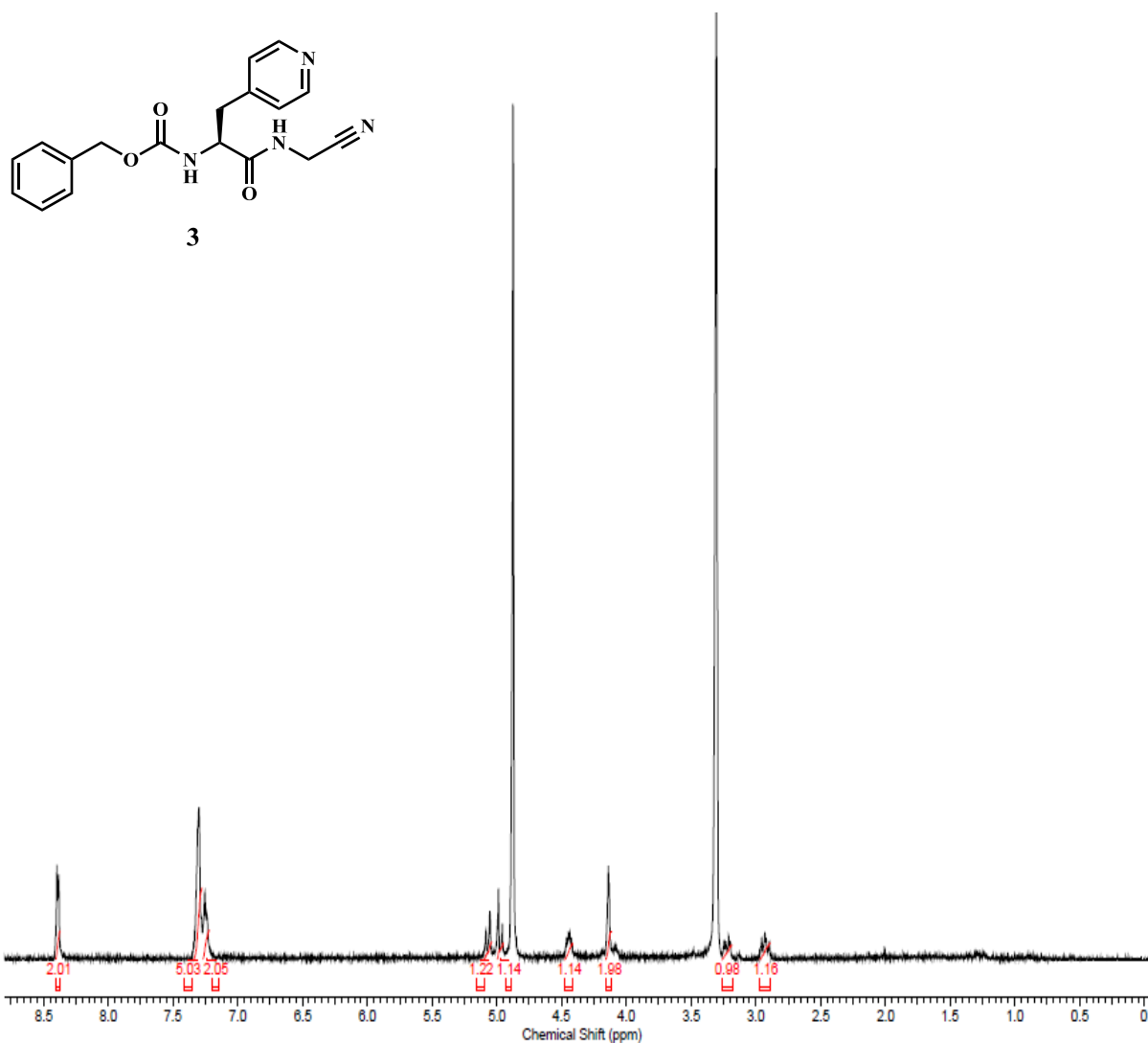


Figure [4.1.0].7 ^1H NMR of Inhibitor **3**.

^1H NMR spectroscopy of **3** was performed in methanol- d_4 , and the resonances were referenced to the residual methanol signal on the Varian FT-NMR Mercury 400: δ 8.39 (d, 2H, 5.67), δ 7.30 (m, 3H), δ 7.25 (m, 2H), δ 5.07 (d, 1H, 12.56), δ 4.97 (d, 1H, 12.56), δ 4.44 (m, 1H), δ 4.14 (m, 2H), δ 3.22 (dd, 1H, 5.67, 14.44), δ 2.93 (dd, 1H, 9.32, 14.44).

MS (ESI) performed in methanol. m/z: $[\text{M} + \text{H}]^+$ Calcd for $\text{C}_{19}\text{H}_{19}\text{N}_3\text{O}_3$: 337.14; Found: 337.88

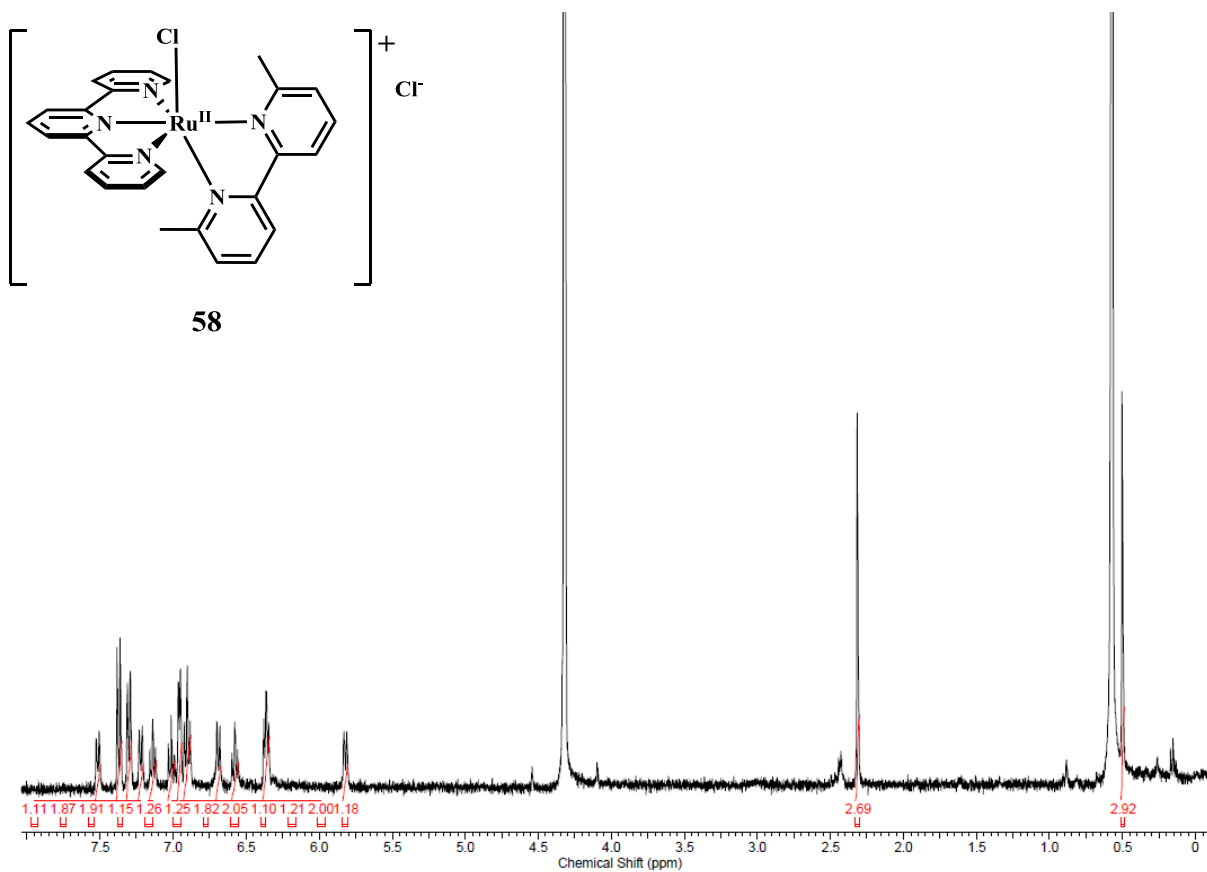


Figure [4.1.0].8 ^1H NMR of Compound **58**.

^1H NMR spectroscopy of **58** was performed in methanol- d_4 , and the resonances were referenced to the residual methanol signal on the Varian FT-NMR Agilent 400: δ 7.51 (d, 1H, 7.77), δ 7.37 (ddd, 2H, 8.31), δ 7.22 (d, 1H, 8.31), δ 7.14 (td, 1H, 1.47, 7.77), δ 7.01 (td, 1H, 1.47, 8.31), δ 6.96 (d, 2H, 5.87), δ 6.90 (tt, 2H, 1.47, 7.83), δ 6.69 (d, 1H, 7.83), δ 6.57 (m, 1H), δ 6.36 (m, 2H), δ 5.82 (d, 1H, 7.83), δ 2.32 (s, 3H), δ 0.50 (s, 3H)

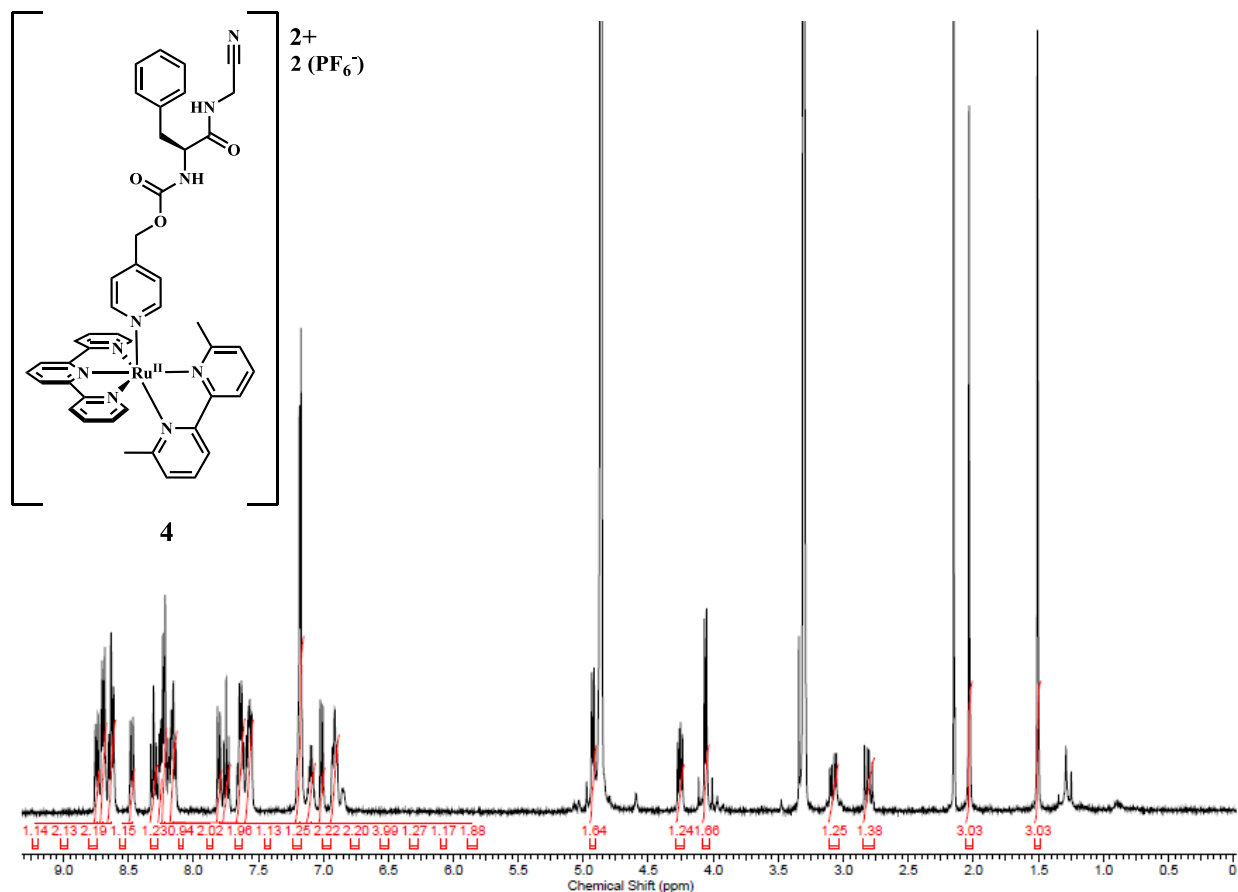


Figure [4.1.0].9 ^1H NMR of Complex **4**.

^1H NMR spectroscopy of **4** was performed in methanol- d_4 , and the resonances were referenced to the residual methanol signal on the Varian FT-NMR Mercury 400: δ 8.74 (d, 1H, 7.83), δ 8.69 (m, 2H), δ 8.63 (t, 2H, 7.83), δ 8.47 (d, 1H, 7.83), δ 8.31 (t, 1H, 8.31), δ 8.26 (d, 1H, 5.87), δ 8.23 (d, 2H, 7.83), δ 8.17 (m, 2H), δ 7.80 (d, 1H, 7.83), δ 7.75 (m, 1H), δ 7.64 (m, 2H), δ 7.57 (m, 2H), δ 7.18 (m, 4H), δ 7.10 (sext, 1H, 4.40), δ 7.01 (d, 1H, 7.83), δ 6.92 (t, 2H, 6.85), δ 4.93 (d, 1H, 6.85), δ 4.26 (dd, 1H, 5.87, 9.29), δ 4.05 (d, 1H, 6.85), δ 3.08 (dd, 1H, 5.87, 13.83), δ 2.81 (dd, 1H, 9.29, 13.83), δ 2.03 (s, 3H), δ 1.51 (s, 3H)

MS (ESI) performed in methanol. m/z : $[M + H]^+$ Calcd for $[C_{45}H_{41}N_9O_3Ru]^+$: 996.21, 997.21, 998.21, 999.20, 1000.20, 1001.20, 1002.20, 1003.20, 1004.20, 1005.21, 1006.21; Found: 996.33, 997.33, 998.29, 999.24, 1000.45, 1001.59, 1002.75, 1004.00, 1004.83, 1005.86, 1006.86

MS (ESI) performed in methanol. m/z : $[M + H]^{2+}$ Calcd for $[C_{45}H_{41}N_9O_3Ru]^{2+}$: 428.62; Found: 428.55.

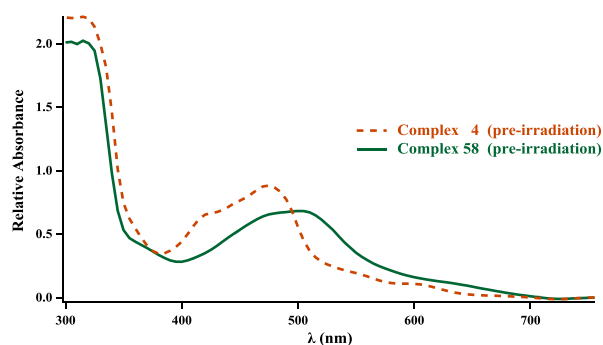


Figure [4.1.0].10 Superimposed UV-Vis Spectra of Complex **4** & **59**. The UV-Vis spectroscopies of complexes **4** and **58** were performed using methanol. This confirms that a hexa-pyridyl complex was synthesized due to the form of the spectrum and maximum absorption.

The experimental λ_{\max} values are as follows:

λ_{\max} of Complex **4** = 475 nm (w. shoulder at 421 nm)

λ_{\max} of Complex **58** = 500 nm.

4.2 PHOTOLYSIS DATA

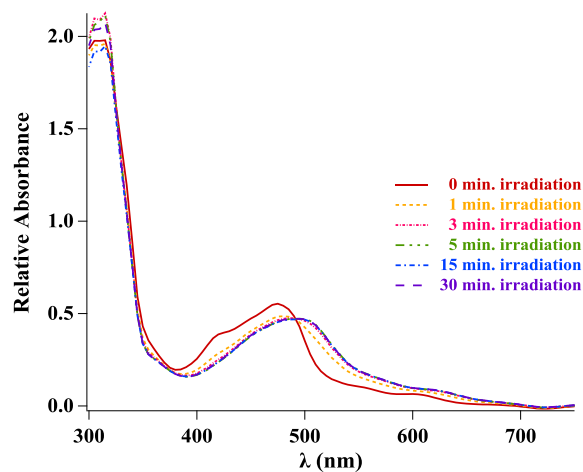


Figure [4.2.0].1 UV-Vis-Photolysis data.

The experimentation of complex **4** was performed in methanol. The hexa-pyridyl complex was not observed after 1 minute of irradiation. This suggests that the monodentate pyridyl ligand was release upon irradiation.

4.3 DATA OF ENZYME INHIBITION ASSAYS

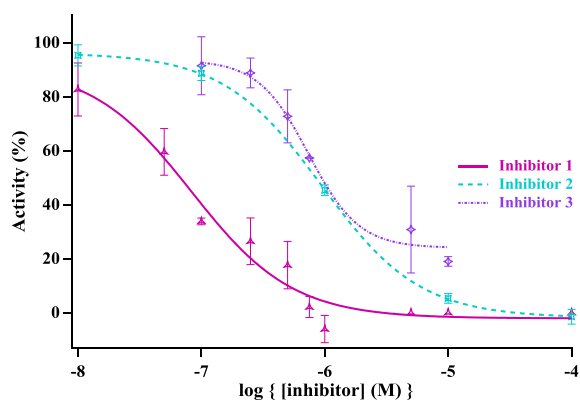


Figure [4.3.0].1 Enzyme assay data of the uncaged CST-K inhibitors.

The IC_{50} values of the free inhibitors were found experimentally using a CST-K enzyme assay protocol. The error bars represent the standard deviation of the mean of three independently prepared sample.

The experimental IC_{50} values are as follows:

IC_{50} of **1** = 67 nM

IC_{50} of **2** = 843 nM

IC_{50} of **3** = 942 nM

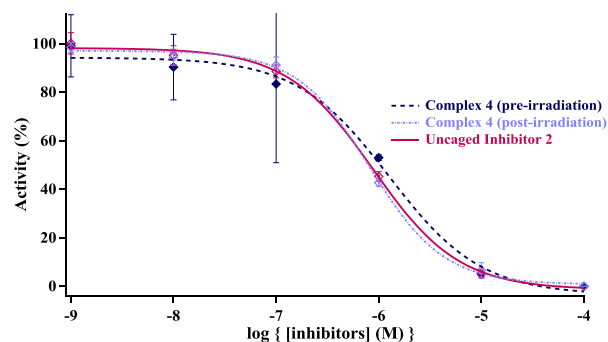


Figure [4.3.0].2 Light inhibition enzyme assay data of the caged CST-K inhibitors plot against the respective uncaged inhibitor **2**.

Dark/light IC_{50} ratio of complex **4** was found using a CST-K enzyme protocol. The dark/light IC_{50} data of the caged inhibitor is plot against the free inhibitor, **2**, for comparison. The error bars represent the standard deviation of the mean of three independently prepared sample.

The experimental IC_{50} values are as follows:

IC_{50} of **4** (pre-irradiation) = 1035 nM

IC_{50} of **4** (post-irradiation) = 794 nM

IC_{50} of **2** (uncaged) = 843 nM.

Chapter 5. Clarifications & Contributions

This study was one in a series, being conducted by the Kodanko Lab that investigates ^(a)the IC_{50} of modified, known inhibitors of cysteine cathepsins (CSTs) and ^(b)the light/dark IC_{50} ratio of the Ru^{II} complexed inhibitor.⁸³ In these studies, the known inhibitors were modified by replacing a phenyl substituent with a pyridyl substituent. This allowed dative binding of the inhibitor to the Ru^{II} chaperone at the nitrogen heteroatom.⁷⁸ Prior to this investment, known dipeptide CST inhibitors were caged at the nitrile group without modification.⁷⁹ However, recent studies showed that Ru^{II} chaperone had a higher binding affinity for the pyridyl group than the nitrile group.⁷⁸ Laboratory experiments also showed that the pyridyl-bound substances had a greater stability in growth media (Li, A; Kodanko, J. Unpublished results). Other inhibitors that are modified and investigated in this series, include irreversible epoxysuccinyl inhibitors,⁸³ and reversible dipeptide inhibitors reported here. The epoxysuccinyl inhibitors are being investigated for inhibition of CST-L and for papain binding affinity.⁸³ They will be referenced in comparison to the dipeptide inhibitor below. The reported dipeptide aminoacetonitrile inhibitor was investigated in relation to cysteine CST-K.

CST-K is a regulatory endopeptidase.³ It binds the substrate at the active site and catalyzes the lysis of the substrate at internal peptide bonds. The activity of these types of enzymes, is therefore described according to its ability to bind a substrate and lyse its peptide bonds. At the active site, the bond breaker (catalytic site) lies between subsites that lock specific substrates into the active site. This active site generally has four important, well-elucidated subsites ranging from S_2 to S_2' , S_3 is also well known, though less important. As such, inhibitors are synthesized such that the P_3 to P_2' substituents have high binding affinity to their corresponding subsites. Other

subsites beyond S_3 and S_2' have not been clearly elucidated, and are not usually a major focus in synthesis. The dipeptide inhibitors presented here bind S_3 – S_1 .²⁷

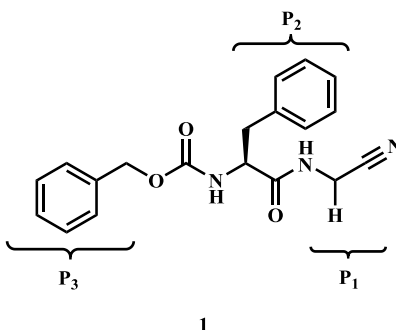


Figure [5.0.0].1 Schechter and Berger residue assignments for inhibitor **1**.

As with previous research in the Kodanko lab,⁸³ exchanging the phenyl ring at P_2 or P_3 with a pyridyl ring was expected to produce increased or similar inhibitory activity to the original inhibitor. Binding of P_3 to the $[Ru^{II}]$ chaperone was also postulated to afford spatio-temporal control over inhibition by way of steric hindrance and decreased binding affinity at P_3 .

The parent inhibitor used had previously been studied by Löser *et alia*.²⁵ In 2005, they showed that synthetic CST-K inhibitors are most active with hydrophobic leucinyl at the P_2 position. However, the compounds presented herein avoid the use of leucinyl as there are no known cageable of this group that would allow for a comparative analysis. The phenyl moiety was instead exchanged with structurally similar pyridyl at P_3 and P_2 instead. The aromatic substituents interact favorably with the S_2 site of CST-K. The inhibitory activity of the cageable and uncageable inhibitors were thus easily compared. The P_2 side chain of the compounds under analysis is therefore, either phenylalanyl or 4-pyridylalanyl, and the P_3 side chain is either carboxybenzyl (Cbz) or carboxy-4-pyridylmethyl (C4pz).

By IC_{50} analysis, inhibitor **2** was 13 times less potent than the parent inhibitor **1**, and inhibitor **3** was 14 times less potent than inhibitor **1**. These results highlight the structural

importance of the P₂ and the P₃ group and their interaction with the subsites of the enzyme. It is also important to note that the structural change at P₂ affected inhibition much more than the structural change at P₃. The findings are not in agreement with the hypothesis and prior studies.⁹

83

The P₁ residue-S₁ subsite interaction

Because the S₁ subsite is adjacent to the catalytic site, a well-tolerated binding or non-binding residue is important for a high substrate binding affinity.³ Though a side chain seems to be unnecessary at this site, a non-proteinogenic side chain was shown to increase the metabolic stability, potency and binding affinity of the inhibitor.⁹ In an account by Altman *et alia*, inhibition increased 4-fold when a benzyloxy group was placed at P₁, in comparison to a hydride however, increasing or decreasing the steric bulk from this point resulted in a loss of activity; S₁ seems to be an all-or-nothing subsite. The P₁ residue did not include a side chain for either of the amino acids used.

The P₂ residue-S₂ subsite interaction

The S₂ and S₁' sites are responsible for the diversity and selectivity of the active site.³ S₂ is well known for accommodating elastic and bulky amino acids; it is a “true deep pocket” and plays a significant role in in facilitating strong binding. This interaction in combination with the covalent thioimidate formation is the most crucial to binding and inhibition.²⁵ The importance of a side chain at the P₂ residue is unquestionable; when glycine is used the inhibitor is completely unreactive. Rigidization and reduction of bulk at this residue typically reduces the potency of CST-K inhibition. One example of this is the change from leucynyl to phenylalanyl. The phenyl to pyridyl exchange here makes for a slightly smaller aromatic ring and a more basic residue.

Although introducing a basic heteroatom improves the solubility and reduces the metabolism of inhibitors, it also increases the hydrogen-bonding capacity of the inhibitor and the hydrophilicity of the residue.⁹⁴ This destabilizes its interaction with the hydrophobic S₂ subsite and stabilizes interaction with residues in the vicinity of the active site, interrupting the usual binding arrangement of the substrate.²⁵ It is also important to note that the experiment were carried out at pH 5.5. At this pH, the pyridine substituent is likely charged and less hydrophobic. These findings support the established notion that the enzyme is selective at S₂ and sensitive to changes at P₂.

The P₃ residue-S₃ subsite interaction

S₃ is less important and more promiscuous than S₂ and S₁ for substrate selectivity.²⁷ The locking of P₃ into S₃ is mediated only by side chain contact over its relatively wide area. In contrast, both main and side chain contact is necessary for S₂-S_{2'} subsites. The S₃ binding site has not been well-defined, thus an accurate trend is yet to be cited. Bulkier substituents at P₃ have been shown to enhance the P₃-S₃ interactions, although, an increase in activity was observed when the *tert*-butyl moiety was replaced with the phenyl moiety.²⁵ In these inhibitor analogues, the introduction of the heteroatom typically affects binding much less than at the S₂ site;³ possibly due to an increase in hydrophilicity.⁹ Polar residues were also found to be well-tolerated at S₃. This is seen in the IC₅₀ increase from **7** to **8** shown in table [5.0.0].1. The decrease in activity that was observed when the 4-pyridyl moiety was used is inconsistent with these findings.

These findings are in drastic contrast to the data reported by Huisman *et alia*.⁸³ The authors noted very little change in inhibition data when the inhibitors were modified. It is however, extremely important to note that the target of Huisman's inhibitors were papain and CST-L which have different subsite characteristics, promiscuity and interaction requirements than CST-K. A closer look at the inhibitors listed in this study also reveal that the inhibitor is able to lock into the

enzyme at P₃-P₁ and P₁' sites. Incorporating subsites on both sides of the warhead may increase the binding stability of the inhibitor to the enzyme.

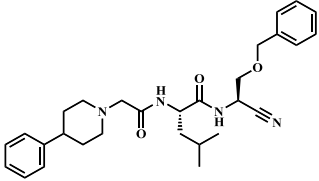
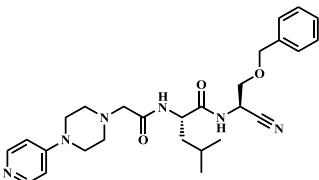
Inhibitor	IC ₅₀ (nM) (recomb. human CSTK)
	83
	9

Table [5.0.0].1 Evidence for increase in efficacy due to increase in basicity at P₃ residue, contrary to the observation presented here

Ru^{II}-complexed inhibitor 4

Of the two modified inhibitors synthesized, the compound with the lowest IC₅₀ was caged to a Ru^{II} metal chaperone at the N-heteroatom of the pyridine. Previously, we caged the inhibitor to the chaperone at the N-heteroatom of the terminal nitrile.⁷⁹ The strategy for investigating aminoacetonitriles changed quite a bit from previous studies due to increased stability in growth media as described in the following paragraph.

In prior studies, the inhibitor was caged at the nitrile terminal rather than through a cageable derivative of the inhibitor. This change was deemed necessary due to the instability of [Ru^{II}]-N≡CR in growth media. The complexes could be unstable due to oxidation of Ru^{II} to Ru^{III} followed by the hydrolysis of the nitrile to an amide.⁹⁵ However, the low dissociation quantum yield of [Ru^{II}(bpy)₂(py)₂]²⁺ highlighted the need for a new chaperone.⁷⁸ The [Ru^{II}]-py bond was too stable for photodissociation. Knoll *et alia* reported a [Ru^{II}(dmbpy)(terpy)]²⁺ chaperone that surpassed the

$[\text{Ru}^{\text{II}}(\text{bpy})_2]^{2+}$ chaperone in pyridine photodissociation with a 27 fold difference in quantum yield. As such, $[\text{Ru}^{\text{II}}(\text{dmbpy})(\text{terpy})(\text{py-R})]^{2+}$ derivatives are currently being studied and were used here. The trend for increasing photodissociation quantum yield with increased steric crowding around the metal center is also seen in other $[\text{Ru}^{\text{II}}]$. See table [5.0.0].2⁹.

	Dichloromethane	Acetonitrile
$[\text{Ru}^{\text{II}}(\text{terpy})(\text{dmbpy})(\text{py})]^{2+}$		$\phi_{500\text{nm}} = 0.16$
$[\text{Ru}^{\text{II}}(\text{terpy})(\text{bpy})(\text{py})]^{2+}$		$\phi_{500\text{nm}} < 0.0001$
$[\text{Ru}^{\text{II}}(\text{dmbpy})_2(\text{py})_2]^{2+}$		$\phi_{436\text{nm}} = 0.025$
$[\text{Ru}^{\text{II}}(\text{bpy})_2(\text{py})_2]^{2+}$		$\phi_{436\text{nm}} = 0.0059$
$[\text{Ru}^{\text{II}}(\text{tpa})(\text{py})_2]^{2+}$	$\phi_{400\text{nm}} = 0.0097$	
$[\text{Ru}^{\text{II}}(\text{tpa})(\text{MeCN})_2]^{2+}$	$\phi_{400\text{nm}} = 0.016$	
$[\text{Ru}^{\text{II}}(\text{mtpa})(\text{MeCN})_2]^{2+}$	$\phi_{400\text{nm}} = 0.041$	

Table [5.0.0].2 Comparison of the quantum yields of dissociation for 3 sets of chaperones. The chaperones of each set have different degrees of metal centered bulk.

The UV-vis photodissociation experiment showed the once irradiated, the inhibitor(s) was photo-released within minutes using white light. As of late, Ru^{II} metal chaperones are tuned by altering the heteroatomic bidentate ligand, bipyridyl.^{78-79, 84, 96-97} Many analogues of bipyridyl have been investigated for their effect on the rate of photo-release of active ligands. Heteroatomic tridentate and tetradentate ligands have also been used. In the Kodanko lab, photo-caging work started with $[\text{Ru}^{\text{II}}(\text{bpy})_2]^{2+}$, followed by $[\text{Ru}^{\text{II}}(\text{tpa})]^{2+}$ complexes, and now using $[\text{Ru}^{\text{II}}(\text{terpy})(\text{bpy})]^{2+}$ complexes and derivatives. With this development came the acknowledgment of pyridine as a cageable ligand.

⁹ tpa - tris(2-pyridylmethyl)amine
mtpa - tris(6-methyl-2-pyridylmethyl)amine;
MeCN - acetonitrile

The metal chaperone used in this study was first investigated, by the Turro group at Ohio State University, for efficient photodissociation of pyridine and pyridine derivatives.^{78,97} Although chaperones $[\text{Ru}^{\text{II}}(\text{bpy})_2]^{2+}$ and $[\text{Ru}^{\text{II}}(\text{bpy})(\text{terpy})]^{2+}$ show good photodissociation for nitriles, photodissociation is poor for pyridine and pyridine derivatives. This is due to the stability of the complex and the strong $[\text{Ru}^{\text{II}}]\text{-py}$ bond. Knoll *et alia* observed that an increase of steric bulk on the ancillary ligands of Ru^{II} chaperones weakened the $\text{Ru}^{\text{II}}\text{-py}$ bond, thus increased its quantum yield of photodissociation. Steric bulk of the bidentate ligand was increased by placing methyl substituents at the 6 and 6' positions of the bpy ligand: $[\text{Ru}^{\text{II}}(\text{dmbpy})(\text{terpy})]^{2+}$.

The dark/light IC_{50} ratio (DLIR) in this experiment was expected to be significant based on previously reported experiments.⁷⁹ The DLIR is a measure of the ability of the chaperone to prohibit inhibition prior to irradiation and facilitate inhibition post-irradiation. This is the main facet being exploited for spatio-temporal control with PACT.

Respondek *et alia* reported a DLIR of 35 and 88 for complexes **35** and **36**, respectively. The DLIR of complex **4** is 1.3. The most obvious difference between **35/36** and **4** is the dual-release capacity of **35** and **36** versus the single release capacity of **4**, although this plays an insignificant role in the observed ratio. Instead, the low DLIR is likely due to the ability of the caged complex to inhibit the CST-K enzyme without irradiation. Recall the structural geometry of **4**, Fig [1.2.0].2, the nitrile warhead is terminal to the complex and unhindered sterically or otherwise. This is in contrast to **35/36**, where the inhibitor is bound to the metal center by the warhead, *id est*, both sterically and datively hindered. In such a case, it is extremely difficult for the enzyme to interact with the warhead. The complex must first be photo-activated, enabling the release of the molecule, before inhibition occurs. Whereas, in **4**, no photo-activation is necessary

since the nitrile warhead is dangling and unhindered. The low DLIR observed is a result of a similar IC_{50} before and after photo-activated release.

This phenomenon was also seen in other experiments performed by a co-researcher in the investigation of papain binding.⁸³ Huisman *et alia* has reported a relative (dark v. light) second order rate constant¹⁰ (k_{rel}) of 10 for complex **43**, whereas complex **40** had a k_{rel} of 1. In complex **43**, the inhibitor is caged such that the epoxysuccinyl warhead is sterically crowded and not easily accessed by substrate prior to irradiation. Whereas, the epoxysuccinyl warhead of **40** is not hindered and is open to attack showing little inhibitory difference whether caged or released, like **4**. Similarly, the metal complex may not have been bulky enough to prohibit binding to the CST-K inhibitor. It is therefore fair to conclude that metallo-binding that renders the warhead unhindered will not contribute to spatio-temporal control over CST inhibition in enzyme assays. These binding arrangements should be coordinated such that the bulk of the ancillary ligands can obstruct interaction with the CST enzyme.

This may also speak to the promiscuity and large size of the P_3 site. It is also possible that the P_3 subsite is large and promiscuous enough to interact with the chaperone. It will be interesting to discover whether the DLIR would be similar in vitro where there is a possibility Ru^{II} -protein complexation that may prevent binding of the caged inhibitor. Further investigations should also include caging at P_2 to determine whether there is enough steric hindrance to reduce inhibition prior to irradiation of the caged inhibitor.

¹⁰ $k_{rel} = (k_{inact}/K_i)_{dark} \div (k_{inact}/K_i)_{light}$

Chapter 6. Conclusion

In conclusion, a new binding protocol for Ru^{II}-dipeptide inhibitor complexes was investigated. By the new protocol, inhibitors are bound by a pyridyl substituent,⁸²⁻⁸³ as an alternative to the nitrile substituent previously reported by the Kodanko group.^{5, 79, 96, 98}

The thesis describes the successful synthesis of a known CST-K inhibitor and two new derivatives. Upon determining and comparing the IC₅₀ of the inhibitors, it became evident that increasing the basicity of the P₂ and P₃ residues decreases the efficacy of the inhibitor to bind to the CST-K active site. These findings are not in complete agreement with previous studies.^{25, 83} The decrease in efficacy resulting from the increase in basicity at P₂ is supported by the literature. However, the decrease in efficacy resulting from the increase in basicity at P₃ is not. The observed deviation may be a result of side-interactions with ionic amino acid residues and hydrogen bond donors and acceptors. The ability of the complex to bind CST-K before photo-release of the dipeptide inhibitor also speaks to the size and promiscuity of the CST-K active site.

The inhibitors described have been successfully caged and photo-released from the synthesized Ru^{II} chaperone. However, the resulting position of the nitrile warhead made it difficult to achieve spatio-temporal control over CST-K binding. This results from the terminal and unhindered position of the nitrile warhead.

The study has shown that for a substantial DLIR/*k*_{rel} to be established, the photo-activatable complex must be designed such that the warhead of the inhibitor is hindered prior to photo-release from the chaperone. This thesis will contribute to the conceptual development of Ru^{II}-inhibitor complexes and future studies of the Kodanko lab as spatio-temporally controlled protein inhibition is pursued. From this and prior studies,^{5, 79, 83} it is so-far determined that successful spatio-temporal

control is best achieved when the nitrile warhead is directly bound to the Ru^{II} complex or sufficiently shielded from attack by the substrate via other measures. As seen here, when the warhead is terminal and far-removed from the Ru^{II} chaperone it is not sufficiently hindered so as to avoid binding the substrate prior to irradiation.

References

1. Turk, V., Cysteine cathepsins: from structure, unction and regulation to new frontiers. *iochim Biophys Acta* **2012**, 68-88.
2. Costa, A. G.; Cusano, N. E.; Silva, B. C.; Cremers, S.; Bilezikian, J. P., Cathepsin K: its skeletal actions and role as a therapeutic target in osteoporosis. *Nature Reviews Rheumatology* **2011**, 7 (8), 447-456.
3. Lecaille, F.; Brömme, D.; Lalmanach, G., Biochemical properties and regulation of cathepsin K activity. *Biochimie* **2008**, 90 (2), 208-226.
4. Mohamed, M. M.; Sloane, B. F., Cysteine cathepsins: multifunctional enzymes in cancer. *Nature Reviews Cancer* **2006**, 6 (10), 764-775.
5. Ramalho, S. D.; Sharma, R.; White, J. K.; Aggarwal, N.; Chalasani, A.; Sameni, M.; Moin, K.; Vieira, P. C.; Turro, C.; Kodanko, J. J., Imaging sites of inhibition of proteolysis in pathomimetic human breast cancer cultures by light-activated ruthenium compound. *PloS one* **2015**, 10 (11), e0142527.
6. Cooper, G. M.; Hausman, R. E., *The cell*. Sinauer Associates Sunderland: 2000.
7. MedIndia. World Cancer Death Clock. 2016.
http://www.medindia.net/patients/calculators/world_cancer_clock.asp (accessed 12/29/2016).
8. Garber, K., Two pioneering osteoporosis drugs finally approach approval. *Nat Rev Drug Discov* **2016**, 15 (7), 445-446.

9. Altmann, E.; Aichholz, R.; Betschart, C.; Buhl, T.; Green, J.; Lattmann, R.; Missbach, M., Dipeptide nitrile inhibitors of cathepsin K. *Bioorganic & medicinal chemistry letters* **2006**, *16* (9), 2549-2554.
10. Levina, A.; Mitra, A.; Lay, P. A., Recent developments in ruthenium anticancer drugs. *Metallomics* **2009**, *1* (6), 458-70.
11. Brömme, D.; Lecaille, F., Cathepsin K inhibitors for osteoporosis and potential off-target effects. *Expert opinion on investigational drugs* **2009**, *18* (5), 585-600.
12. Venditto, V. J.; Simanek, E. E., Cancer therapies utilizing the camptothecins: a review of the in vivo literature. *Molecular pharmaceutics* **2010**, *7* (2), 307-349.
13. Gocheva, V.; Joyce, J. A., Cysteine cathepsins and the cutting edge of cancer invasion. *Cell cycle* **2007**, *6* (1), 60-64.
14. Kovac, A. L., Prevention and treatment of postoperative nausea and vomiting. *Drugs* **2000**, *59* (2), 213-243.
15. Aujard, I.; Benbrahim, C.; Gouget, M.; Ruel, O.; Baudin, J. B.; Neveu, P.; Jullien, L., o-Nitrobenzyl Photolabile Protecting Groups with Red-Shifted Absorption: Syntheses and Uncaging Cross-Sections for One-and Two-Photon Excitation. *Chemistry—A European Journal* **2006**, *12* (26), 6865-6879.
16. Auzel, F., Upconversion and anti-stokes processes with f and d ions in solids. *Chemical reviews* **2004**, *104* (1), 139-174.

17. Cuenoud, B.; Tarasow, T. M.; Schepartz, A., A new strategy for directed protein cleavage. *Tetrahedron letters* **1992**, *33* (7), 895-898.
18. Dakin, K.; Li, W.-h., Infrared-LAMP: two-photon uncaging and imaging of gap junctional communication in three dimensions. *Nature methods* **2006**, *3* (12), 959-959.
19. Hagen, V.; Frings, S.; Bendig, J.; Lorenz, D.; Wiesner, B.; Kaupp, U. B., Fluorescence Spectroscopic Quantification of the Release of Cyclic Nucleotides from Photocleavable [Bis (carboxymethoxy) coumarin-4-yl] methyl Esters inside Cells. *Angewandte Chemie International Edition* **2002**, *41* (19), 3625-3628.
20. Tran, C.; Gallavardin, T.; Petit, M.; Slimi, R.; Dhimane, H.; Blanchard-Desce, M.; Acher, F. C.; Ogden, D.; Dalko, P. I., Two-photon “caging” groups: effect of position isomery on the photorelease properties of aminoquinoline-derived photolabile protecting groups. *Organic letters* **2015**, *17* (3), 402-405.
21. Wachter, E.; Heidary, D. K.; Howerton, B. S.; Parkin, S.; Glazer, E. C., Light-activated ruthenium complexes photobind DNA and are cytotoxic in the photodynamic therapy window. *Chemical Communications* **2012**, *48* (77), 9649-9651.
22. Farrer, N. J.; Salassa, L.; Sadler, P. J., Photoactivated chemotherapy (PACT): the potential of excited-state d-block metals in medicine. *Dalton Transactions* **2009**, (48), 10690-10701.
23. Lee, J.; Yu, P.; Xiao, X.; Kodadek, T., A general system for evaluating the efficiency of chromophore-assisted light inactivation (CALI) of proteins reveals Ru (II) tris-bipyridyl as an unusually efficient “warhead”. *Molecular BioSystems* **2008**, *4* (1), 59-65.

24. Powers, J. C.; Asgian, J. L.; Ekici, Ö. D.; James, K. E., Irreversible inhibitors of serine, cysteine, and threonine proteases. *Chemical reviews* **2002**, *102* (12), 4639-4750.
25. Löser, R.; Schilling, K.; Dimmig, E.; Gütschow, M., Interaction of papain-like cysteine proteases with dipeptide-derived nitriles. *Journal of medicinal chemistry* **2005**, *48* (24), 7688-7707.
26. Schechter, I.; Berger, A., On the size of the active site in proteases. I. Papain. *Biochemical and Biophysical Research Communications* **1967**, *27* (2), 157-162.
27. Turk, B.; Turk, D.; Turk, V., Lysosomal cysteine proteases: more than scavengers. *Biochimica et Biophysica Acta (BBA)-Protein Structure and Molecular Enzymology* **2000**, *1477* (1), 98-111.
28. Lutgens, S. P. M.; Cleutjens, K. B. J. M.; Daemen, M. J. A. P.; Heeneman, S., Cathepsin cysteine proteases in cardiovascular disease. *The FASEB Journal* **2007**, *21* (12), 3029-3041.
29. Brömme, D.; Okamoto, K., Human cathepsin O2, a novel cysteine protease highly expressed in osteoclastomas and ovary molecular cloning, sequencing and tissue distribution. *Biological chemistry Hoppe-Seyler* **1995**, *376* (6), 379-384.
30. Frizler, M.; Stirnberg, M.; Sisay, M. T.; Gutschow, M., Development of nitrile-based peptidic inhibitors of cysteine cathepsins. *Current topics in medicinal chemistry* **2010**, *10* (3), 294-322.
31. Singh, J.; Petter, R. C.; Baillie, T. A.; Whitty, A., The resurgence of covalent drugs. *Nature reviews Drug discovery* **2011**, *10* (4), 307-317.

32. Altmann, E.; Renaud, J.; Green, J.; Farley, D.; Cutting, B.; Jahnke, W., Arylaminoethyl amides as novel non-covalent cathepsin K inhibitors. *Journal of medicinal chemistry* **2002**, *45* (12), 2352-2354.
33. Kim, T.-S.; Tasker, A. S., Non-covalent cathepsin K inhibitors for the treatment of osteoporosis. *Current topics in medicinal chemistry* **2006**, *6* (4), 355-360.
34. Altmann, E.; Green, J.; Tintelnot-Blomley, M., Arylaminoethyl amides as inhibitors of the cysteine protease cathepsin K—investigating P 1' substituents. *Bioorganic & medicinal chemistry letters* **2003**, *13* (12), 1997-2001.
35. Oballa, R. M.; Truchon, J.-F.; Bayly, C. I.; Chauret, N.; Day, S.; Crane, S.; Berthelette, C., A generally applicable method for assessing the electrophilicity and reactivity of diverse nitrile-containing compounds. *Bioorganic & medicinal chemistry letters* **2007**, *17* (4), 998-1002.
36. Löser, R.; Frizler, M.; Schilling, K.; Gütschow, M., Azadipeptide Nitriles: Highly Potent and Proteolytically Stable Inhibitors of Papain-Like Cysteine Proteases. *Angewandte Chemie International Edition* **2008**, *47* (23), 4331-4334.
37. Mullard, A., Merck & Co. drops osteoporosis drug odanacatib. *Nat Rev Drug Discov* **2016**, *15* (10), 669-669.
38. Asboth, B.; Stokum, E.; Khan, I. U.; Polgar, L., Mechanism of action of cysteine proteinases: oxyanion binding site is not essential in the hydrolysis of specific substrates. *Biochemistry* **1985**, *24* (3), 606-609.

39. Horstkotte, E.; Schröder, T.; Niewöhner, J.; Thiel, E.; Jay, D. G.; Henning, S. W., Toward Understanding the Mechanism of Chromophore-assisted Laser Inactivation—Evidence for the Primary Photochemical Steps¶. *Photochemistry and photobiology* **2005**, *81* (2), 358-366.
40. Wild, M.; Griebel, J.; Hajduk, A.; Friedrich, D.; Stark, A.; Abel, B.; Siefermann, K. R., Efficient synthesis of triarylamine-based dyes for p-type dye-sensitized solar cells. *Scientific Reports* **2016**, *6*, 26263.
41. Velusamy, M.; Justin Thomas, K. R.; Lin, J. T.; Hsu, Y.-C.; Ho, K.-C., Organic Dyes Incorporating Low-Band-Gap Chromophores for Dye-Sensitized Solar Cells. *Organic Letters* **2005**, *7* (10), 1899-1902.
42. Jay, D. G., Selective destruction of protein function by chromophore-assisted laser inactivation. *Proceedings of the National Academy of Sciences* **1988**, *85* (15), 5454-5458.
43. Jacobson, K.; Rajfur, Z.; Vitriol, E.; Hahn, K., Chromophore-assisted laser inactivation in cell biology. *Trends in cell biology* **2008**, *18* (9), 443-450.
44. Hoffman-Kim, D.; Diefenbach, T. J.; Eustace, B. K.; Jay, D. G., Chromophore-Assisted Laser Inactivation. *Methods in cell biology* **2007**, *82*, 335-354.
45. Eustace, B. K.; Buchstaller, A.; Jay, D. G., Adapting chromophore-assisted laser inactivation for high throughput functional proteomics. *Briefings in Functional Genomics and Proteomics* **2002**, *1*, 257-265.
46. Beermann, A. E.; Jay, D. G., Chromophore-assisted laser inactivation of cellular proteins. *Methods in cell biology* **1994**, *44*, 715-732.

47. Klán, P.; Šolomek, T. s.; Bochet, C. G.; Blanc, A. l.; Givens, R.; Rubina, M.; Popik, V.; Kostikov, A.; Wirz, J., Photoremovable protecting groups in chemistry and biology: reaction mechanisms and efficacy. *Chemical reviews* **2012**, *113* (1), 119-191.
48. Pelliccioli, A. P.; Wirz, J., Photoremovable protecting groups: reaction mechanisms and applications. *Photochemical & photobiological sciences* **2002**, *1* (7), 441-458.
49. Jana, A.; Saha, B.; Karthik, S.; Barman, S.; Iqbal, M.; Ghosh, S. K.; Singh, N. P., Fluorescent photoremovable precursor (acridin-9-ylmethyl) ester: synthesis, photophysical, photochemical and biological applications. *Photochemical & Photobiological Sciences* **2013**, *12* (6), 1041-1052.
50. Jana, A.; Atta, S.; Sarkar, S. K.; Singh, N. P., 1-Acetylpyrene with dual functions as an environment-sensitive fluorophore and fluorescent photoremovable protecting group. *Tetrahedron* **2010**, *66* (52), 9798-9807.
51. Zhu, Y.; Pavlos, C. M.; Toscano, J. P.; Dore, T. M., 8-Bromo-7-hydroxyquinoline as a photoremovable protecting group for physiological use: mechanism and scope. *Journal of the American Chemical Society* **2006**, *128* (13), 4267-4276.
52. Kulikov, A.; Arumugam, S.; Popik, V. V., Photolabile protection of alcohols, phenols, and carboxylic acids with 3-hydroxy-2-naphthalenemethanol. *The Journal of organic chemistry* **2008**, *73* (19), 7611-7615.
53. Schmidt, R.; Geissler, D.; Hagen, V.; Bendig, J., Mechanism of photocleavage of (coumarin-4-yl) methyl esters. *The Journal of Physical Chemistry A* **2007**, *111* (26), 5768-5774.

54. Goswami, P. P.; Syed, A.; Beck, C. L.; Albright, T. R.; Mahoney, K. M.; Unash, R.; Smith, E. A.; Winter, A. H., BODIPY-derived photoremovable protecting groups unmasked with green light. *Journal of the American Chemical Society* **2015**, *137* (11), 3783-3786.
55. Venkatesh, Y.; Rajesh, Y.; Karthik, S.; Chetan, A.; Mandal, M.; Jana, A.; Singh, N. P., Photocaging of Single and Dual (Similar or Different) Carboxylic and Amino Acids by Acetyl Carbazole and its Application as Dual Drug Delivery in Cancer Therapy. *The Journal of Organic Chemistry* **2016**, *81* (22), 11168-11175.
56. Yang, Y.; Shao, Q.; Deng, R.; Wang, C.; Teng, X.; Cheng, K.; Cheng, Z.; Huang, L.; Liu, Z.; Liu, X., In vitro and in vivo uncaging and bioluminescence imaging by using photocaged upconversion nanoparticles. *Angewandte Chemie International Edition* **2012**, *51* (13), 3125-3129.
57. Li, W., Near-Infrared Upconversion Controls Photocaged Cell Adhesion. *Journal of the American Chemical Society* *136* (6), 2248-2251.
58. Brown, E. B.; Shear, J. B.; Adams, S. R.; Tsien, R. Y.; Webb, W. W., Photolysis of caged calcium in femtoliter volumes using two-photon excitation. *Biophysical journal* **1999**, *76* (1), 489-499.
59. Weissleder, R., A clearer vision for in vivo imaging. *Nature biotechnology* **2001**, *19* (4), 316-316.
60. Weissleder, R.; Mahmood, U., Molecular imaging 1. *Radiology* **2001**, *219* (2), 316-333.

61. Dendramis, K. A.; Allen, P. B.; Reid, P. J.; Chiu, D. T., Spectrally tunable uncaging of biological stimuli from nanocapsules. *Chemical Communications* **2008**, (39), 4795-4797.
62. Falvey, D. E.; Sundararajan, C., Photoremovable protecting groups based on electron transfer chemistry. *Photochemical & Photobiological Sciences* **2004**, 3 (9), 831-838.
63. So, P. T.; Dong, C. Y.; Masters, B. R.; Berland, K. M., Two-photon excitation fluorescence microscopy. *Annual review of biomedical engineering* **2000**, 2 (1), 399-429.
64. Denk, W.; Strickler, J. H.; Webb, W. W., Two-photon laser scanning fluorescence microscopy. *Science* **1990**, 248 (4951), 73-76.
65. Banerjee, A.; Falvey, D. E., Protecting Groups That Can Be Removed through Photochemical Electron Transfer: Mechanistic and Product Studies on Photosensitized Release of Carboxylates from Phenacyl Esters. *The Journal of Organic Chemistry* **1997**, 62 (18), 6245-6251.
66. Bomben, P. G.; Gordon, T. J.; Schott, E.; Berlinguette, C. P., A Trisheteroleptic Cyclometalated RuII Sensitizer that Enables High Power Output in a Dye-Sensitized Solar Cell. *Angewandte Chemie* **2011**, 123 (45), 10870-10873.
67. Dibenedetto, A.; Stufano, P.; Nocito, F.; Aresta, M., RuII-Mediated Hydrogen Transfer from Aqueous Glycerol to CO₂: From Waste to Value-Added Products. *ChemSusChem* **2011**, 4 (9), 1311-1315.
68. Hartinger, C. G.; Zorbas-Seifried, S.; Jakupec, M. A.; Kynast, B.; Zorbas, H.; Keppler, B. K., From bench to bedside—preclinical and early clinical development of the anticancer agent

indazolium trans-[tetrachlorobis (1H-indazole) ruthenate (III)](KP1019 or FFC14A). *Journal of inorganic biochemistry* **2006**, *100* (5), 891-904.

69. Vatansever, F.; de Melo, W. C.; Avci, P.; Vecchio, D.; Sadasivam, M.; Gupta, A.; Chandran, R.; Karimi, M.; Parizotto, N. A.; Yin, R., Antimicrobial strategies centered around reactive oxygen species–bactericidal antibiotics, photodynamic therapy, and beyond. *FEMS microbiology reviews* **2013**, *37* (6), 955-989.
70. Bayley, H.; Gasparro, F.; Edelson, R., Photoactivatable drugs. *Trends in Pharmacological Sciences* **1987**, *8* (4), 138-143.
71. Mari, C.; Gasser, G., Lightening up Ruthenium Complexes to Fight Cancer? *CHIMIA International Journal for Chemistry* **2015**, *69* (4), 176-181.
72. Smith, N. A.; Sadler, P. J., Photoactivatable metal complexes: from theory to applications in biotechnology and medicine. The Royal Society: 2013.
73. Clarke, M. J.; Bitler, S.; Rennert, D.; Buchbinder, M.; Kelman, A. D., Reduction and Subsequent Binding of Ruthenium Ions Catalyzed by Subcellular Components. *Journal of Inorganic Biochemistry* **1980**, *12* (1), 79-87.
74. Yasbin, R. E.; Matthews, C. R.; Clarke, M. J., Mutagenic and toxic effects of ruthenium. *Chemico-Biological Interactions* **1980**, *31* (3), 355-365.
75. Wiltshaw, E., Cisplatin in the treatment of cancer. *Platinum Metals Review* **1979**, *23* (3), 90-98.

76. Leanne B, J.; Ross W, B., Photodynamic therapy and the development of metal-based photosensitisers. *Metal-based drugs* **2008**, 2008.
77. Wilson, B. C.; Patterson, M. S., The physics, biophysics and technology of photodynamic therapy. *Physics in medicine and biology* **2008**, 53 (9), R61.
78. Knoll, J. D.; Albani, B. A.; Durr, C. B.; Turro, C., Unusually efficient pyridine photodissociation from Ru (II) complexes with sterically bulky bidentate ancillary ligands. *The Journal of Physical Chemistry A* **2014**, 118 (45), 10603-10610.
79. Respondek, T.; Sharma, R.; Herroon, M. K.; Garner, R. N.; Knoll, J. D.; Cueny, E.; Turro, C.; Podgorski, I.; Kodanko, J. J., Inhibition of Cathepsin Activity in a Cell-Based Assay by a Light-Activated Ruthenium Compound. *ChemMedChem* **2014**, 9 (6), 1306-1315.
80. In the studies presented a drug chaperone is referred to as the portion of the complex containing the Ru(II) metal center that is separated from the inhibitor upon irradiation.
81. Respondek, T.; Garner, R. N.; Herroon, M. K.; Podgorski, I.; Turro, C.; Kodanko, J. J., Light activation of a cysteine protease inhibitor: caging of a peptidomimetic nitrile with RuII (bpy) 2. *Journal of the American Chemical Society* **2011**, 133 (43), 17164-17167.
82. Li, A.; White, J. K.; Arora, K.; Herroon, M. K.; Martin, P. D.; Schlegel, H. B.; Podgorski, I.; Turro, C.; Kodanko, J. J., Selective Release of Aromatic Heterocycles from Ruthenium Tris (2-pyridylmethyl) amine with Visible Light. *Inorganic chemistry* **2015**, 55 (1), 10-12.

83. Huisman, M.; White, J. K.; Lewalski, V. G.; Podgorski, I.; Turro, C.; Kodanko, J. J., Caging the uncageable: using metal complex release for photochemical control over irreversible inhibition. *Chemical Communications* **2016**, 52 (85), 12590-12593.
84. Garner, R. N.; Gallucci, J. C.; Dunbar, K. R.; Turro, C., [Ru (bpy) 2 (5-cyanouracil) 2] 2+ as a potential light-activated dual-action therapeutic agent. *Inorganic chemistry* **2011**, 50 (19), 9213-9215.
85. Sgambellone, M. A.; David, A.; Garner, R. N.; Dunbar, K. R.; Turro, C., Cellular toxicity induced by the photorelease of a caged bioactive molecule: design of a potential dual-action Ru (II) complex. *Journal of the American Chemical Society* **2013**, 135 (30), 11274-11282.
86. Smith, N. A.; Zhang, P.; Greenough, S. E.; Horbury, M. D.; Clarkson, G. J.; McFeely, D.; Habtemariam, A.; Salassa, L.; Stavros, V. G.; Dowson, C. G., Combatting AMR: photoactivatable ruthenium (ii)-isoniazid complex exhibits rapid selective antimycobacterial activity. *Chemical Science* **2017**, 8 (1), 395-404.
87. Araújo, N.; Fontana, C. R.; Bagnato, V.; Gerbi, M., Photodynamic antimicrobial therapy of curcumin in biofilms and carious dentine. *Lasers in medical science* **2014**, 29 (2), 629-635.
88. Hamblin, M. R.; Hasan, T., Photodynamic therapy: a new antimicrobial approach to infectious disease? *Photochemical & Photobiological Sciences* **2004**, 3 (5), 436-450.
89. Ryskova, L.; Buchta, V.; Slezak, R., Photodynamic antimicrobial therapy. *Open Life Sciences* **2010**, 5 (4), 400-406.

90. Asahina, Y.; Kamitori, S.; Takao, T.; Nishi, N.; Hojo, H., Chemoenzymatic Synthesis of the Immunoglobulin Domain of Tim-3 Carrying a Complex-Type N-Glycan by Using a One-pot Ligation. *Angewandte Chemie International Edition* **2013**, *52* (37), 9733-9737.
91. Halpern, B.; Nitecki, D., The deblocking of t-butyloxycarbonyl-peptides with formic acid. *Tetrahedron letters* **1967**, *8* (31), 3031-3133.
92. Leising, R. A.; Kubow, S. A.; Churchill, M. R.; Buttrey, L. A.; Ziller, J. W.; Takeuchi, K. J., Synthesis, characterization, and x-ray crystal structure of nitro (terpyridine) bis (trimethylphosphine) ruthenium (1+) perchlorate. *Inorganic Chemistry* **1990**, *29* (7), 1306-1312.
93. Bahreman, A.; Limburg, B.; Siegler, M. A.; Bouwman, E.; Bonnet, S., Spontaneous Formation in the Dark, and Visible Light-Induced Cleavage, of a Ru-S Bond in Water: A Thermodynamic and Kinetic Study. *Inorganic chemistry* **2013**, *52* (16), 9456-9469.
94. Rafi, S. B.; Hearn, B. R.; Vedantham, P.; Jacobson, M. P.; Renslo, A. R., Predicting and improving the membrane permeability of peptidic small molecules. *Journal of medicinal chemistry* **2012**, *55* (7), 3163-3169.
95. Yeh, J.; Liu, K.; Lien, M. H.; Yeh, A., Nitrile Hydrolysis of 4-Cyanopyridinepentaammineruthenium (III) Complex. *Journal of the Chinese Chemical Society* **2003**, *50* (3A), 381-386.
96. Sharma, R.; Knoll, J. D.; Martin, P. D.; Podgorski, I.; Turro, C.; Kodanko, J. J., Ruthenium tris (2-pyridylmethyl) amine as an effective photocaging group for nitriles. *Inorganic chemistry* **2014**, *53* (7), 3272-3274.

97. Knoll, J. D.; Albani, B. A.; Turro, C., Excited state investigation of a new Ru (ii) complex for dual reactivity with low energy light. *Chemical Communications* **2015**, 51 (42), 8777-8780.
98. Prakash, J.; Kodanko, J. J., Metal-based methods for protein inactivation. *Current opinion in chemical biology* **2013**, 17 (2), 197-203.

Abstract

DESIGN, SYNTHESIS AND ANALYSIS OF POTENTIAL PHOTO-ACTIVATABLE CATHEPSIN K INHIBITORS

by

KHALIN EVANIA NISBETT

May 2017

Advisor: Dr. Jeremy Kodanko

Major: Chemistry

Degree: Master of Science

Tightly regulated cysteine CA proteases play a major role in maintaining the homeostasis within cells. Subsequently, when these proteases are dysregulated and mislocalized they disrupt healthy cell dynamics and contribute to many life-threatening pathologies such as arteriosclerosis, osteoporosis and cancer. As such many pharmaceutical companies and research teams are highly interested in these proteases as targets. One emergent strategy is the spatiotemporal control of biological processes. In relation to this, a series of spatiotemporally controlled inhibitors of CA proteases are being developed by the Kodanko Lab. This thesis describes the investigation of two new cathepsin K (CST-K) inhibitor derivatives and a new Ru^{II}-inhibitor binding protocol.

With regards to the free inhibitor derivatives, increased basicity at P₂ and P₃ decreased the efficacy of the inhibitors. Also, described herein is the successful caging and photo-release of one of the dipeptide nitrile inhibitors. The new Ru^{II} chaperone ([Ru^{II}])–inhibitor binding protocol is aimed at increasing the stability of Ru^{II}-inhibitor complexes in cell growth media. The investigation has revealed the drawbacks of the new binding protocol. Spatiotemporal control over protein inhibition was ineffective as a result of the promiscuity of the CST-K active site and the

terminal and unshielded position of the warhead. It became clear that the warhead of the inhibitor must be sufficiently hindered when caged to produce a substantial dark/light IC_{50} ratio (DLIR). This work is expected to improve the conceptualization of future investigations.

Autobiographical Statement

My name is Khalin Evania Nisbett. I was born and raised on a 36 square mile island (Nevis) that now habituates 12,000 people. I have long been interested in the complex dynamics behind how people think, behave and develop mentally illnesses, as well as, the very fundamental concept of how molecules interact. To me, they are one and the same: every action gives way to a reaction. My goal is to find the action – to improve our understanding of psychiatric and neurodegenerative diseases and their therapies.

PRIOR EDUCATION

University of the Virgin Islands | *Summa Cum Laude* | BSc. in Chemistry & AAS Physics | Dec 2014
Nevis Sixth Form College | AAS Math & Chemistry | May 2011

PRIOR RESEARCH EXPERIENCE

UVI Research Intern | 2014 | Analysis of citral, a major component of *Cymbopogon Citratus*
 Principal Investigator: Yakini Brandy, Ph.D.

UVI Research Intern | 2013 | Screening of Ciguatoxins found in the invasive *Pterois Miles/ Volitans*
 Principally Investigator: Bernard Castillo, Ph.D.

TEACHING & MENTORING EXPERIENCE

Graduate-Undergraduate Mentor | Wayne State University | Fall 2016

Graduate Teaching Assistant | Wayne State University | Aug 2015 – May 2017

Instructor | General Chemistry & General Physis Laboratory | University of the Virgin Islands | Winter 2015
Assistant | University of the Virgin Islands | Winter 2015

HONORS & AWARDS

Graduate School Honor Citation for Excellence in Teaching | WSU | 2017

Dean's List Award Recipient | UVI | 2012, 2013 & 2014

Award for outstanding presentation | ABRCMS, San Antonio, Texas | 2014

Outstanding Senior Chemistry Major Award | UVI | 2014

Barnett Frank Class Award-Highest Cumulated Junior GPA | UVI | 2014

Who's Who Among College & University Award Recipient | UVI | 2014

Distinction in Human & Social Biology | Nevis | 2012

Outstanding Results in Chemistry (A-Level) | NSFC | 2011

Outstanding Results in Mathematics (A-Level) | NSFC | 2011

Essay Competition Winner | Organization of the Eastern Caribbean States | 2010

CONFERENCE & SYMPOSIUM PRESENTATIONS

2014 14th Annual Biomedical Research Conference for Minority Students | San Antonio, TX

2014 Annual Fall Research Symposium | St Thomas, USVI

2014 Emerging Researchers' National Conference in STEM | Washington, D.C.

2014 UVI Research Day | St. Thomas, USVI

2013 Annual Fall Research Symposium | St Thomas, USVI

2013 12th Annual Spring Research Symposium | St Croix, USVI

COMMUNITY INVOLVEMENT

Graduate Student Alumni Representative | ACS UVI Student Chemistry Club | Current as @ 5/9/2017

President | ACS UVI Student Chemistry Club | Fall 2013 – Spring 2014

Member | UVI Sisters With Purpose | 2013 – 2014

Secretary/Financial Comptroller | HOPE Nevis Incorporated | 2009 - 2012

Founder & President | Nevis Creatively Inspired Scientists | 2010-2011